Mobile Information Systems

Cognition and Cooperation in Advanced Wireless and Mobile Information Systems

Guest Editors: Chao Chen, Carlos Pomalaza-Ráez, Yunfei Chen, Kun Xie, and Tricha Anjali

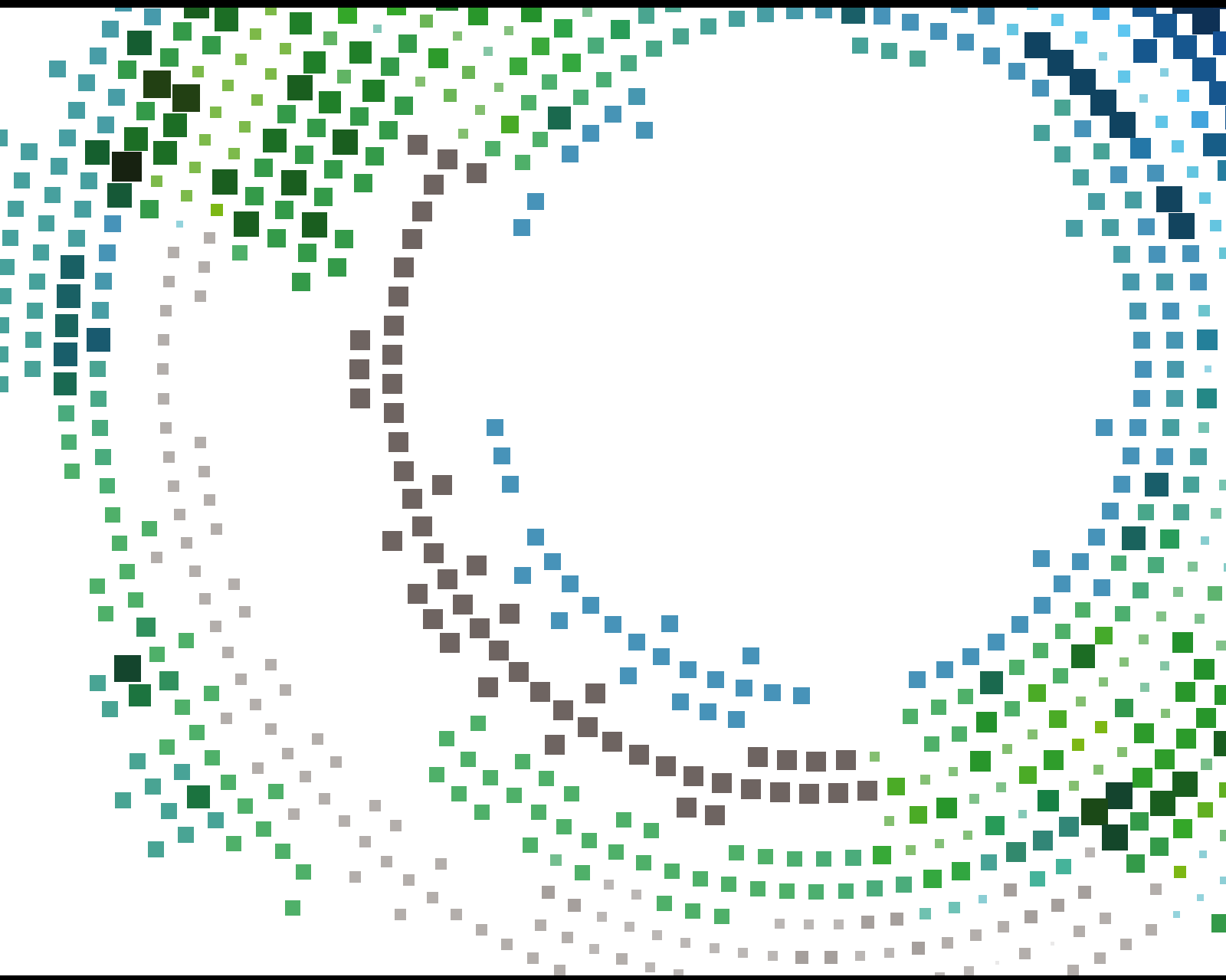

Cognition and Cooperation in Advanced Wireless and Mobile Information Systems

Mobile Information Systems

Cognition and Cooperation in Advanced Wireless and Mobile Information Systems

Guest Editors: Chao Chen, Carlos Pomalaza-Ráez, Yunfei Chen, Kun Xie, and Tricha Anjali

Contents

Hindawi Publishing Corporation
Mobile Information Systems
Volume 2016, Article ID 5404986, 2 pages
http://dx.doi.org/10.1155/2016/5404986

Editorial

Cognition and Cooperation in Advanced Wireless and Mobile Information Systems

Chao Chen,[1] Carlos Pomalaza-Ráez,[2] Yunfei Chen,[3] Kun Xie,[4] and Tricha Anjali[5]

[1]*Department of Electrical and Computer Engineering, Indiana University–Purdue University Fort Wayne, Fort Wayne, IN, USA*
[2]*Center for Wireless Communications, University of Oulu, 90570 Oulu, Finland*
[3]*School of Engineering, University of Warwick, Coventry CV4 7AL, UK*
[4]*College of Computer Science and Electronic Engineering, Hunan University, Changsha, China*
[5]*International Institute of Information Technology, Bangalore, India*

Correspondence should be addressed to Chao Chen; chenc@ipfw.edu

Received 18 August 2016; Accepted 18 August 2016

With the recent development in advanced sensing technology, processing capability, memory capacity, and battery innovations, modern wireless devices become increasingly aware of the conditions of their components and the surrounding environment. Based on learning results, a cognitive wireless device is able to reconfigure its operation dynamically and allocate resources efficiently to improve performance. In addition, cooperation among networked peer devices enables them to make intelligent adaptations based on the aggregated learning results to optimize the whole network performance.

A cognitive radio is an intelligent radio that can detect available frequency bands in its vicinity and reconfigure its transceiver parameters adaptively. Several of the selected papers investigate algorithms such as spectrum sensing, access control, and interference suppression that allow secondary users (SUs) to exploit the transmission opportunities in the primary network. S. S. Ali et al. propose new spectrum sensing methods in a multiantenna setting by weighting all eigenvalues of the covariance matrix, with the goal of detecting the existence of primary users (PUs) more effectively. SUs can choose one of few proposed weighting schemes depending on what prior information about PU is available. When a PU-vacant channel is detected in a cognitive radio network, traffic from SUs needs to be regulated to allow multiple cognitive radios to coexist in the same spectrum band. Y. Zhao et al. propose an access control scheme for prioritized traffic from SUs. They use a discrete-time queuing model to analyze the system performance and derive a dynamic access threshold for the SU packets with lower priority according to actual network status. D. Zhang et al. develop a rank-constrained beamforming algorithm for underlay multiple-input multiple-output (MIMO) cognitive radio networks. The proposed design aligns the interference caused by SUs into a reduced-dimensional subspace. At the same time, the PUs' receivers select the optimal precoding and receiving beamforming matrices to minimize the dimension of the interference.

Cooperative relaying can improve throughput and energy efficiency in wireless communications through additional spatial and spectrum diversity at the relay node. N. Cao et al. compare two strategies of cooperative relay, that is, decode-and-forward relaying and amplify-and-forward relaying, and their outage performance in cognitive radio systems. They propose the concept of rate decaying factor and use it to derive the SUs maximum SNR of these two relay strategies in a PU-occupied channel. Y. Yao et al. consider energy-harvesting relay nodes that can transform received RF signal into stored energy. In such systems, the sender first allocates its transmission power to simultaneously transmit information and transfer power to the relay, which then forwards the information to the destination using harvested energy. Through joint optimization of the power splitting and time switching ratios, the network throughput is maximized.

Besides those, the paper by M. Radenkovic addresses the problem of "cognitive privacy" in the mobile social world. An open-source distributed virtual platform called cognitive privacy framework is proposed, in which each personal cloud may decide on the fly to use different transmission network for different types of data and privacy requirements.

These papers are excellent examples of how cognition and cooperation in various wireless and mobile systems can improve system performance and user experience. By compiling these papers, we hope to encourage our readers and researchers to apply cognitive and cooperative principles in designing future wireless and mobile information systems.

Chao Chen
Carlos Pomalaza-Ráez
Yunfei Chen
Kun Xie
Tricha Anjali

Hindawi Publishing Corporation
Mobile Information Systems
Volume 2016, Article ID 3297938, 8 pages
http://dx.doi.org/10.1155/2016/3297938

Research Article

Optimization of Access Threshold for Cognitive Radio Networks with Prioritized Secondary Users

Yuan Zhao, Jialiang Wang, Jiemin Liu, and Luyi Bai

School of Computer and Communication Engineering, Northeastern University at Qinhuangdao, Qinhuangdao 066004, China

Correspondence should be addressed to Yuan Zhao; yuanzh85@163.com

Received 29 January 2016; Accepted 1 June 2016

Academic Editor: Carlos Pomalaza-Ráez

We propose an access control scheme in cognitive radio networks with prioritized Secondary Users (SUs). Considering the different types of data in the networks, the SU packets in the system are divided into SU1 packets with higher priority and SU2 packets with lower priority. In order to control the access of the SU2 packets (including the new arrival SU2 packets and the interrupted SU2 packets), a dynamic access threshold is set. By building a discrete-time queueing model and constructing a three-dimensional Markov chain with the number of the three types of packets in the system, we derive some performance measures of the two types of the SU packets. Then, with numerical results, we show the change trends for the different performance measures. At last, considering the tradeoff between the throughput and the average delay of the SU2 packets, we build a net benefit function to make optimization for the access threshold.

1. Introduction

In conventional cognitive radio networks, two types of users, namely, Primary Users (PUs) and Secondary Users (SUs), share the spectrum resource in the system. The SUs can occupy the spectrum when the spectrum is not occupied by the PUs. The PUs have higher priority than the SUs and the PUs can interrupt the transmission of the SUs to take over the spectrum [1]. Most of existing researches for cognitive radio networks were studied under the assumption of single type of SUs [2–4]. However, in practical networks, there are different types of data in the system. So, it is necessary to consider the different types and prioritization among the SUs in cognitive radio networks.

In recent years, some researches began to focus on the performance analysis of the cognitive radio networks with prioritized SUs.

Lee et al. considered a cognitive radio network with three types of calls, namely, PU call, SU1 call, and SU2 call, in the system [5]. They denoted the high priority and the low priority SU calls as SU1 calls and SU2 calls. By building a continuous-time Markov chain and applying the Gauss-Seidel method, they gave the steady-state probability distribution of the system. Moreover, they presented some performance measures, such as the blocking rate and the throughput of the SU2 call.

Zhang et al. analyzed the transmission delay of priority-based SUs in the opportunistic spectrum access (OSA) based cognitive radio networks [6]. By employing a preemptive resume priority (PRP) M/M/1 queuing model, they derived some performance measures, such as the transmission delay of the interrupted SUs with each priority level and the overall transmission delay of the interrupted SUs.

Zhao and Yue considered cognitive radio networks with multiple SUs [7]. A nonpreemptive priority scheme for the SU packets with higher priority was proposed and compared with the preemptive priority scheme. By constructing and analyzing a three-dimensional Markov chain, they derived the expression for the interrupted rate of the two types of SU packets, respectively.

However, the above researches about cognitive radio networks with prioritized SUs did not consider the access control for the SU packets with lower priority. In cognitive radio network, larger number of SU packets with lower priority which access the system without any restriction will disturb the transmission of the PUs and the SUs with higher priority. So, it is necessary to control the access of the SU packets

with lower priority reasonably. In this paper, we consider setting an access threshold for the SU packets with lower priority (called SU2 packets) to control the access of the SU2 packets. Specially, we also make optimization for the access threshold, while the optimization research was not shown up in [5–7].

On the other hand, we can find that the researches about cognitive radio networks with priority SUs mentioned above were analyzed by using continuous-time models. However, considering the digital nature of model networks, the discrete-time models are more suitable when analyzing the system performance of the networks [8]. So, in this paper, we evaluate the system performance of the proposed cognitive radio networks with the discrete-time queueing analysis. By building a discrete-time queueing model with multiple priority levels, we construct a three-dimensional Markov chain and give the transition probability matrix of the Markov chain. Then with the obtained steady-state distribution, we derive some performance measures of the system. At last, we make optimization for the access threshold by building a net benefit function.

The remainder of this paper is organized as follows. The system model with model assumption and model analysis is demonstrated in Section 2. In Section 3, different performance measures for the SU1 packets and the SU2 packets are derived, respectively. In Section 4, numerical results for different performance measures are shown. Considering the tradeoff between different performance measures, the optimization for the access threshold is given in Section 5. Finally, conclusions are drawn in Section 6.

2. System Model

2.1. Model Assumption. We focus on a cognitive radio network with a single channel. The PU packets have higher priority to occupy the channel than the SU packets. There are two types of SU packets, namely, SU1 packets and SU2 packets. We assume that the SU1 packets have higher priority than the SU2 packets. That is to say, the PU packets have the highest priority, and the SU2 packets have the lowest priority. The PU packets can interrupt the transmission of the SU1 packets and the SU2 packets, while the SU1 packets can interrupt the transmission of the SU2 packets.

In order to reduce the latency of the PU packets and the SU1 packets, no buffers are set for the PU packets and the SU1 packets.

When a PU packet arrives at the system, if the channel is occupied by another PU packet, this newly arriving PU packet will leave the system to find another available channel directly. If the channel is occupied by an SU packet (an SU1 packet or an SU2 packet), this newly arriving PU packet will interrupt the transmission of the SU packet and occupy the channel.

When an SU1 packet arrives at the system, if the channel is occupied by a PU packet or an SU1 packet, this newly arriving SU1 packet will also leave the system to find another available channel. If the channel is occupied by an SU2 packet, this newly arriving SU1 packet will interrupt the transmission of the SU2 packet and occupy the channel.

A buffer called SU2 buffer is prepared for the SU2 packets. In order to control the access of the SU2 packets, an access threshold is set for the SU2 packets. When an SU2 packet arrives at the system, if the number of SU2 packets in the SU2 buffer is equal to the access threshold, this SU2 packet will be blocked by the system. The access threshold can also control the return action of the interrupted SU2 packet. When the transmission of an SU2 packet is interrupted, if the number of SU2 packets in the SU2 buffer is smaller than the access threshold, this interrupted SU2 packet can return back to the SU2 buffer; otherwise, this interrupted SU2 packet has to leave the system. Specially, we assume that the interrupted SU2 packets have higher priority than the newly arriving SU2 packets.

Based on the access control scheme mentioned above, we can build a queueing model with multiple priority levels and finite waiting room.

Considering the digital nature of modern networks, the time axis is assumed to be divided into slots with equal size. The slot boundary is denoted as $t = 1, 2, \ldots$. The arrival intervals of the PU packets, the SU1 packets, and the SU2 packets are assumed to follow geometric distribution with arrival rates p_1, p_{21}, and p_{22}. The transmission time of the PU packets, the SU1 packets, and the SU2 packets is assumed to follow geometric distribution with service rates r_1, r_{21}, and r_{22}. The access threshold is denoted as T, where $T > 0$.

Let L_n be the total number of packets (including PU packets, SU1 packets, and SU2 packets) in the system at the instant $t = n^+$. Let S_n be the number of SU1 packets in the system at the instant $t = n^+$. Let P_n be the number of PU packets in the system at the instant $t = n^+$. We note that $\{L_n, S_n, P_n\}$ constitutes a three-dimensional discrete-time Markov chain. With the access threshold T, we can give the state space Ω of $\{L_n, S_n, P_n\}$ as follows:

$$\begin{aligned}\Omega = {} & (0,0,0) \\ & \cup \{(i,0,0) \cup (i,1,0) \cup (i,0,1) : 1 \le i \le T+1\}.\end{aligned} \tag{1}$$

2.2. Model Analysis. Let $\mathbf{P}$ be the state transition probability matrix for the three-dimensional Markov chain $\{L_n, S_n, P_n\}$. $\mathbf{P}$ can be given as a $(T+2) \times (T+2)$ block-structured matrix as follows:

$$\mathbf{P} = \begin{pmatrix} \mathbf{U}_0 & \mathbf{V}_0 & \mathbf{W}_0 & & & & \\ \mathbf{D}_0 & \mathbf{C} & \mathbf{B} & \mathbf{A} & & & \\ & \mathbf{D} & \mathbf{C} & \mathbf{B} & \mathbf{A} & & \\ & \ddots & \ddots & \ddots & \ddots & \ddots & \\ & & \mathbf{D} & \mathbf{C} & \mathbf{B} & \mathbf{A} & \\ & & & \mathbf{D} & \mathbf{C} & \mathbf{E} & \\ & & & & \mathbf{D} & \mathbf{F} & \end{pmatrix}. \tag{2}$$

Hereafter, we use the overbar notation to denote the probability of the complement of an event, for instance, $\overline{p}_1 = 1 - p_1$. Moreover, we denote $\lambda = \overline{p}_{22}\overline{r}_{22} + p_{22}r_{22}$, $\xi = \overline{r}_{21} + p_{21}r_{21}$. The elements of $\mathbf{P}$ can be discussed by following subblock matrices.

$\mathbf{U}_0$ is the probability for the total number of packets in the system being fixed at 0. $\mathbf{U}_0$ can be given as follows:

$$\mathbf{U}_0 = \overline{p}_1\overline{p}_{21}\overline{p}_{22}. \tag{3}$$

$\mathbf{V}_0$ is the transition probability subblock when the total number of packets in the system transfers from 0 to 1. $\mathbf{V}_0$ can be given as follows:

$$\mathbf{V}_0 = \left(\overline{p}_1\overline{p}_{21}p_{22}, \overline{p}_1p_{21}\overline{p}_{22}, p_1\overline{p}_{22}\right). \tag{4}$$

$\mathbf{W}_0$ is the transition probability subblock when the total number of packets in the system transfers from 0 to 2. $\mathbf{W}_0$ can be given as follows:

$$\mathbf{W}_0 = \left(0, \overline{p}_1p_{21}p_{22}, p_1p_{22}\right). \tag{5}$$

$\mathbf{D}_0$ is the transition probability subblock when the total number of packets in the system transfers from 1 to 0. $\mathbf{D}_0$ can be given as follows:

$$\mathbf{D}_0 = \left(\overline{p}_1\overline{p}_{21}\overline{p}_{22}r_{22}, \overline{p}_1\overline{p}_{21}\overline{p}_{22}r_{21}, \overline{p}_1\overline{p}_{21}\overline{p}_{22}r_1\right)^{\mathrm{T}}, \tag{6}$$

where T describes the transpose operator of the matrix.

$\mathbf{D}$ is the transition probability subblock when the total number of packets in the system transfers from u to $(u-1)$, where $2 \le u \le T+1$. $\mathbf{D}$ can be given as follows:

$$\mathbf{D} = \begin{pmatrix} \overline{p}_1\overline{p}_{21}\overline{p}_{22}r_{22} & 0 & 0 \\ \overline{p}_1\overline{p}_{21}\overline{p}_{22}r_{21} & 0 & 0 \\ \overline{p}_1\overline{p}_{21}\overline{p}_{22}r_1 & 0 & 0 \end{pmatrix}. \tag{7}$$

$\mathbf{C}$ is the transition probability subblock when the total number of packets in the system transfers from u to u, where $1 \le u \le T$. $\mathbf{C}$ can be given as follows:

$$\mathbf{C} = \begin{pmatrix} \overline{p}_1\overline{p}_{21}\lambda & \overline{p}_1p_{21}\overline{p}_{22}r_{22} & p_1\overline{p}_{22}r_{22} \\ \overline{p}_1\overline{p}_{21}p_{22}r_{21} & \overline{p}_1\overline{p}_{22}\xi & \overline{p}_{22}p_1 \\ \overline{p}_1\overline{p}_{21}p_{22}r_1 & \overline{p}_1p_{21}\overline{p}_{22}r_1 & \overline{p}_{22}\left(\overline{r}_1 + r_1p_1\right) \end{pmatrix}. \tag{8}$$

$\mathbf{B}$ is the transition probability subblock when the total number of packets in the system transfers from u to $(u+1)$, where $1 \le u \le T-1$. $\mathbf{B}$ can be given as follows:

$$\mathbf{B} = \begin{pmatrix} \overline{p}_1\overline{p}_{21}p_{22}\overline{r}_{22} & \overline{p}_1p_{21}\lambda & p_1\lambda \\ 0 & \overline{p}_1p_{22}\xi & p_{22}p_1 \\ 0 & \overline{p}_1p_{21}p_{22}r_1 & p_{22}\left(\overline{r}_1 + r_1p_1\right) \end{pmatrix}. \tag{9}$$

$\mathbf{A}$ is the transition probability subblock when the total number of packets in the system transfers from u to $(u+2)$, where $1 \le u \le T-1$. $\mathbf{A}$ can be given as follows:

$$\mathbf{A} = \begin{pmatrix} 0 & \overline{p}_1p_{21}p_{22}\overline{r}_{22} & p_1p_{22}\overline{r}_{22} \\ 0 & 0 & 0 \\ 0 & 0 & 0 \end{pmatrix}. \tag{10}$$

$\mathbf{E}$ is the transition probability subblock when the total number of packets in the system transfers from T to $(T+1)$. $\mathbf{E}$ can be given as follows:

$$\mathbf{E} = \begin{pmatrix} \overline{p}_1\overline{p}_{21}p_{22}r_{22} & \overline{p}_1p_{21}\left(1-\overline{p}_{22}r_{22}\right) & p_1\left(1-\overline{p}_{22}r_{22}\right) \\ 0 & \overline{p}_1p_{22}\xi & p_{22}p_1 \\ 0 & \overline{p}_1p_{21}p_{22}r_1 & p_{22}\left(\overline{r}_1 + r_1p_1\right) \end{pmatrix}. \tag{11}$$

$\mathbf{F}$ is the transition probability subblock when the total number of packets in the system is fixed at $(T+1)$. $\mathbf{F}$ can be given as follows:

$$\mathbf{F} = \begin{pmatrix} \overline{p}_1\overline{p}_{21}\left(1-\overline{p}_{22}r_{22}\right) & \overline{p}_1p_{21} & p_1 \\ \overline{p}_1\overline{p}_{21}p_{22}r_{21} & \overline{p}_1\xi & p_1 \\ \overline{p}_1\overline{p}_{21}p_{22}r_1 & \overline{p}_1p_{21}r_1 & \overline{r}_1 + r_1p_1 \end{pmatrix}. \tag{12}$$

The structure of the transition probability matrix $\mathbf{P}$ indicates that the three-dimensional Markov chain $\{L_n, S_n, P_n\}$ is nonperiodic, irreducible, and positive recurrent [9]. The steady-state distribution $\pi_{i,j,k}$ of the three-dimensional Markov chain is defined as follows:

$$\pi_{i,j,k} = \lim_{n\to\infty} P\left\{L_n = i, S_n = j, P_n = k\right\}. \tag{13}$$

Let $\mathbf{\Pi}$ be the steady-state probability vector, which is the unique solution of equations $\mathbf{\Pi P} = \mathbf{\Pi}$, $\mathbf{\Pi e} = 1$, where $\mathbf{e}$ is a one column vector.

We partition $\mathbf{\Pi}$ as $\mathbf{\Pi} = (\mathbf{\Pi}_0, \mathbf{\Pi}_1, \ldots, \mathbf{\Pi}_T, \mathbf{\Pi}_{T+1})$, where $\mathbf{\Pi}_0 = \pi_{0,0,0}$ and $\mathbf{\Pi}_i = (\pi_{i,0,0}, \pi_{i,1,0}, \pi_{i,0,1})$ for $1 \le i \le T+1$. By applying a Gauss-Seidel method, we can obtain the steady-state probability vector $\mathbf{\Pi}$.

3. Performance Measures

3.1. Performance Measures of the SU1 Packets. The average queue length $E[\mathrm{SU1}]$ of the SU1 packets is defined as the number of SU1 packets in the system per slot. We can give the expression of the average queue length $E[\mathrm{SU1}]$ of the SU1 packets as follows:

$$E\left[\mathrm{SU1}\right] = \sum_{i=1}^{T+1} \pi_{i,1,0}. \tag{14}$$

The blocking rate β_{21} of the SU1 packets is defined as the number of SU1 packets that are blocked by the system per slot. We can give the expression of the blocking rate β_{21} of the SU1 packets as follows:

$$\begin{aligned} \beta_{21} &= p_{21}\left(\sum_{i=1}^{T+1}\left(\pi_{i,1,0}\left(\overline{r}_{21} + r_{21}p_1\right) + \pi_{i,0,1}\left(\overline{r}_1 + r_1p_1\right)\right)\right. \\ &\quad \left. + \sum_{i=0}^{T+1}\pi_{i,0,0}p_1\right). \end{aligned} \tag{15}$$

The interrupted rate γ_{21} of the SU1 packets is defined as the number of SU1 packets that are interrupted by the PU packets per slot. We can give the expression of the interrupted rate γ_{21} of the SU1 packets as follows:

$$\gamma_{21} = \sum_{i=1}^{T+1} \pi_{i,1,0} \overline{r}_{21} p_1. \tag{16}$$

The throughput θ_{21} of the SU1 packets is defined as the number of SU1 packets that are transmitted completely by the system per slot. We can give the expression of the throughput θ_{21} of the SU1 packets as follows:

$$\theta_{21} = p_{21} - \beta_{21} - \gamma_{21}. \tag{17}$$

3.2. Performance Measures of the SU2 Packets. The average queue length $E[\mathrm{SU2}]$ of the SU2 packets is defined as the number of SU2 packets in the system per slot. We can give the expression of the average queue length $E[\mathrm{SU2}]$ of the SU2 packets as follows:

$$E[\mathrm{SU2}] = \sum_{i=0}^{T+1} i\pi_{i,0,0} + \sum_{i=1}^{T+1} (i-1)\left(\pi_{i,1,0} + \pi_{i,0,1}\right). \tag{18}$$

The blocking rate β_{22} of the SU2 packets is defined as the number of SU2 packets that are blocked by the system per slot. We can give the expression of the blocking rate β_{22} of the SU2 packets as follows:

$$\begin{aligned}\beta_{22} = {} & p_{22}\left(\pi_{T+1,0,0}\left(1 - r_{22}\overline{p}_1\overline{p}_{21}\right)\right. \\ & \left. + \pi_{T+1,1,0}\left(1 - r_{21}\overline{p}_1\overline{p}_{21}\right)\right) \\ & + p_{22}\left(\pi_{T+1,0,1}\left(1 - r_1\overline{p}_1\overline{p}_{21}\right)\right. \\ & \left. + \pi_{T,0,0}\overline{r}_{22}\left(1 - \overline{p}_1\overline{p}_{21}\right)\right).\end{aligned} \tag{19}$$

The interrupted losing rate γ_{22} of the SU2 packets is defined as the number of SU2 packets that are interrupted by the PU packets or the SU1 packets and being forced to leave the system because of the number of SU2 packets in the buffer achieving the access threshold. We can give the expression of the interrupted losing rate γ_{22} of the SU2 packets as follows:

$$\gamma_{22} = \pi_{T+1,0,0}\overline{r}_{22}\left(1 - \overline{p}_1\overline{p}_{21}\right). \tag{20}$$

The throughput θ_{22} of the SU2 packets is defined as the number of SU2 packets that are transmitted completely by the system per slot. We can give the expression of the throughput θ_{22} of the SU2 packets as follows:

$$\theta_{22} = p_{22} - \beta_{22} - \gamma_{22}. \tag{21}$$

The average delay δ_{22} of the SU2 packets is defined as the average time length from an SU2 packet joining the system to this SU2 packet leaving the system (being transmitted completely or being interrupted to leave). With Little's formula [10], we can give the expression of the average delay δ_{22} of the SU2 packets as follows:

$$\delta_{22} = \frac{E[\mathrm{SU2}]}{p_{22} - \beta_{22}}. \tag{22}$$

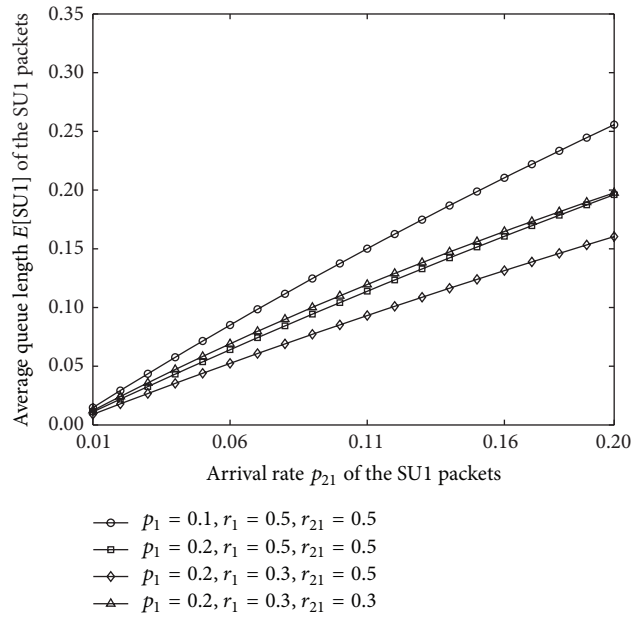

Figure 1: Average queue length $E[\mathrm{SU1}]$ of the SU1 packets.

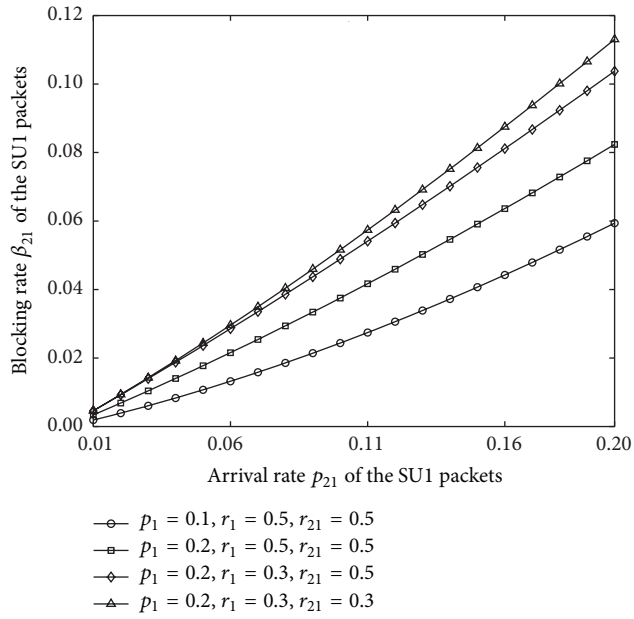

Figure 2: Blocking rate β_{21} of the SU1 packets.

4. Numerical Results

In this section, we show the change trends for different performance measures with numerical results for the SU1 packets and the SU2 packets, respectively.

4.1. Numerical Results for the SU1 Packets. According to the working principle of the system model, the performance of the SU1 packets will be influenced by the PU packets. Figures 1–3 show the change trends for the average queue length $E[\mathrm{SU1}]$, the blocking rate β_{21}, and the throughput θ_{21} of the

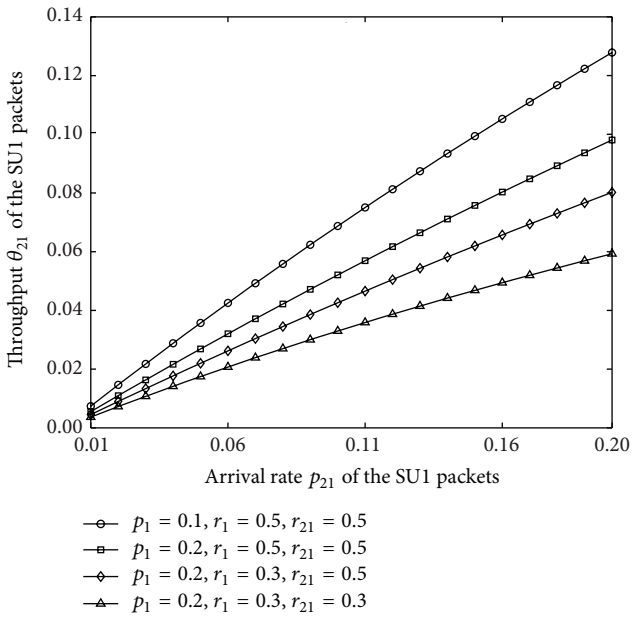

Figure 3: Throughput θ_{21} of the SU1 packets.

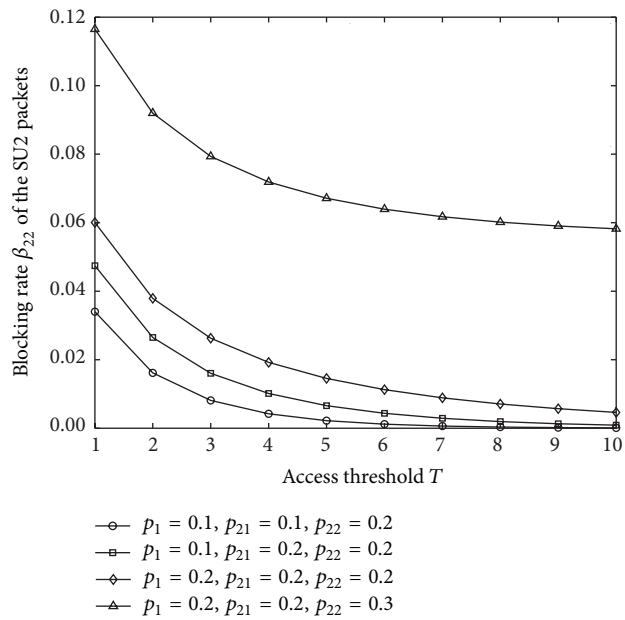

Figure 4: Blocking rate β_{22} of the SU2 packets.

SU1 packets with different parameter settings of PU packets and SU1 packets.

From Figures 1–3, we find that as the arrival rate p_{21} of the SU1 packets increases, the average queue length $E[\text{SU1}]$, the blocking rate β_{21}, and the throughput θ_{21} of the SU1 packets will increase. This is because the larger the arrival rate of the SU1 packets is, the more the SU1 packets will join the system. As a result, the average queue length of the SU1 packets in the system will be higher. On the other hand, the larger the number of SU1 packets joining the system is, the more the possibility for the SU1 packets being blocked by the system is and the higher the blocking rate of the SU1 packets will be. Moreover, the more the SU1 packets joining the system are, the more the SU1 packets will be transmitted and the greater the throughput of the SU1 packets will be.

From Figures 1–3, we also find that as the arrival rate p_1 of the PU packets increases, the blocking rate β_{21} of the SU1 packets will increase and the average queue length $E[\text{SU1}]$ and the throughput θ_{21} of the SU1 packets will decrease. The reason is that as the arrival rate of the PU packets increases, the possibility for the channel being occupied by the PU packets will also increase. As a result, the number of SU1 packets joining the system and being transmitted completely will decrease, and this will decrease the average queue length and the throughput of the SU1 packets. Moreover, larger number of SU1 packets will be blocked by the system, and the blocking rate of the SU1 packets will be increased.

Moreover, from Figures 1–3, we conclude that as the service rate r_1 of the PU packets increases, the average queue length $E[\text{SU1}]$ and the throughput θ_{21} of the SU1 packets will increase and the blocking rate β_{21} of the SU1 packets will decrease. This is because the higher the service rate of the PU packets is, the larger the possibility for the SU1 packets occupying the channel is, and this will increase the average queue length and the throughput of the SU1 packets. At the same time, the blocking rate of the SU1 packets will be lower.

Additionally, Figures 1–3 show that as the service rate r_{21} of the SU1 packets increases, the average queue length $E[\text{SU1}]$ and the blocking rate β_{21} of the SU1 packets will decrease and the throughput θ_{21} of the SU1 packets will increase. The reason is that as the service rate of the SU1 packets increases, the SU1 packets on the channel will be transmitted more quickly and then the throughput of the SU1 packets will be greater. Along with the increase of the service rate of the SU1 packets, the average number of SU1 packets in the system will be lower and then the average queue length and the blocking rate of the SU1 packets will decrease.

4.2. Numerical Results for the SU2 Packets. According to the working principle of the system model, the performance of the SU2 packets will be influenced not only by the PU packets but also by the SU1 packets. Figures 4–6 show the change trends for the blocking rate β_{22}, the throughput θ_{22}, and the average delay δ_{22} of the SU2 packets with respect to the access threshold under different parameter settings of PU packets and SU1 packets. In Figures 4–6, without loss of generality, the service rates r_1, r_{21}, and r_{22} are assumed to be fix at 0.5.

From Figures 4–6, we find that as the access threshold T increases, the blocking rate β_{22} of the SU2 packets will decrease and the throughput θ_{22} and the average delay δ_{22} of the SU2 packets will increase. This is because the higher the access threshold is, the more the SU2 packets can be admitted to join the system and the more the SU2 packets will wait in the system. As a result, the average delay of the SU2 packets will be higher. On the other hand, as the access threshold increases, the number of SU2 packets being blocked by system will decrease and then the blocking rate of the SU2 packets will decrease too. Moreover, the more the SU2 packets joining the system are, the more the SU2 packets will be

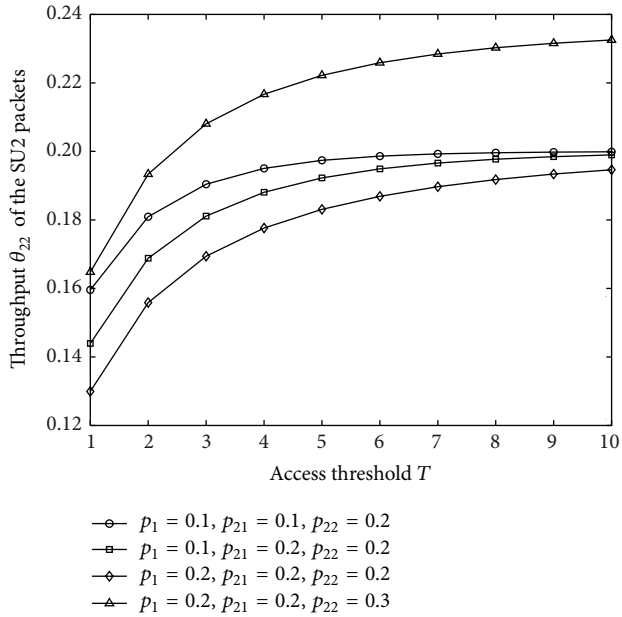

Figure 5: Throughput θ_{22} of the SU2 packets.

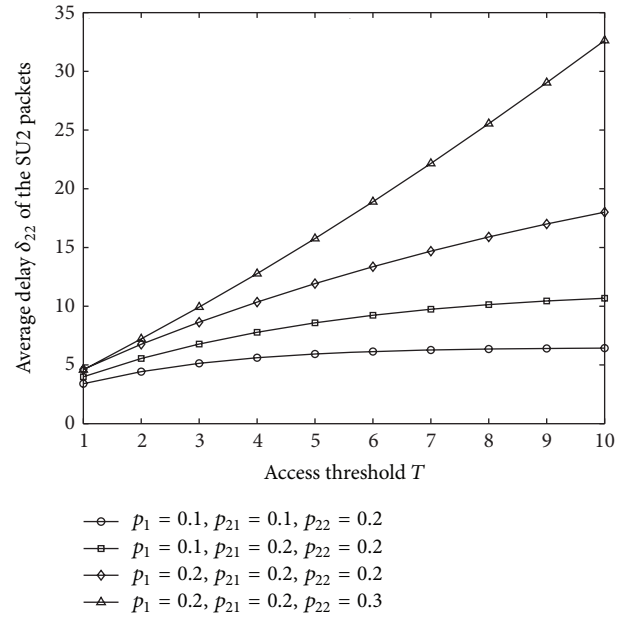

Figure 6: Average delay δ_{22} of the SU2 packets.

transmitted completely and the greater the throughput of the SU2 packets will be. Specially, from Figure 4, we find that as the access threshold T increases, the blocking rete β_{22} of the SU2 packets will decrease. As a result, the number of SU2 packets being in the system will increase and the possibility for the channel being occupied will be higher. Therefore, we conclude that the possibility for the channel being occupied can be increased by setting a greater access threshold.

From Figures 4–6, we also find that as the arrival rate p_1 of the PU packets or the arrival rate p_{21} of the SU1 packets increases, the blocking rate β_{22} and the average delay δ_{22} of the SU2 packets will increase and the throughput θ_{22} of the SU2 packets will decrease. The reason is that as the arrival rate of the PU packets or the arrival rate of the SU1 packets increases, the possibility for the channel being occupied by the SU2 packets will decrease. Then the number of SU2 packets waiting in the system will increase, and this will induce the increase in the average delay and the blocking rate of the SU2 packets. Moreover, the less the number of SU2 packets occupying the channel is, the less the number of SU2 packets will be transmitted completely. As a result, the throughput of the SU2 packets will be lower.

Additionally, Figures 4–6 show that as the arrival rate p_{22} of the SU2 packets increases, the blocking rate β_{22}, the throughput θ_{22}, and the average delay δ_{22} of the SU2 packets will increase too. The reason is that as the arrival rate of the SU2 packets increases, the number of SU2 packets with joining need will increase. The more the SU2 packets joining the system are, the more the SU2 packets waiting in the system are and the more the SU2 packets will be transmitted completely. So the blocking rate, the throughput, and the average delay of the SU2 packets will be higher.

5. Optimization for the Access Threshold

In this section, we focus on the optimal setting for the access threshold of the SU2 packets. From the numerical results, we conclude that as the access threshold T increases, the throughput θ_{22} of the SU2 packets increases, and this is what we want to see. On the other hand, as the access threshold T increases, the average delay δ_{22} of the SU2 packets also increases, which is not what we want to see. So in order to balance the throughput of the SU2 packets and the average delay of the SU2 packets, we build a net benefit function $F(T)$ with the access threshold T as follows:

$$F(T) = b\theta_{22} - c\delta_{22}, \tag{23}$$

where b and c are the impact factors for the net benefit function. Moreover, b and c can be set according to the actual network situation.

From (23), we can derive the optimal access threshold T^* as follows:

$$T^* = \arg\max_{T} \{F(T)\}. \tag{24}$$

In order to find the optimal access threshold T^*, by setting $b = 300$ and $c = 2$ as an example, we depict the change trend for the net benefit function $F(T)$ in Figure 7.

From Figure 7, we find that as the access threshold increases, the net benefit function shows an upper convex change trend. The reason may be that when the access threshold is smaller, the access threshold is the main factor to control the access actions of the SU2 packets. As the access threshold increases, the throughput will increase quickly, which will induce the increasing trend of the net benefit function. However, as the access threshold continues to increase, the average delay of the SU2 packets increases rapidly, which will cause the decrease of the net benefit. So, from Figure 7, we can find that there exists an optimal access threshold to

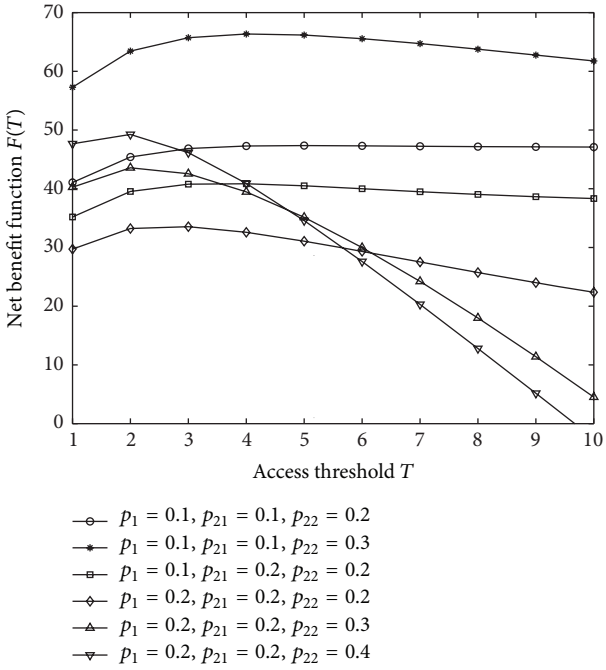

Figure 7: Change trend for the net benefit function $F(T)$.

Table 1: Numerical results for the optimal access threshold and the corresponding net benefit.

p_1	p_{21}	p_{22}	T^*	$F(T^*)$
0.1	0.1	0.2	5	47.3504
0.1	0.1	0.3	4	66.3590
0.1	0.2	0.2	4	40.8567
0.2	0.2	0.2	3	33.5409
0.2	0.2	0.3	2	43.5728
0.2	0.2	0.4	2	49.2551

achieve the maximum net benefit. We summarize the optimal access threshold and the corresponding net benefit in Table 1 for different parameter settings.

From Table 1, we conclude that as the arrival rate p_1 of the PU packets or the arrival rate p_{21} of the SU1 packets increases, the optimal access threshold T^* shows a decreasing tendency. This is because as the arrival rate of the PU packets increases or the arrival rate p_{21} of the SU1 packets increases, the possibility for the SU2 packets occupying the channel will be lower and larger number of SU2 packets have to wait in the system, which will result in the increase of the average delay of the SU2 packets. In order to reduce the average delay of the SU2 packets, the access threshold should be set lower.

On the other hand, from Table 1, we find that as the arrival rate p_{22} of the SU2 packets increases, the optimal access threshold T^* shows a decreasing tendency when we compare $p_1 = 0.1$, $p_{21} = 0.1$, $p_{22} = 0.2$ with $p_1 = 0.1$, $p_{21} = 0.1$, $p_{22} = 0.3$ and $p_1 = 0.2$, $p_{21} = 0.2$, $p_{22} = 0.2$ with $p_1 = 0.2$, $p_{21} = 0.2$, $p_{22} = 0.3$. The reason for the interesting tendency may be that the higher the arrival rate of the SU2 packets is, the more the SU2 packets will join the system, which will induce an increase in the average delay of the SU2 packets. So, in order to reduce the average delay of the SU2 packets, the access threshold should be set lower. Moreover, from Table 1, we also find that for $p_1 = 0.2$, $p_{21} = 0.2$, the optimal access threshold T^* will be fixed at $T^* = 2$ when the arrival rate of the SU2 packets increases from $p_{22} = 0.3$ to $p_{22} = 0.4$. The reason for this change trend may be that when the access threshold is decreased to a low level, considering the tradeoff between the average delay and the throughput of the SU2 packets, the optimal access threshold will not be decreased in order to guarantee the throughput of the SU2 packets.

Therefore, from the numerical results shown in Table 1, we conclude that we should set the access threshold based on the different network running status in practice.

6. Conclusion

In this paper, we consider a cognitive radio network with prioritized SU packets. In order to control the access of the SU2 packets (i.e., the SU packets with lower priority), an access threshold was set not only for the newly arriving SU2 packets but also for the interrupted SU2 packets. By building and analyzing a discrete-time Markov chain, some performance measures for the two kinds of SU packets (SU1 packets and SU2 packets) were derived. With numerical results, we investigated the change trends for different performance measures and found that there was a tradeoff between the throughput and the average delay of the SU2 packets. At last, by constructing a net benefit function, we derived the numerical results for the optimal access threshold which balanced different performance measures of the SU2 packets.

Competing Interests

The authors declare that the funding mentioned in Acknowledgments section does not lead to any conflict of interests. Additionally, the authors declare that there is no conflict of interests regarding the publication of this paper.

Acknowledgments

This work was supported by the Doctoral Fund Project of Northeastern University at Qinhuangdao (XNB201606), the National Natural Science Foundation of China (61402087), the Natural Science Foundation of Hebei Province (F2016501073 and F2015501049), the Scientific Research Fund of Hebei Education Department (QN2016307), and the Fundamental Research Fund for the Central Universities (N152303007), China.

References

[1] E. Z. Tragos, S. Zeadally, A. G. Fragkiadakis, and V. A. Siris, "Spectrum assignment in cognitive radio networks: a comprehensive survey," *IEEE Communications Surveys & Tutorials*, vol. 15, no. 3, pp. 1108–1135, 2013.

[2] S. Tang, "A general model of opportunistic spectrum sharing with unreliable sensing," *International Journal of Communication Systems*, vol. 27, no. 1, pp. 31–44, 2014.

[3] S. Jin, Y. Zhao, W. Yue, and Z. Saffer, "Performance analysis and optimization of an adaptive admission control scheme in cognitive radio networks," *Mathematical Problems in Engineering*, vol. 2013, Article ID 727310, 2013.

[4] J. Wang, A. Huang, W. Wang, and T. Q. S. Quek, "Admission control in cognitive radio networks with finite queue and user impatience," *IEEE Wireless Communications Letters*, vol. 2, no. 2, pp. 175–178, 2013.

[5] Y. Lee, C. G. Park, and D. B. Sim, "Cognitive radio spectrum access with prioritized secondary users," *Applied Mathematics & Information Sciences*, vol. 6, no. 2, supplement, pp. 595S–601S, 2012.

[6] Y. Zhang, T. Jiang, L. Zhang, D. Qu, and W. Peng, "Analysis on the transmission delay of priority-based secondary users in cognitive radio networks," in *Proceedings of the International Conference on Wireless Communications and Signal Processing (WCSP '13)*, IEEE Press, Hangzhou, China, October 2013.

[7] Y. Zhao and W. Yue, "Performance comparison between two kinds of priority schemes in cognitive radio networks," in *Queueing Theory and Network Applications*, T. V. Do, Y. Takahashi, W. Yue, and V.-H. Nguyen, Eds., vol. 383 of *Advances in Intelligent Systems and Computing*, pp. 73–80, Springer, New York, NY, USA, 2016.

[8] H. Takagi, *Queueing Analysis, Volume 3: Discrete-Time Systems*, North-Holland Elsevier, Amsterdam, The Netherlands, 1993.

[9] A. S. Alfa, *Queueing Theory for Telecommunication: Discrete Time Modelling of a Single Node System*, Springer, New York, NY, USA, 2010.

[10] N. Tian and Z. G. Zhang, *Vacation Queueing Models: Theory and Applications*, Springer, New York, NY, USA, 2006.

Hindawi Publishing Corporation
Mobile Information Systems
Volume 2016, Article ID 8907267, 11 pages
http://dx.doi.org/10.1155/2016/8907267

Research Article

Throughput Characterization for Cooperative Wireless Information Transmission with RF Energy Harvesting-Based Relay

Yuanyuan Yao,[1] Changchuan Yin,[1] and Sai Huang[2]

[1]*Beijing Laboratory of Advanced Information Networks and the Beijing Key Laboratory of Network System Architecture and Convergence, Beijing University of Posts and Telecommunications, Beijing 100876, China*
[2]*Key Laboratory of Universal Wireless Communications Ministry of Education, Wireless Technology Innovation Institute (WTI), Beijing University of Posts and Telecommunications, Beijing 100876, China*

Correspondence should be addressed to Yuanyuan Yao; yyyao@bupt.edu.cn

Received 25 January 2016; Accepted 27 March 2016

Academic Editor: Yunfei Chen

The simultaneous wireless information and power transfer (SWIPT) in a cooperative relaying system is investigated, where the relay node is self-sustained by harvesting radiofrequency (RF) energy from the source node. In this paper, we propose a time switching and power splitting (TSPS) protocol for the cooperative system with a mobile destination node. In the first part of the transmission slot, a portion of the received signal power is used for energy transfer, and the remaining power is used for information transmission from the source to the relay. For the remaining time of the transmission slot, information is transmitted from the relay to a mobile destination node. To coordinate the wireless information and power transfer, two transmission modes are investigated, namely, relay-assisted transmission mode and nonrelay mode, respectively. Under these two modes, the outage probability and the network throughput are characterized. By joint optimization of the power splitting and the time switching ratios, we further compare the network throughput under the two transmission modes with different parameters. Results indicate that the relay-assisted transmission mode significantly improves the throughput of the wireless network.

1. Introduction

Recently, to prolong the lifetime of energy-constrained wireless network, energy harvesting has drawn great attentions due to the growing energy demands and the increasing energy prices [1]. It enables the wireless nodes to collect energy from ambient renewable energy sources (e.g., wind and solar power), which eliminates the need for manual battery replacement/recharging, and effectively reduces the cost of energy bills and degrades the level of carbon dioxide emissions [2]. However, for some devices, such as military nodes or wireless sensor nodes which are located in a harsh environment that is difficult to access, the recharging of the batteries remains an open problem, especially when the number of nodes is huge and the nodes are distributed in a wide area. Radiofrequency (RF) energy harvesting is proposed as a solution or partial solution to overcome these problems [3].

RF energy harvesting can be regarded as a far-field energy transfer technique and has become a promising solution for generating a small amount of electrical power to replenish the power sources in energy-constrained wireless networks [4, 5]. The RF harvester in the node is equipped with a power conversion circuit, which can transform the received electromagnetic wave into direct-current (DC) power. As such, the devices can utilize the harvested energy from RF signals to augment/replenish their batteries [6]. Wireless nodes which are equipped with omnidirectional antennas can radiate RF signals in all directions, and thus the wireless signals can be used to deliver information as well as energy, which indicates that the energy-constrained wireless devices can simultaneously process wireless information and

power transfer (SWIPT) [7]. With SWIPT, the available wireless resources can be effectively utilized by developing the transceiver designs.

The idea of SWIPT was first proposed in [8], where a capacity-energy function was utilized to investigate the trade-off between energy harvesting and information transmission. Since the traditional receiver cannot extract the RF energy from the same signals used for information transmission, a new SWIPT receiver that can split the received signal into two separate streams was proposed in [9], where the two streams can be used for information decoding and energy harvesting with different power levels. Liu et al. in [10] derived the optimal information decoding and energy harvesting mode switching rules at the receiver targeting the optimization of the outage probability by using time switching (TS) or power splitting (PS) protocols. In [11], Ng et al. investigated the resource allocation algorithm that is designed to maximize the energy efficiency of data transmission in orthogonal frequency division multiple access (OFDMA) systems with SWIPT, and suboptimal iterative resource allocation algorithms were formulated and solved.

The cooperative relaying techniques can overcome the fading and the attenuation by using the intermediate relay, which significantly improve the efficiency and reliability of the network. Therefore, it is appropriate to be used in energy-constrained networks such as the RF energy harvesting networks [7]. Relaying cooperation is integrated in some standards and systems for providing different levels of assistance. In [12], PS-based relaying (PSR) protocol and the TS-based relaying (TSR) protocol were investigated to enable information decoding and energy harvesting at the energy-constrained relay in wireless amplify-and-forward (AF) relaying networks. In the PSR protocol, the relay used part of the received signal power for energy harvesting and the remaining signal power for information transmission. In the TSR protocol, the relay spent a portion of time for energy harvesting and the remaining time for information transmission. The SWIPT in an OFDM relaying system was considered in [13], where a source node transmitted energy and information simultaneously to a relay, and then the relay forwards the source information by using the harvested energy to the destination node. However, in [12, 13], some issues need to be further addressed: (a) the network throughput is analyzed separately in terms of power splitting ratio or time switching ratio, and joint optimization in terms of the two parameters is never considered; (b) in the cooperative relaying system, the location of the relay or the distances between nodes are restricted; for example, in [12], the authors assume that the distance between the relay and the destination node is a constant, and, in [13], the relay is located on a line between the source and the destination; (c) most of the prior works assumed that there is no direct link between the source and the destination node in the cooperative relaying system, and thus we could not evaluate whether the performance is improved by exploiting the cooperative relaying concept with energy harvesting.

In this paper, as shown in Figure 1, we consider a three-node cooperative relaying system, where two transmission modes are investigated, that is, (a) the nonrelay mode, where the access-point (AP) directly transmits the information to the user device (UD), no matter when the UD is far away from the AP or not, and (b) the relay-assisted transmission mode, where the AP transmits the information directly to the UD when the UD is relatively nearer to the AP; for the UD located far away from the AP, an energy harvesting relay assists the message transmission from the source to the UD [14]. Time is partitioned into slots. For the relay-assisted transmission mode, a time switching and power splitting (TSPS) protocol for the relaying path is proposed. In each transmission slot, during the first part of the slot, a portion of the signal power in the source is used for energy transfer, and the remaining power is used for information transmission from the source to the relay; for the remaining transmission time, information is transmitted from the relay to the destination. The position of the destination node is assumed to be changed uniformly within a circular area on R^2 around the relay from slot to slot. The main contributions of the paper are summarized as follows. (1) We analyze the performance for cooperative relaying system with a mobile destination, assuming that the position of the destination node uniformly changes from slot to slot. (2) A function describing the relationship between the network performance (i.e., the outage probability and the network throughput) and both the power splitting and the time switching ratios is given. (3) We evaluate and compare the performance for the two transmission modes with different parameters, and the relay-assisted mode considerably improves the reliability of the wireless network.

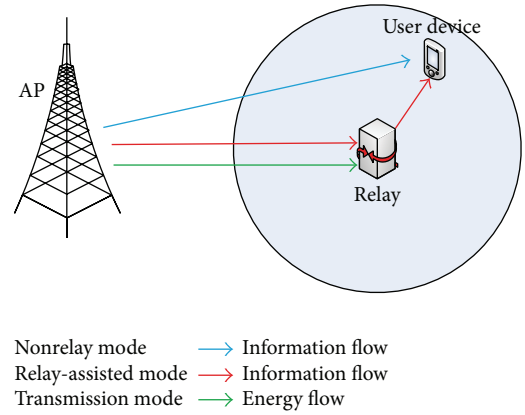

Figure 1: System model for RF energy harvesting-based relay network.

The remainder of this paper is organized as follows. The system model and performance metrics are described in Section 2. Section 3 investigates the network throughput with the relay-assisted transmission mode. The network throughput with nonrelay mode is studied in Section 4. Numerical results are presented in Section 5. Finally, we conclude the paper in Section 6.

Notations. Throughout this paper, we use $E[\cdot]$ and $|\cdot|$ to denote the expectation operator and the absolute value operations, respectively. $X \sim \mathcal{CN}(\mu, \sigma^2)$ stands for a circularly symmetric complex Gaussian random variable X

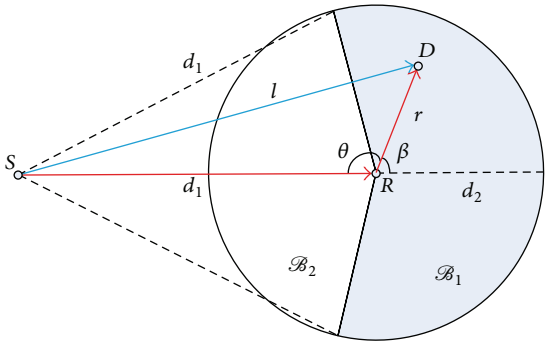

Figure 2: System topology for energy-constrained relay-assisted network.

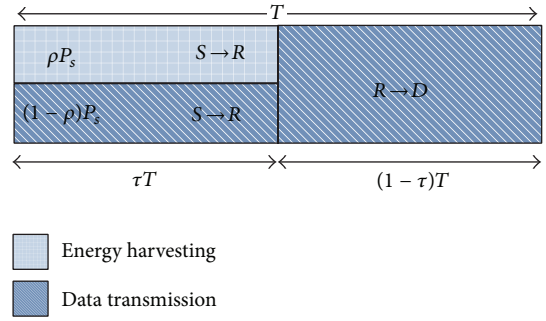

Figure 3: Transmission slot structure for TSPS protocol.

with mean μ and variance σ^2, while $X \sim \exp(\lambda)$ represents an exponentially distributed random variable X with mean λ.

2. System Model

2.1. Network Model. We consider a wireless communication network which consists of one single-antenna AP named source S, one user device named destination node D, and another terminal considered as an energy-constrained relay, denoted by R. As shown in Figure 2, the information is transmitted from S to D, with/without R. It is assumed that the source is continuously connected to a power supply and the transmission power is P_s; the relay has no direct power supply but is embedded with a rechargeable battery and thus could harvest energy from the RF signal broadcasted by the source. In addition, the relay has no traffic and is dedicated to help the source forward the information from source to destination. Furthermore, we assume the relay receives and transmits signals over two different frequency bands.

The propagation channel is modeled as the combination of small-scale Rayleigh fading and large-scale path loss given by

$$h_{XY} = \widetilde{h}_{XY}\sqrt{r_{XY}^{-\alpha}}, \tag{1}$$

where $\widetilde{h}_{XY} \sim \mathcal{CN}(0, \mu_{XY})$ denotes the channel coefficients from X to Y with $X, Y \in \{S, R, D\}$ and $X \neq Y$, the channel power gain $|\widetilde{h}_{XY}|^2$ follows the exponential distribution with the mean μ_{XY}, that is, $|\widetilde{h}_{XY}|^2 \sim \exp(\mu_{XY})$, r_{XY} denotes the propagation distance from X to Y, and $\alpha > 2$ is the path-loss exponent.

Time is partitioned into slots with duration T. During each slot, the channel gains remain constant but are independently and identically distributed (i.i.d.) from one slot to another. The distance between the source and the relay is d_1; that is, $r_{SR} = d_1$. We assume that, within a time slot, the position of the destination node uniformly changes from slot to slot within the transmitting area (available region) of the relay, named $\mathscr{B}$, which denotes a disk centered at R with radius d_2. Therefore, the probability density function (PDF) of the distance from the relay to the destination r_{RD} is given by $f_{r_{RD}}(r) = 2r/d_2^2$.

2.2. Selection Sector Model. The considered network does not require the source to choose the relaying path all the time. Provided that the S-D link is poor and the destination node is far away from the source, the relay can help deliver the source signals to the destination in order to combat fading and path-loss degradation effects. However, when the destination node is relatively nearer to the source, choosing the S-R-D path can not only lead to a waste of resources but also limit the network capacity. Therefore, we define two complementary sectors $\mathscr{B}_1$ and $\mathscr{B}_2$, as shown in Figure 2, which have a significant influence on the network performance.

We define $\theta \triangleq \angle SRD$ as the angle which is formed by the source S, the relay R, and the destination node D. In addition, we use subscript l for r_{SD} and use subscript r for r_{RD}. We define the area $\mathscr{B}_2$ as $\mathscr{B}_2 = \{r \in [0, d_2],\ \theta \in [-\theta_0, \theta_0]\}$, with $\theta_0 = \arccos(d_2/2d_1)$. By using the cosine rule, the source-relay distance is given by $l = \sqrt{d_1^2 + r^2 - 2d_1 r\cos\theta}$.

Then, we define $\beta = \pi - \theta$ as the center angle of the shaded area $\mathscr{B}_1$; the selection region is denoted by $\mathscr{B}_1 = \{r \in [0, d_2],\ \beta \in [-\beta_0, \beta_0]\}$, with $\beta_0 = \pi - \arccos(d_2/2d_1)$. It is worth noting that β_0 is the maximum range of the angle.

The remaining area $\mathscr{B}_2$ is the direct-link area, which means that the relay is ineffective if the destination node D is inside this area.

2.3. Transmission Mode. To analyze the system performance, we consider two transmission modes: (a) the nonrelay mode and (b) the relay-assisted transmission mode, respectively. In mode (a), the source directly transfers the information to the destination, no matter when the destination node is far away from the source or not. However, in mode (b), the source only transmits the information directly to the destination during the whole time when the destination node is relatively nearer to the source than the relay, that is, the destination node located inside the area $\mathscr{B}_2$. When the destination node is located inside the area $\mathscr{B}_1$, the cooperative relaying concept is exploited; a TSPS protocol for the relaying path is proposed; as depicted in Figure 3, in each transmission slot, denoted by T, during the first part of the time τT, where τ is the time switching ratio with $0 < \tau < 1$, a portion of the transmission power, ρP_s, is used for energy transfer from the source to the relay, and the remaining power, $(1-\rho)P_s$, is used for information transmission from the source to the relay, where

ρ is the power splitting ratio $0 < \rho < 1$. The remaining part of the time, $(1-\tau)T$, is used for information transmission from relay to destination.

Note that we assume the circuit power (i.e., the power consumed by the hardware during data transmission) is negligible; therefore, all the energy harvested from the source is consumed by the relay when the information is delivered from the relay to the destination. The values of the time fraction τ and the power fraction ρ, used for wireless information and energy transfer by the relay, have a significant impact on the achievable throughput at the destination.

The notations and symbols used in the paper are listed in Symbol Notation.

2.4. Performance Metric. In this paper, two performance metrics are studied, which are defined as follows.

2.4.1. Outage Probability. The outage probability is defined as the probability that a receiver decodes the received data packets unsuccessfully from its corresponding transmitter. Specifically, given the signal-to-noise ratio (SNR) and a corresponding SNR target, denoted by γ, the outage probability of the network is defined as

$$p_{\text{out}} = \mathbb{P}\left(\text{SNR} < \gamma\right). \tag{2}$$

2.4.2. Network Throughput. The network throughput is the maximum rate that the system can achieve with successful transmissions. Assume that the source transmission rate target is $R_r = \log(1+\gamma)$, and the total transmission time is t. Consequently, the network throughput is given by

$$C = \left(1 - p_{\text{out}}\right) \cdot R_r \cdot t. \tag{3}$$

3. Relay-Assisted Transmission Mode

In this mode, as shown in Figure 2, the transmitting area of the relay $\mathscr{B}$ is split into two parts, the relay selection sector $\mathscr{B}_1$ for the relay path *S*-*R*-*D* and direct-link area $\mathscr{B}_2$ for the path *S*-*D*. In this section, we first derive the outage probability based on the TSPS protocol for the *S*-*R*-*D* link and the direct link *S*-*D*, respectively. Then, we characterize the average network throughput by considering different locations of the destination node.

3.1. Cooperative Link (S-R-D). As shown in Figure 2, the probability that the destination node D is located inside the area $\mathscr{B}_1$ is derived as

$$p_1 = \frac{1}{2\pi}\int_{-\beta_0}^{\beta_0} \mathrm{d}\beta = \frac{\pi - \arccos\left(d_2/2d_1\right)}{\pi}. \tag{4}$$

Note that p_1 increases with d_2 and decreases with d_1.

During the first part of the transmission slot with duration τT, the received signal from the source by the relay, denoted by y_r, is split into two parts by a ratio ρ. The first part $\sqrt{\rho}y_r$ is sent to the energy harvesting receiver, which can collect RF signal directly and transform it into DC power, while the remaining part $\sqrt{1-\rho}y_r$ is sent to the information receiver. We have

$$y_r = \sqrt{P_s}h_{SR} \cdot s(m) + n_a, \tag{5}$$

where $h_{SR} = \widetilde{h}_{SR}\sqrt{d_1^{-\alpha}}$, $s(m)$ is the normalized transmitted signal from the source, $\mathbb{E}\{|s(m)|^2\} = 1$, and n_a is the additive white Gaussian noise (AWGN) caused by the receiving antenna of the relay. Then, the energy harvested by the relay from the source is given by

$$E_h = \eta\rho P_s \left|h_{SR}\right|^2 \tau T, \tag{6}$$

where η $(0 < \eta \le 1)$ denotes the harvesting efficiency.

The information receiver transforms the received RF signal to baseband and accomplishes baseband signal processing, and then the sampled signal, $y_r(m) = \sqrt{1-\rho}y_r$, at the relay is obtained as

$$y_r(m) = \sqrt{(1-\rho)P_s}h_{SR} \cdot s(m) + \sqrt{(1-\rho)}n_a + n_b, \tag{7}$$

where n_b is the AWGN caused by baseband signal processing.

For the remaining part of the time slot, $(1-\tau)T$, the relay will amplify and forward the sampled signal to the destination using the power P_r, which is given by

$$P_r = \frac{E_h}{(1-\tau)T} = \frac{\eta\rho P_s \left|h_{SR}\right|^2 \tau}{(1-\tau)}. \tag{8}$$

The amplification factor is given by [15]

$$\xi = \frac{1}{\sqrt{A}} = \frac{1}{\sqrt{(1-\rho)P_s\left|h_{SR}\right|^2 + (1-\rho)\sigma_a^2 + \sigma_b^2}}, \tag{9}$$

where σ_a^2 and σ_b^2 are the variances of AWGN n_a and n_b, respectively.

After amplifying the signal $y_r(m)$, the transmitted information of the relay is given by

$$\begin{aligned} x_r(m) &= \frac{\sqrt{P_r}y_r(m)}{\sqrt{A}} \\ &= \frac{\sqrt{P_r}y_r(m)}{\sqrt{(1-\rho)P_s\left|h_{SR}\right|^2 + (1-\rho)\sigma_a^2 + \sigma_b^2}}. \end{aligned} \tag{10}$$

Therefore, the received signal at the destination node, $y_d(m)$, is obtained as

$$y_d(m) = h_{RD} \cdot x_r(m) + n_c, \tag{11}$$

where $h_{RD} = \widetilde{h}_{RD}\sqrt{r^{-\alpha}}$, n_c is the overall AWGN at the destination node, and σ_c^2 is the variance of AWGN n_c. Substituting (7) and (10) into (11), we can get

$$\begin{aligned} y_d(m) &= \frac{h_{RD}\sqrt{(1-\rho)P_sP_r}h_{SR}s(m)}{\sqrt{(1-\rho)P_s|h_{SR}|^2 + (1-\rho)\sigma_a^2 + \sigma_b^2}} \\ &\quad + \frac{h_{RD}\sqrt{(1-\rho)P_r}n_a + h_{RD}\sqrt{P_r}n_b}{\sqrt{(1-\rho)P_s|h_{SR}|^2 + (1-\rho)\sigma_a^2 + \sigma_b^2}} + n_c \\ &= \frac{h_{RD}\sqrt{(1-\rho)P_sP_r}h_{SR}s(m)}{\sqrt{(1-\rho)P_s|h_{SR}|^2 + \sigma_1^2}} \\ &\quad + \frac{h_{RD}\sqrt{P_r}n_1}{\sqrt{(1-\rho)P_s|h_{SR}|^2 + \sigma_1^2}} + n_c, \end{aligned} \tag{12}$$

where we assume $n_1 = \sqrt{1-\rho}\cdot n_a + n_b$ is the total AWGN at the relay and $\sigma_1^2 = (1-\rho)\cdot\sigma_a^2 + \sigma_b^2$. The first part of (12) is the signal part, and the second and the third part are the noise part. Therefore, the SNR of the *S-R-D* path at the destination node is obtained as

$$\begin{aligned} \gamma_{SRD} &= \frac{|h_{RD}|^2(1-\rho)P_sP_r|h_{SR}|^2 / \left((1-\rho)P_s|h_{SR}|^2 + \sigma_1^2\right)}{|h_{RD}|^2 P_r\sigma_1^2 / \left((1-\rho)P_s|h_{SR}|^2 + \sigma_1^2\right) + \sigma_c^2} \\ &= \frac{|h_{RD}|^2(1-\rho)P_sP_r|h_{SR}|^2}{|h_{RD}|^2 P_r\sigma_1^2 + (1-\rho)P_s|h_{SR}|^2\sigma_c^2 + \sigma_1^2\sigma_c^2}. \end{aligned} \tag{13}$$

Substituting (8) into (13), we have

$$\gamma_{SRD} = \frac{|h_{RD}|^2(1-\rho)P_s^2|h_{SR}|^4\eta\rho(\tau/(1-\tau))}{|h_{RD}|^2|h_{SR}|^2\eta\rho P_s\sigma_1^2(\tau/(1-\tau)) + (1-\rho)P_s|h_{SR}|^2\sigma_c^2 + \sigma_1^2\sigma_c^2}. \tag{14}$$

From (2), the probability that the destination decodes the received data packets unsuccessfully, that is, the outage probability, is given by

$$p_{\text{out\_1}} = \mathbb{P}(\gamma_{SRD} < \gamma). \tag{15}$$

Then, we have the following theorem.

Theorem 1. *The outage probability p_{out_1} for S-R-D link with TSPS protocol is obtained as*

$$\begin{aligned} p_{out\_1} = \int_0^{d_2} &\left(1 - e^{-\Psi/\Omega\cdot\mu_{SR}}\sqrt{\frac{4\Lambda r^\alpha}{\Omega\cdot\mu_{SR}\mu_{RD}}}K_1\left(\sqrt{\frac{4\Lambda r^\alpha}{\Omega\cdot\mu_{SR}\mu_{RD}}}\right)\right) \\ &\cdot\frac{2r}{d_2^2}\mathrm{d}r, \end{aligned} \tag{16}$$

where $\Lambda = (1-\rho)P_s\sigma_c^2\gamma$, $\Omega = d_1^{-\alpha}P_s^2\rho(1-\rho)\eta(\tau/(1-\tau))$, and $\Psi = P_s\eta\rho\sigma_1^2\gamma(\tau/(1-\tau))$. μ_{SR} and μ_{RD} are the mean value of the exponential distributions $|\widetilde{h}_{SR}|^2$ and $|\widetilde{h}_{RD}|^2$, respectively. $K_1(\cdot)$ denotes the first-order modified Bessel function of the second kind [16].

Proof. We derive the outage probability $p_{\text{out\_1}}$ by substituting (14) into (15), and $p_{\text{out\_1}}$ is given by

$$\begin{aligned} p_{\text{out\_1}} &= \mathbb{P}\left(\frac{|h_{RD}|^2(1-\rho)P_s^2|h_{SR}|^4\eta\rho(\tau/(1-\tau))}{|h_{RD}|^2|h_{SR}|^2\eta\rho P_s\sigma_1^2(\tau/(1-\tau)) + (1-\rho)P_s|h_{SR}|^2\sigma_c^2 + \sigma_1^2\sigma_c^2} < \gamma\right) \\ &= \mathbb{P}\left(|h_{RD}|^2 < \frac{(1-\rho)P_s|h_{SR}|^2\sigma_c^2\gamma + \sigma_1^2\sigma_c^2\gamma}{\left||h_{SR}|^4P_s^2\rho(1-\rho)\eta(\tau/(1-\tau)) - |h_{SR}|^2P_s\eta\rho\sigma_1^2\gamma(\tau/(1-\tau))\right|}\right) \\ &\overset{(a)}{=} \mathbb{P}\left(\left|\widetilde{h}_{RD}\right|^2 < \frac{(1-\rho)P_s\left|\widetilde{h}_{SR}\right|^2 r^\alpha\sigma_c^2\gamma + \sigma_1^2\sigma_c^2\gamma r^\alpha d_1^\alpha}{\left|\left|\widetilde{h}_{SR}\right|^4 d_1^{-\alpha}P_s^2\rho(1-\rho)\eta(\tau/(1-\tau)) - \left|\widetilde{h}_{SR}\right|^2P_s\eta\rho\sigma_1^2\gamma(\tau/(1-\tau))\right|}\right) \\ &\overset{(b)}{=} \mathbb{P}\left(\left|\widetilde{h}_{RD}\right|^2 < \frac{\Lambda r^\alpha\left|\widetilde{h}_{SR}\right|^2 + \Gamma}{\left|\Omega\left|\widetilde{h}_{SR}\right|^4 - \Psi\left|\widetilde{h}_{SR}\right|^2\right|}\right), \end{aligned} \tag{17}$$

where (a) follows from $h_{SR} = \widetilde{h}_{SR}\sqrt{d_1^{-\alpha}}$ and $h_{RD} = \widetilde{h}_{RD}\sqrt{r^{-\alpha}}$ and (b) follows from $\Lambda = (1-\rho)P_s\sigma_c^2\gamma$, $\Gamma = \sigma_1^2\sigma_c^2\gamma r^\alpha d_1^\alpha$, $\Omega = d_1^{-\alpha}P_s^2\rho(1-\rho)\eta(\tau/(1-\tau))$, and $\Psi = P_s\eta\rho\sigma_1^2\gamma(\tau/(1-\tau))$. For simplicity, we consider a high SNR case; the factor $\sigma_1^2\sigma_c^2$ in

the denominator of (14) is approximately 0, such that $\Gamma \approx 0$. Then, we have

$$p_{\text{out\_1}} \approx \mathbb{P}\left(\left|\widetilde{h}_{RD}\right|^2 < \frac{\Lambda r^{\alpha}\left|\widetilde{h}_{SR}\right|^2}{\left|\Omega\left|\widetilde{h}_{SR}\right|^4 - \Psi\left|\widetilde{h}_{SR}\right|^2\right|}\right)$$
$$= \begin{cases} \mathbb{P}\left(\left|\widetilde{h}_{RD}\right|^2 < \dfrac{\Lambda r^{\alpha}\left|\widetilde{h}_{SR}\right|^2}{\Omega\left|\widetilde{h}_{SR}\right|^4 - \Psi\left|\widetilde{h}h_{SR}\right|^2}\right), & \left|\widetilde{h}_{SR}\right|^2 > \dfrac{\Psi}{\Omega} \\ \mathbb{P}\left(\left|\widetilde{h}_{RD}\right|^2 > \dfrac{\Lambda r^{\alpha}\left|\widetilde{h}_{SR}\right|^2}{\Omega\left|\widetilde{h}_{SR}\right|^4 - \Psi\left|\widetilde{h}_{SR}\right|^2}\right) = 1, & \left|\widetilde{h}_{SR}\right|^2 < \dfrac{\Psi}{\Omega}. \end{cases} \quad (18)$$

It is worth noting that we have mentioned that $|\widetilde{h}_{XY}|^2 \sim \exp(\mu_{XY})$; the PDF of the exponential variables $|\widetilde{h}_{SR}|^2$ and $|\widetilde{h}_{RD}|^2$ are $f_{|\widetilde{h}_{SR}|^2}(z) = (1/\mu_{SR})e^{-z/\mu_{SR}}$ and $f_{|\widetilde{h}_{RD}|^2}(z) = (1/\mu_{RD})e^{-z/\mu_{RD}}$, respectively. Thus, $p_{\text{out\_1}}$ is approximately given by

$$\begin{aligned} p_{\text{out\_1}} &= E_r\left[E_{|\widetilde{h}_{SR}|^2}\left[1 - e^{-\Lambda r^{\alpha}|\widetilde{h}_{SR}|^2/|\Omega|\widetilde{h}_{SR}|^4 - \Psi|\widetilde{h}_{SR}|^2|\cdot 1/\mu_{RD}}\right]\right] \\ &= E_r\left[\int_0^{\Psi/\Omega}\left(\frac{1}{\mu_{SR}}e^{-z/\mu_{SR}}\right)\cdot 1\,\mathrm{d}z\right] \\ &\quad + E_r\left[\int_{\Psi/\Omega}^{\infty}\left(\frac{1}{\mu_{SR}}e^{-z/\mu_{SR}}\right)\right. \\ &\quad \left.\cdot\left(1 - e^{-(1/\mu_{RD})(\Lambda r^{\alpha}z/(\Omega z^2 - \Psi z))}\right)\mathrm{d}z\right] \\ &\overset{(a)}{=} \int_0^{d_2}\int_{\Psi/\Omega}^{\infty}\left(1 - \frac{1}{\mu_{SR}}e^{-(z/\mu_{SR} + \Lambda r^{\alpha}z/(\Omega z^2 - \Psi z)\cdot 1/\mu_{RD})}\right) \\ &\quad \cdot f(r)\,\mathrm{d}z\,\mathrm{d}r \\ &\overset{(b)}{=} \int_0^{d_2}\int_{\Psi/\Omega}^{\infty}\left(1 - \frac{1}{\mu_{SR}}e^{-(z/\mu_{SR} + \Lambda r^{\alpha}/(\Omega z - \Psi)\cdot 1/\mu_{RD})}\right) \\ &\quad \cdot \frac{2r}{d_2^2}\mathrm{d}z\,\mathrm{d}r \overset{(c)}{=} \int_0^{d_2}\left(1\right. \\ &\quad \left. - e^{-\Psi/\Omega\mu_{SR}}\sqrt{\frac{4\Lambda r^{\alpha}}{\Omega\mu_{SR}\mu_{RD}}}K_1\left(\sqrt{\frac{4\Lambda r^{\alpha}}{\Omega\mu_{SR}\mu_{RD}}}\right)\right)\frac{2r}{d_2^2}\mathrm{d}r, \end{aligned} \quad (19)$$

where (a) follows from $0 < r \le d_2$, (b) follows from the notion that the PDF of the distance from the relay to the destination is $f(r) = 2r/d_2^2$, and (c) is obtained by the formula $\int_0^{\infty} e^{-\beta/4x - \gamma x}\mathrm{d}x = \sqrt{\beta/\gamma}K_1(\sqrt{\beta\gamma})$ [16]. This ends the proof for Theorem 1. □

3.2. Direct Link (S-D). As shown in Figure 2, consider the case where the destination node D is located in $\mathscr{B}_2$, which is the complementary sector of $\mathscr{B}_1$. We have mentioned in Section 2.2 that $l^2 = d_1^2 + r^2 - 2d_1 r\cos\theta$; we have $\mathscr{B}_2 = \{r \in [0, d_2],\ \theta \in [-\theta_0, \theta_0]\}$, with $\theta_0 = \arccos(d_2/2d_1)$. Thus, the probability that the destination node is located inside the area $\mathscr{B}_2$ is derived as

$$p_2 = \frac{1}{2\pi}\int_{-\theta_0}^{\theta_0}\mathrm{d}\theta = \frac{\arccos(d_2/2d_1)}{\pi}. \quad (20)$$

Note that p_2 decreases with d_2 and increases with d_1.

In this case, the source transmits towards the destination node directly, and thus the communication is performed within an overall time slot. Therefore, the received signal at the destination node, $y_d(t)$, is obtained as

$$y_d(t) = \sqrt{P_s}h_{SD}\cdot s(t) + n_3, \quad (21)$$

where $h_{SD} = \widetilde{h}_{SD}\sqrt{l^{-\alpha}}$, n_3 is the AWGN at the destination node, σ_3^2 is the variance of AWGN n_3, and $s(t)$ is normalized transmitted signal from the source. Therefore, the SNR of the *S-D* path at the destination node is obtained as

$$\gamma_{SD} = \frac{P_s\left|\widetilde{h}_{SD}\right|^2 l^{-\alpha}}{\sigma_3^2}. \quad (22)$$

From (2), the probability that the destination decodes the received data packets unsuccessfully, that is, the outage probability $p_{\text{out\_2}}$, is

$$p_{\text{out\_2}} = \mathbb{P}(\gamma_{SD} < \gamma). \quad (23)$$

Then, we have the following theorem.

Theorem 2. *The outage probability p_{out_2} for the direct link at the destination node is obtained as*

$$p_{out\_2} = \int_{-\arccos[d_2/2d_1]}^{\arccos[d_2/2d_1]}\int_0^{d_2}\frac{r}{\pi d_2^2}\frac{\sigma_3^2\gamma\left(d_1^2 + r^2 - 2d_1 r\cos[\theta]\right)^{\alpha/2}}{P_s\mu_{SD}}\mathrm{d}r\,\mathrm{d}\theta. \quad (24)$$

Proof. Using (22) in (23), $p_{\text{out\_2}}$ is given by

$$\begin{aligned} p_{\text{out\_2}} &= \mathbb{P}\left(\frac{P_s\left|\widetilde{h}_{SD}\right|^2 l^{-\alpha}}{\sigma_3^2} < \gamma\right) \\ &= \mathbb{P}\left(\left|\widetilde{h}_{SD}\right|^2 < \frac{\sigma_3^2\gamma l^{\alpha}}{P_s}\right) \\ &\overset{(a)}{=} E_{\mathscr{B}_2}\left[1 - e^{-\sigma_3^2\gamma l^{\alpha}/P_s\mu_{SD}}\right], \end{aligned} \quad (25)$$

where (a) follows from the notion that the PDF of the exponential variable $|\widetilde{h}_{SD}|^2$ is $f_{|\widetilde{h}_{SD}|^2}(z) = (1/\mu_{SD})e^{-z/\mu_{SD}}$.

Due to the fact that $l^2 = d_1^2 + r^2 - 2d_1 r\cos\theta$ and $\mathscr{B}_2 = \{r \in [0, d_2],\ \theta \in [-\theta_0, \theta_0]\}$, with $\theta_0 = \arccos(d_2/2d_1)$, thus, we have

$$\begin{aligned} p_{\text{out\_2}} &= \int_{-\theta_0}^{\theta_0}\int_0^{d_2}\frac{1}{2\pi}\left(1 - e^{-\sigma_3^2\gamma(d_1^2 + r^2 - 2d_1 r\cos(\theta))^{\alpha/2}/P_s\mu_{SD}}\right) \\ &\quad \cdot f(r)\,\mathrm{d}r\,\mathrm{d}\theta. \end{aligned} \quad (26)$$

For high SNR, we assume $\sigma_3^2 \approx 0$. From the Taylor series $e^x \approx 1 + x$, the outage probability $p_{\text{out\_2}}$ can be approximately written as

$$p_{\text{out\_2}} = \int_{-\theta_0}^{\theta_0} \int_0^{d_2} \frac{1}{2\pi} \cdot \frac{\sigma_3^2 \gamma \left(d_1^2 + r^2 - 2d_1 r \cos(\theta)\right)^{\alpha/2}}{P_s \mu_{SD}} \frac{2r}{d_2^2} \mathrm{d}r \, \mathrm{d}\theta. \tag{27}$$

This completes the proof for Theorem 2. □

3.3. Throughput Analysis. For the different locations of the destination node, we have analyzed two conditions for the relay-assisted transmission mode, *S-R-D* by using the TSPS protocol and direct link *S-D*, and obtained the outage probabilities $p_{\text{out\_1}}$ and $p_{\text{out\_2}}$, respectively. The throughput is characterized by evaluating the outage probability at a source transmission rate target, which is defined as $R_r = \log(1 + \gamma)$. From (3), we denote the throughput with TSPS protocol at the destination node by C_a; we have

$$C_a = R_r \cdot \left(1 - p_{\text{out\_1}}\right)(1 - \tau) T. \tag{28}$$

It is worth noting that, for $\tau \to 0$ or $\rho \to 0$, there is less time or less power available for energy harvesting. Consequently, the energy harvested by the relay is smaller and less throughput is obtained due to larger outage probability. On the other hand, for the value of $\tau \to 1$ or $\rho \to 1$, there is less time for information transmission or less power portion for data transmission. Furthermore, larger ρ results in poor signal strength at the relay, and when the relay amplifies the noise signal and forwards it to the destination node, small throughput occurs due to larger outage probability and less transmission time. Therefore, there is a tradeoff between energy harvesting and data transmission, and there exist optimal τ and ρ which yields the maximum network throughput C_a.

The throughput for the *S-D* link denoted by C_b is obtained by

$$C_b = R_r \left(1 - p_{\text{out\_2}}\right) T. \tag{29}$$

Therefore, the throughput for the relay-assisted transmission mode C_1, at the destination node, is obtained by

$$\begin{aligned} C_1 &= C_a \cdot p_1 + C_b \cdot p_2 \\ &= R_r \cdot \left(1 - p_{\text{out\_1}}\right)(1 - \tau) T \cdot p_1 \\ &\quad + R_r \left(1 - p_{\text{out\_2}}\right) T \cdot p_2, \end{aligned} \tag{30}$$

where p_1 and p_2 are given by (4) and (20), respectively. It is worth highlighting that C_b is a constant for different τ and ρ; consequently, the optimal value of C_1 mainly depends on C_a.

It seems intractable to evaluate the closed-form expressions for the optimal value of C_1. However, the optimization can be done offline by numerical calculation of the optimal values of ρ^* and τ^* for the given system parameters.

4. Nonrelay Mode

In this section, we will characterize the outage probability and the network throughput for the link from source to the destination. As shown in Figure 2, consider the case where the destination node D is located inside the area $\mathscr{B}$, and the communication is performed in an overall time slot. Similar to that in Section 3.2, the SNR of the nonrelay mode at the destination node can be obtained as

$$\gamma_{SD} = \frac{P_s \left|\widetilde{h}_{SD}\right|^2 l^{-\alpha}}{\sigma_4^2}, \tag{31}$$

where σ_4^2 is the variance of the overall AWGN at the destination node. From (2), the probability that the destination node decodes the received data packets unsuccessfully, that is, the outage probability $p_{\text{out\_3}}$, is

$$p_{\text{out\_3}} = \mathbb{P}\left(\gamma_{SD} < \gamma\right). \tag{32}$$

Then, we have the following theorem.

Theorem 3. *The outage probability p_{out_3} for the nonrelay mode at the destination node is obtained as*

$$p_{out\_3} = \int_{-\pi}^{\pi} \int_0^{d_2} \frac{\sigma_4^2 \gamma \left(d_1^2 + r^2 - 2d_1 r \cos(\delta)\right)^{\alpha/2}}{P_s \mu_{SD}} \frac{r}{\pi d_2^2} \mathrm{d}r \, \mathrm{d}\delta. \tag{33}$$

Proof. Substituting (31) into (32), $p_{\text{out\_3}}$ is given by

$$\begin{aligned} p_{\text{out\_3}} &= \mathbb{P}\left(\frac{P_s \left|\widetilde{h}_{SD}\right|^2 l^{-\alpha}}{\sigma_4^2} < \gamma\right) \\ &= E_{\mathscr{B}}\left[1 - e^{-\sigma_4^2 \gamma l^{\alpha} / P_s \mu_{SD}}\right]. \end{aligned} \tag{34}$$

From Section 2.2, we get that $\mathscr{B} = \{r \in [0, d_2], \delta \in [-\pi, \pi]\}$. Thus, we have

$$\begin{aligned} p_{\text{out\_3}} &= \int_{-\pi}^{\pi} \int_0^{d_2} \left(1 - e^{-\sigma_4^2 \gamma (d_1^2 + r^2 - 2d_1 r \cos(\delta))^{\alpha/2} / P_s \mu_{SD}}\right) \frac{1}{2\pi} \\ &\quad \cdot f(r) \, \mathrm{d}r \, \mathrm{d}\delta. \end{aligned} \tag{35}$$

Similarly, from the Taylor series $e^x \approx 1 + x$, the outage probability $p_{\text{out\_3}}$ can be approximately written as

$$p_{\text{out\_3}} = \int_{-\pi}^{\pi} \int_0^{d_2} \frac{\sigma_4^2 \gamma \left(d_1^2 + r^2 - 2d_1 r \cos(\delta)\right)^{\alpha/2}}{P_s \mu_{SD}} \frac{1}{2\pi} \cdot \frac{2r}{d_2^2} \mathrm{d}r \, \mathrm{d}\delta. \tag{36}$$

This completes the proof for Theorem 3. □

The throughput C_2 at the destination node in the nonrelay transmission mode is obtained by

$$C_2 = R_r \cdot \left(1 - p_{\text{out\_3}}\right) T. \tag{37}$$

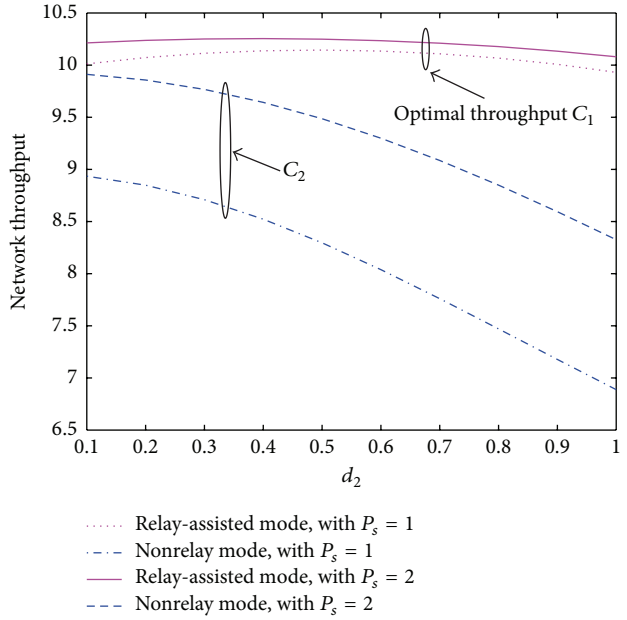

FIGURE 4: The network throughput C of the two transmission modes versus the transmission rate target R_r, with $\sigma_1^2 = 0.01$ and $\sigma_c^2 = 0.001$.

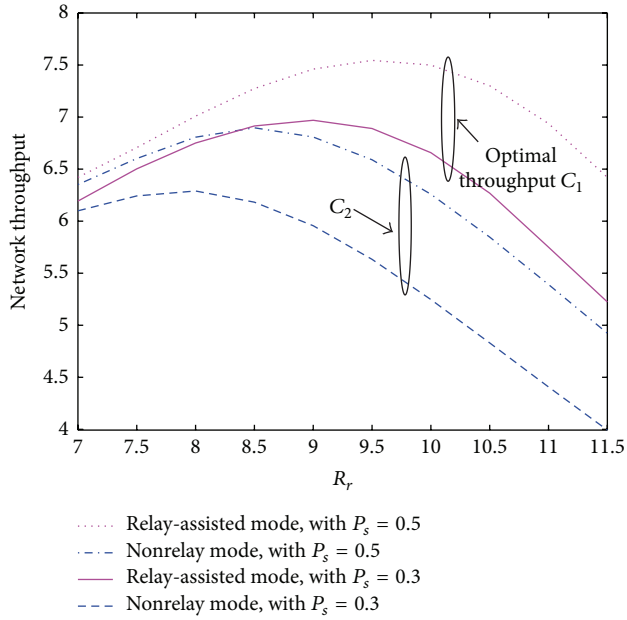

FIGURE 5: The network throughput C of the two transmission modes versus the radius of selection sector d_2, with $\sigma_1^2 = \sigma_c^2 = 0.001$.

5. Numerical Results

In this section, based on our theoretical analysis, we present some numerical results and give some interpretations. First of all, we compare the optimal throughput in relay-assisted transmission mode with that in nonrelay mode. By using the TSPS protocol, we characterize the optimal values C_1 of the network throughput in relay-assisted mode, the optimal values of the time switching ratio τ, and the power splitting ratio ρ for different parameters, respectively.

Unless otherwise specified, we set the path-loss exponent as $\alpha = 4$, which corresponds to a city cellular network environment. Transmission time slot is normalized to $T = 1$; the energy harvesting efficiency $\eta = 1$; the source transmission power $P_s = 1$ W; the source transmission rate target $R_r = 11$ bits/s/Hz; the distance between the source node and the relay and the radius of the selection sector are both normalized to $d_1 = d_2 = 1$; and the mean value of the channel power gain $\mu_{SR} = \mu_{RD} = \mu_{SD} = 1$.

5.1. Comparison between the Relay-Assisted Transmission Mode and the Nonrelay Mode. Figure 4 shows the optimal throughput in the relay-assisted transmission mode and the network throughput in the nonrelay mode for different values of the transmission rate target R_r. We have the following observations. First of all, the optimal throughput C_1 in the relay-assisted transmission mode renders larger values of throughput compared to the throughput in the nonrelay mode C_2, as much as 30.8%, when the rate target is 11.5 at $P_s = 0.3$. Moreover, the network throughput first increases as R_r increases but starts to decrease when the rate target is above a certain threshold. This is due to the fact that, for smaller R_r, the network throughput mainly depends on the rate target R_r, and the throughput increases as R_r increases. However, when R_r increases above a certain value, the destination node fails to decode the signal correctly, which results in a larger outage probability, and thus the throughput decreases. Furthermore, it is observed that the throughput increases with increasing P_s; the reason is that large source transmission power P_s is beneficial to reducing the network outage probability and thus enhances the network throughput.

Figure 5 shows the optimal throughput in the relay-assisted transmission mode and the network throughput in the nonrelay mode for different values of the radius of selection sector d_2. Similar to Figure 4, the optimal throughput in the relay-assisted transmission mode, C_1, renders larger values of throughput compared to the throughput in the nonrelay mode, C_2, as much as 44.2%, when $d_2 = 1$ at $P_s = 1$, and the throughput increases with increasing P_s. Moreover, the throughput in the nonrelay mode C_2 decreases as d_2 increases due to the fact that the path loss increases with increasing d_2 and thus results in a large outage probability $p_{\text{out\_3}}$ (see (37)). However, the optimal throughput in the relay-assisted transmission mode C_1 is not monotonously changed with d_2; this is because d_2 mainly affects the throughput in relay-assisted transmission mode with TSPS protocol (see the first portion of (30)). On the one hand, small d_2 leads to a small path loss, which imposes a small outage probability $p_{\text{out\_1}}$, and thus results in large throughput C_a (see (28)), but the probability p_1 from (4) is decreased. On the other hand, for large values of d_2, the throughput C_a degrades since the outage probability $p_{\text{out\_1}}$ increases, but the probability p_1 is increased. Therefore, there exists an optimal d_2 which yields the maximum throughput in the relay-assisted transmission mode C_1. In Figure 5, the optimal d_2 is 0.4 and 0.5, with $P_s = 2$ and $P_s = 1$, respectively.

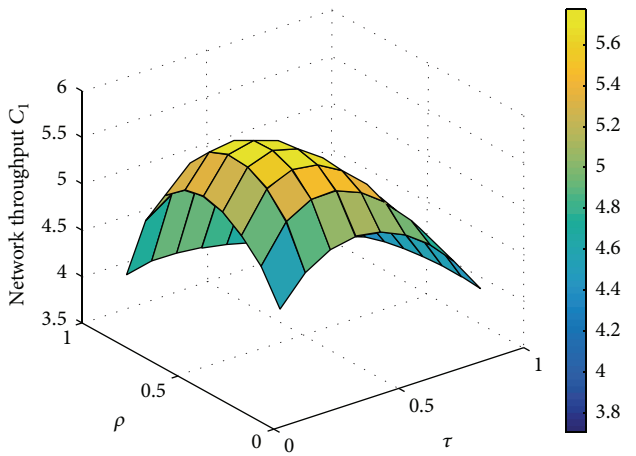

FIGURE 6: The network throughput C_1 with different settings of the time switching ratio τ and the power splitting ratio ρ in the relay-assisted mode, with $\sigma_1^2 = \sigma_c^2 = 0.01$.

5.2. Optimization with the Relay-Assisted Transmission Mode. Figure 6 demonstrates how the time switching ratio τ and the power splitting ratio ρ would affect the network throughput C_1. As observed, the maximum C_1 can be obtained as $C_1 = 5.7752$ with $\tau = 0.3$ and $\rho = 0.4$. This is because, for small values of τ or ρ, there is less time and there is less power available for energy harvesting. Consequently, the energy harvested by the relay is smaller and less throughput is obtained due to larger outage probability. On the other hand, for the value of τ or ρ larger than the optimal values, there is less time for information transmission and there is less power portion for data transmission. Moreover, larger ρ results in poor signal strength at the relay, and when the relay amplifies and transmits the noise signal to the destination node, small throughput occurs due to larger outage probability at the destination node. Our results can be used to find the feasible region in the τ-ρ plane for given allowable throughput. Figure 7 demonstrates the network throughput for TSPS protocol with $0 < \rho < 1$. We see that the simulation results are consistent with our analytical results for the different values of ρ and τ, which verifies the analytical expression for the network throughput.

Figure 8 shows the optimal throughput C_1 with relay-assisted transmission protocol as well as the TSR and the PSR protocols for different values of energy harvesting efficiency η. It is observed that the optimal throughput C_1 is in proportion to energy harvesting efficiency η. Furthermore, the TSPS protocol outperforms the TSR and the PSR protocols in terms of throughput, as much as 5.9% and 28%, respectively, when the energy harvesting efficiency = 1. Figure 9 plots the optimal throughput C_1 with relay-assisted transmission protocol as well as the TSR and the PSR protocols for different values of the noise variance for the R-D link σ_c^2. It is observed that the optimal throughput C_1 is inversely proportional to the noise variance for the R-D link σ_c^2. Similarly, the TSPS protocol outperforms the TSR and the PSR protocols in terms of throughput, as much as 7.3% and 28%, respectively, when the noise variance for the R-D link $\sigma_c^2 = 10^{-3}$. We can see

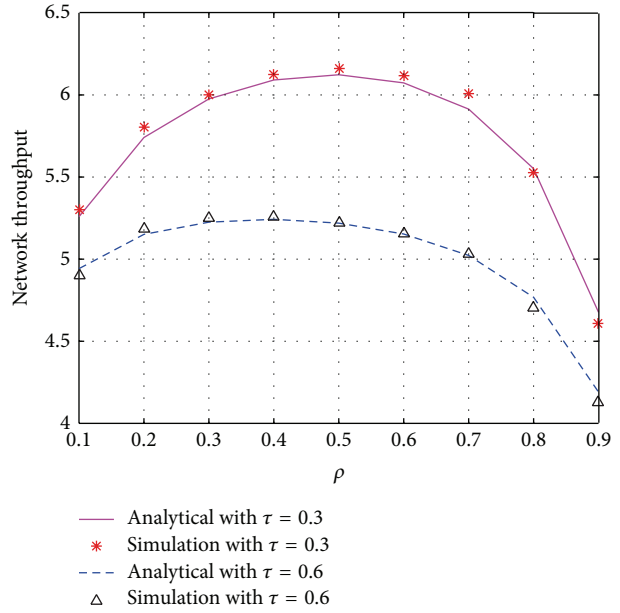

FIGURE 7: The network throughput C_1 with different settings of the power splitting ratio ρ in the relay-assisted mode.

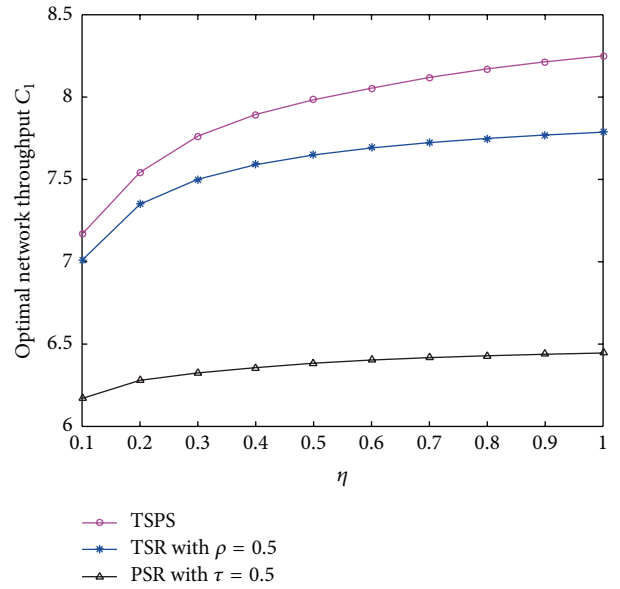

FIGURE 8: The optimal network throughput C_1 with relay-assisted transmission mode versus the energy harvesting efficiency η, with $\sigma_1^2 = 0.01$ and $\sigma_c^2 = 0.001$.

that joint optimization of both ρ and τ improves the network throughput significantly.

In Figure 10, we characterized the optimal values of τ and ρ for the TSPS protocol for different values of the noise variance for the R-D link σ_c^2. It can be observed from Figure 10 that the optimal value of τ or ρ increases by increasing σ_c^2, and the optimal values of τ and ρ jointly maximize the network throughput as shown in Figure 9 with TSPS protocol.

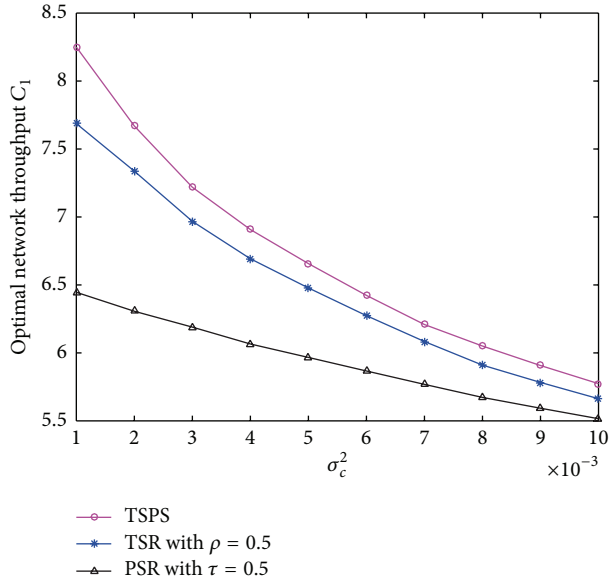

FIGURE 9: The optimal network throughput C_1 with relay-assisted transmission mode versus the noise variance for the R-D link σ_c^2, with $\sigma_1^2 = 0.01$.

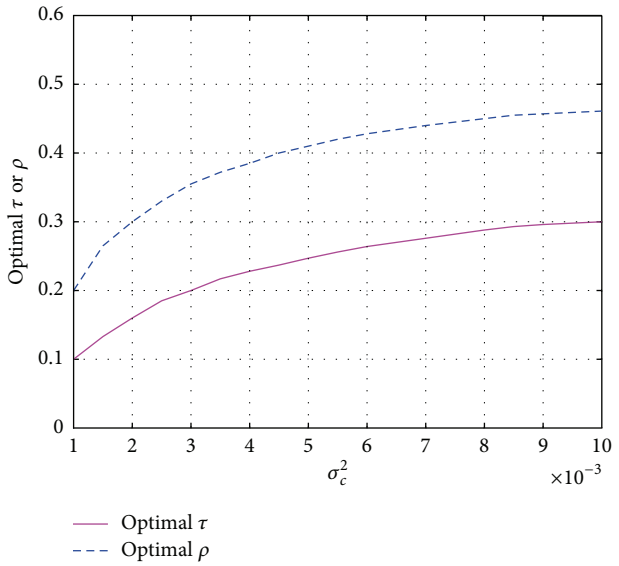

FIGURE 10: The optimal time switching ratio τ and power splitting ratio ρ versus the noise variance for the R-D link σ_c^2, with $\sigma_1^2 = 0.01$.

6. Conclusion

In this paper, we investigated two transmission modes: the relay-assisted transmission mode and the nonrelay mode, respectively. In the relay-assisted transmission mode, we proposed a TSPS protocol in a cooperative relaying system to improve network performance in terms of efficiency and reliability. During the first amount of the time slot, a portion of the received signal power is used for energy harvesting by the relay, and the remaining power is used for information transmission from the source to the relay, while the remaining part of the time is used for information transfer from the relay to the destination. The outage probability and the network throughput are characterized, by using the two transmission modes, respectively. With the TSPS protocol, the network throughput is maximized by joint optimization of the power splitting and time switching ratios. In particular, theoretical analysis shows that the optimal throughput in the relay-assisted transmission mode achieves larger values of throughput compared to the throughput in the nonrelay mode as much as 44.2%.

Symbol Notation

γ: The signal-to-noise (SNR) target
R_r: The transmission rate target
τ: Time switching ratio
ρ: Power splitting ratio
P_s: Transmission power of the source
h: Rayleigh fading gain
p_{out}: Outage probability of the network
C: Network throughput
d_1: The fixed distance between the source and the relay
d_2: The radius of the available region of the relay
$\mathscr{B}_1$: Selection sector of the relaying path
l: The distance between the source and the destination node
r: The distance between the relay and the destination node
η: Energy harvesting efficiency
α: Path-loss exponent
T: One transmission slot time
σ_1^2: The variance of the additive white Gaussian noise (AWGN) over the S-R link
σ_c^2: The variance of the AWGN over the R-D link.

Competing Interests

The authors declare that they have no competing interests.

Acknowledgments

This work was supported in part by the National Science and Technology Major Project under Grant 2015ZX03003012-005, the NSFC under Grant 61271257, and the National Research Foundation for the Doctoral Program of Higher Education of China under Grant 20120005110007.

References

[1] H. Chen, Y. Li, J. L. Rebelatto, B. F. Uchôa-Filho, and B. Vucetic, "Harvest-then-cooperate: wireless-powered cooperative communications," *IEEE Transactions on Signal Processing*, vol. 63, no. 7, pp. 1700–1711, 2015.

[2] H. Li, J. Xu, R. Zhang, and S. Cui, "A general utility optimization framework for energy-harvesting-based wireless communications," *IEEE Communications Magazine*, vol. 53, no. 4, pp. 79–85, 2015.

[3] A. Sinha and A. Chandrakasan, "Dynamic power management in wireless sensor networks," *IEEE Design and Test of Computers*, vol. 18, no. 2, pp. 62–74, 2001.

[4] D. Bouchouicha, F. Dupont, M. Latrach, and L. Ventura, "Ambient RF energy harvesting," in *Proceedings of the International Conference on Renewable Energies and Power Quality (ICREPQ '10)*, Granada, Spain, March 2010.

[5] A. M. Zungeru, L.-M. Ang, S. R. S. Prabaharan, and K. P. Seng, "Radio frequency energy harvesting and management for wireless sensor networks," in *Green Mobile Devices and Networks: Energy Optimization and Scavenging Techniques*, H. Venkataraman and G.-M. Muntean, Eds., chapter 13, pp. 341–368, CRC Press, New York, NY, USA, 2012.

[6] S. Lee, R. Zhang, and K. Huang, "Opportunistic wireless energy harvesting in cognitive radio networks," *IEEE Transactions on Wireless Communications*, vol. 12, no. 9, pp. 4788–4799, 2013.

[7] X. Lu, P. Wang, D. Niyato, D. I. Kim, and Z. Han, "Wireless networks with rf energy harvesting: a contemporary survey," *IEEE Communications Surveys and Tutorials*, vol. 17, no. 2, pp. 757–789, 2015.

[8] L. R. Varshney, "Transporting information and energy simultaneously," in *Proceedings of the IEEE International Symposium on Information Theory (ISIT '08)*, pp. 1612–1616, Toronto, Canada, July 2008.

[9] X. Zhou, R. Zhang, and C. K. Ho, "Wireless information and power transfer: architecture design and rate-energy tradeoff," *IEEE Transactions on Communications*, vol. 61, no. 11, pp. 4754–4767, 2013.

[10] L. Liu, R. Zhang, and K.-C. Chua, "Wireless information transfer with opportunistic energy harvesting," *IEEE Transactions on Wireless Communications*, vol. 12, no. 1, pp. 288–300, 2013.

[11] D. W. K. Ng, E. S. Lo, and R. Schober, "Wireless information and power transfer: energy efficiency optimization in OFDMA systems," *IEEE Transactions on Wireless Communications*, vol. 12, no. 12, pp. 6352–6370, 2013.

[12] A. A. Nasir, X. Zhou, S. Durrani, and R. A. Kennedy, "Relaying protocols for wireless energy harvesting and information processing," *IEEE Transactions on Wireless Communications*, vol. 12, no. 7, pp. 3622–3636, 2013.

[13] Y. Liu and X. Wang, "Information and energy cooperation in OFDM relaying," in *Proceedings of the IEEE ICC*, London, UK, June 2015.

[14] M. O. Hasna and M.-S. Alouini, "Performance analysis of two-hop relayed transmissions over Rayleigh fading channels," in *Proceedings of the IEEE 56th Vehicular Technology Conference (VTC-Fall '02)*, vol. 4, pp. 1992–1996, Vancouver, Canada, 2002.

[15] S. Ikki and M. H. Ahmed, "Performance analysis of cooperative diversity wireless networks over Nakagami-m fading channel," *IEEE Communications Letters*, vol. 11, no. 4, pp. 334–336, 2007.

[16] I. S. Gradshteyn and I. M. Ryzhik, *Table of Integrals, Series, and Products*, Academic Press, New York, NY, USA, 4th edition, 1980.

Hindawi Publishing Corporation
Mobile Information Systems
Volume 2016, Article ID 3848734, 8 pages
http://dx.doi.org/10.1155/2016/3848734

Research Article

On the Eigenvalue Based Detection for Multiantenna Cognitive Radio System

Syed Sajjad Ali,[1] Chang Liu,[1] Jialong Liu,[1] Minglu Jin,[1] and Jae Moung Kim[2]

[1]*School of Information and Communication Engineering, Dalian University of Technology, Dalian 116024, China*
[2]*Department of Information and Communication Engineering, INHA University, Incheon 402-751, Republic of Korea*

Correspondence should be addressed to Jae Moung Kim; jaekim@inha.ac.kr

Received 29 December 2015; Revised 4 April 2016; Accepted 5 May 2016

Academic Editor: Yunfei Chen

Eigenvalue based spectrum sensing can make detection by catching correlation features in space and time domains, which can not only reduce the effect of noise uncertainty, but also achieve high detection probability. Hence, the eigenvalue based detection is always a hot topic in spectrum sensing area. However, most existing algorithms only consider part of eigenvalues rather than all the eigenvalues, which does not make full use of correlation of eigenvalues. Motivated by this, this paper focuses on multiantenna system and makes all the eigenvalues weighted for detection. Through the analysis of system model, we transfer the eigenvalue weighting issue to an optimal problem and derive the theoretical expression of detection threshold and probability of false alarm and obtain the close form expression of optimal solution. Finally, we propose new weighting schemes to give promotions of the detection performance. Simulations verify the efficiency of the proposed algorithms.

1. Introduction

The rapid development of wireless services leads to the scarcity of the public radio spectrum becoming more and more serious. Traditionally, licensed spectrum is allocated over relatively long time periods and is intended to be used only by legitimate users. Cognitive radio (CR) technology was proposed to handle the contradiction between the shortage of spectrum resource and the underutilization of licensed spectrum [1, 2]. Spectrum sensing which is a fundamental task of CR is aimed at obtaining the awareness of licensed spectrum usage and existence of primary users (PUs) in a specific geographical location [3–7]. The main function of spectrum sensing is to frequently explore the spectrum holes for the secondary users (SUs) by detecting the presence of primary users so that the SUs can share the licensed spectrum. Therefore, spectrum sensing becomes critical in cognitive radio system.

There have been many discussions and proposed solutions for spectrum sensing [8]. Of these methods, likelihood ratio test (LRT) [9], cyclostationary detection (CSD) [10, 11], and matched filtering (MF) detection [12, 13] can achieve optimal performance while requiring both source signal and noise power information, which is not available in practice. Hence, semiblind methods such as energy detection (ED) [9, 14] and maximum eigenvalue detection (MED) [15] are proposed. Among these, ED is the most commonly chosen scheme for study and implementation due to its relatively low complexity and satisfactory performance under low signal-to-noise ratio (SNR) environment. However, ED heavily relies on the accuracy of the knowledge of noise power which is generally changing over time. This so-called noise uncertainty problem [16] can significantly degrade the performance of ED algorithm.

To overcome these shortcomings, blind detection algorithms which require no information on source signal or noise power have been intensively studied recently [17–21]. The classical blind detection algorithms are the eigenvalue based methods. For example, maximum-minimum eigenvalue (MME) detection [22], arithmetic to geometric mean (AGM) detection [23], and signal-subspace eigenvalues (SSE) method [23] can overcome the shortcoming of ED and

achieve outstanding performance. On the other hand, eigenvalue based methods have also been studied in new scenarios, such as cooperative adaptive versions [24] and Multiple Primary Transmit Power (MPTP) scenario [25].

However, most algorithms only consider part of eigenvalues, such as maximum, minimum, and mean value, which does not make full use of all the eigenvalues to make detection. Motivated by this, we focus on the problem of eigenvalue weighting in multiantenna system and analyze the related problems. By analyzing the model of eigenvalue weighting, we transfer the weighting problem to an optimal problem. Using the latest random matrix theory (RMT) [26, 27], we derive the close form expression of probability of detection and probability of false alarm and obtain the optimal solution. Finally, we propose new weighting schemes to give promotions of the detection performance. Simulations verify the efficiency of the proposed algorithms. The main contributions of this paper include the following:

(i) Different from the traditional eigenvalue based detection, we consider making detection by utilizing all of the eigenvalues in the multiantenna system. By transferring the weighting problem to an optimal problem, we analyze and derive an energy based maximum ratio combination (EN-MRC) method.

(ii) Considering the case of correlated signals is common in applications, we use the idea of MRC weighting in EN-MRC method to design an eigenvalue based MRC (EIG-MRC) scheme: signal eigenvalue weighting (SEW) based detection, which needs the a priori information of signals' covariance matrix and noise power.

(iii) To make the detection more practical, we use the maximum likelihood estimation (MLE) approach to design a method of signal eigenvalue approximation weighting (SEAW) based detection, in which only the noise power is needed.

The rest of the paper is organized as follows. Section 2 explains the system model. The eigenvalue weighting based detection is studied in Section 3. Section 4 presents simulation results and conclusion is presented in Section 5. Some notations used in the paper are listed as follows: superscripts T and H stand for transpose and Hermitian transpose (transpose-conjugate), respectively.

2. System Model

Figure 1 illustrates a classical multiantenna spectrum sensing scenario with D randomly distributed primary users (PU in figure) and P randomly distributed secondary users (SU in figure). Once PUs begin to communicate, the surrounding SUs can receive the PU signals and then capture the samples to operate the spectrum sensing.

According to Figure 1, the SUs are equipped with M receiving antennas and there are D PU signals arriving in the antenna array. In this case, the sensing problem in multiantenna cognitive radio system can be written as

$$\begin{aligned} H_0 &: x_i(k) = n_i(k) \\ H_1 &: x_i(k) = \sum_{j=1}^{D} h_{ij} s_j(k) + n_i(k), \end{aligned} \tag{1}$$

where $i = 1, 2, \ldots, M$ represents the ith receiving antenna and $k = 0, 1, \ldots, N-1$ is the kth sample. $x_i(k)$ is the sample of the ith receiving antenna. h_{ij} is the channel gain between the jth PU signal $s_j(k)$ and the ith receiving antenna. $n_i(k)$ is the additive white Gaussian noise (AWGN) with 0 mean, σ_n^2 variance.

Stacking the samples at the same time we can get the following receiving vector of antenna array:

$$\begin{aligned} \mathbf{x}(k) &= \left[x_1(k), x_2(k), \ldots, x_M(k)\right]^T, \\ \mathbf{s}(k) &= \left[s_1(k), s_2(k), \ldots, s_D(k)\right]^T, \\ \mathbf{n}(k) &= \left[n_1(k), n_2(k), \ldots, n_M(k)\right]^T. \end{aligned} \tag{2}$$

Hence, formula (1) can be rewritten as the matrix form:

$$\begin{aligned} H_0 &: \mathbf{X} = \mathbf{N}, \\ H_1 &: \mathbf{X} = \mathbf{HS} + \mathbf{N}, \end{aligned} \tag{3}$$

where $\mathbf{X} = [\mathbf{x}(0), \mathbf{x}(1), \ldots, \mathbf{x}(N-1)]^T$ and $\mathbf{N} = [\mathbf{n}(0), \mathbf{n}(1), \ldots, \mathbf{n}(N-1)]^T$ are the antenna receiving matrix and noise matrix, respectively. $\mathbf{H} \in \mathbb{C}^{M \times D}$ is the channel gain matrix of the signal matrix $\mathbf{S} = [\mathbf{s}(0), \mathbf{s}(1), \ldots, \mathbf{s}(N-1)]^T$.

3. Eigenvalue Weighting Based Detection

3.1. Fundamental of Eigenvalue Weighting Based Detection. Based on (3), the corresponding covariance matrix can be written as

$$\begin{aligned} \mathbf{R_X} &= E\left(\mathbf{XX}^H\right), \\ \mathbf{R_S} &= E\left(\mathbf{SS}^H\right), \\ \mathbf{R_N} &= E\left(\mathbf{NN}^H\right). \end{aligned} \tag{4}$$

Hence, we can rewrite $\mathbf{R_X}$ as

$$\mathbf{R_X} = \mathbf{HR_S H}^H + \mathbf{R_N}. \tag{5}$$

Let $\lambda_1 \geq \lambda_2 \geq \cdots \geq \lambda_M$ and $\rho_1 \geq \rho_2 \geq \cdots \geq \rho_D$ represent the eigenvalues of $\mathbf{R_X}$ and $\mathbf{HR_S H}^H$, respectively. Obviously, when PUs are present, we can get $\lambda_i = \rho_i + \sigma_n^2$; when PUs are absent, that is, $\mathbf{R_X} = \mathbf{R_N}$, we can have $\lambda_1 = \lambda_2 = \cdots = \lambda_M = \sigma_n^2$.

Based on the analysis above, we can make detection by weighting the eigenvalues. Considering the number of samples is finite in reality we can get the following test statistic:

$$T = \sum_{i=1}^{M} w_i \lambda_i \left(\mathbf{R_X}(N)\right), \tag{6}$$

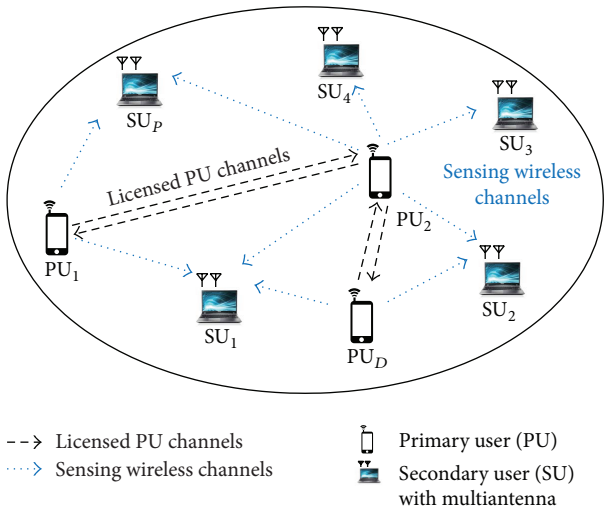

FIGURE 1: Scenario of spectrum sensing for multiantenna cognitive radio system.

where $\lambda(\cdot)$ is the eigenvalues and w_i is the weighting coefficient. $\mathbf{R_X}(N) = (1/N)\mathbf{X}\mathbf{X}^H$ is the samples covariance matrix. Obviously, if $T > \gamma$ (γ is the test threshold), then PUs are present; otherwise, PUs are absent.

Finally, we summarize the general eigenvalue weighting algorithm steps as follows.

Eigenvalue Weighting Based Spectrum Sensing Algorithm for Multiantenna Cognitive Radio System

Step 1 (compute the sample covariance matrix of the received signal). Since the number of samples is finite, we can only use the sample covariance matrix $\mathbf{R_X}(N) = (1/N)\mathbf{X}\mathbf{X}^H$.

Step 2 (obtain the eigenvalues of sample covariance matrix). Make eigenvalue decomposition (EVD) of $\mathbf{R_X}(N)$, obtain M eigenvalues, and sort them in a descending order: $\lambda_1 \geq \lambda_2 \geq \cdots \geq \lambda_M$.

Step 3 (calculate the test statistic of the eigenvalue weighting). Let all the eigenvalues be weighted by w_i and compute the sum of them. Thus, we can obtain the test statistic in (6).

Step 4 (decision). If $T > \gamma$, then signal exists ("yes" decision); otherwise, signal does not exist ("no" decision), where γ is a threshold.

3.2. Theoretical Analysis of Eigenvalue Weighting Based Detection. Note that how to select weights w_i is of great importance, which can affect the performance of the algorithm directly. Based on the Neyman-Pearson rule, we can express the weighting selection problem as the following optimal problem [28, 29]:

$$\begin{aligned} \max_{\mathbf{w}} \quad & P_d = \int_r^\infty f_{T|H_1}(x;\mathbf{w})\,dx \\ \text{s.t.} \quad & P_{fa} = \int_r^\infty f_{T|H_0}(x;\mathbf{w})\,dx, \end{aligned} \tag{7}$$

where $\mathbf{w} = [w_1, w_2, \ldots, w_M]^T$ is the weighting coefficient vector; P_d and P_{fa} represent the probability of detection and the probability of false alarm. $f_{T|H_1}(\cdot)$ and $f_{T|H_0}(\cdot)$ are the probability density function of test statistic under H_1 and H_0, respectively.

Based on (6), we find that it is possible to analyze the distribution of the test statistic whereas the joint probability density function is rather complex, whose close form expression is not available. However, we can transfer the problem of eigenvalue weighting of the matrix to a problem of the trace of a new matrix and the analysis of distribution of the trace is a simple problem. The detailed analysis is showed in the following.

Let $\mathbf{Y} = \mathbf{G}\mathbf{X} \in \mathbb{C}^{M\times N}$ and $\mathbf{G} = \text{diag}[g_1, g_2, \ldots, g_M] = \text{diag}[\sqrt{w_1}, \sqrt{w_2}, \ldots, \sqrt{w_M}]^T$. Hence,

$$\mathbf{W_Y} = \mathbf{Y}\mathbf{Y}^H = \mathbf{G}\mathbf{W_X}\mathbf{G}^H, \tag{8}$$

where $\mathbf{W_X} = \mathbf{X}\mathbf{X}^H$. When the number of samples N tends to infinite, the $\mathbf{W_X}$ tends to a diagonal matrix and we can get the following:

$$\text{EVD}\left(\mathbf{W_Y}\right) = \text{EVD}\left(\mathbf{G}\mathbf{W_X}\mathbf{G}^H\right) \approx \mathbf{G}\text{EVD}\left(\mathbf{W_X}\right)\mathbf{G}^H, \tag{9}$$

where EVD$(\cdot)$ represents the diagonal matrix of eigenvalues and the equality holds when the number of samples N tends to infinite. Hence, if we make eigenvalue weighting of $\mathbf{W_X}$ by $\mathbf{w} = [w_1, w_2, \ldots, w_M]^T$ and calculate the sum of the eigenvalues after weighting, then it is equivalent to compute the trace of $\mathbf{W_Y}$. Since $\mathbf{W_X} = N\mathbf{R_X}(N)$, we can rewrite (6) as the following:

$$\begin{aligned} T &= \sum_{i=1}^{M} w_i \lambda_i\left(\mathbf{R_X}(N)\right) \approx \sum_{i=1}^{M} \lambda_i\left(\mathbf{R_Y}(N)\right) \\ &= \text{Trace}\left(\mathbf{R_Y}(N)\right) = \text{Trace}\left(\mathbf{G}\mathbf{R_X}(N)\mathbf{G}^H\right) \\ &= \frac{1}{N}\sum_{i=1}^{M}\sum_{k=0}^{N-1} w_i \left|r_{\mathbf{X}i}(k)\right|^2, \end{aligned} \tag{10}$$

where $r_{\mathbf{X}i}(k)$ is the ith row, $(k+1)$th element of $\mathbf{R_X}(N)$. Let $a_i = \sum_{k=0}^{N-1} |r_{\mathbf{X}i}(k)|^2$ and thus the test statistic T can be written as

$$T' = NT = \sum_{i=1}^{M} w_i a_i. \tag{11}$$

For simplification, we assume the noise variance $\sigma_n^2 = 1$. When the number of samples is large enough we can get the following expression based on central limit theorem (CRT):

$$a_i \sim \begin{cases} \mathcal{N}\left(N\sum_{i=1}^{M} w_i, 2N\sum_{i=1}^{M} w_i^2\right), & H_0 \\ \mathcal{N}\left(N\sum_{i=1}^{M} w_i(1+r_i), 2N\sum_{i=1}^{M} w_i^2(1+2r_i)\right), & H_1, \end{cases} \tag{12}$$

where $r_i = E|\sum_{j=1}^{D} h_{ij}s_j(k)|^2$ is the power of the PU signals. Therefore, we can obtain the expressions of P_{fa} and P_d, respectively:

$$P_{fa} = P\left\{T' > \gamma \mid H_0\right\} = Q\left(\frac{\gamma - N\sum_{i=1}^{M} w_i}{\sqrt{2N\sum_{i=1}^{M} w_i^2}}\right), \tag{13}$$

$$\begin{aligned} P_d &= P\left\{T' > \gamma \mid H_1\right\} \\ &= Q\left(\frac{\gamma - N\sum_{i=1}^{M} w_i\left(1 + r_i\right)}{\sqrt{2N\sum_{i=1}^{M} w_i^2\left(1 + 2r_i\right)}}\right), \end{aligned} \tag{14}$$

where $Q(x) = \int_x^{+\infty}(1/\sqrt{2\pi})e^{-t^2/2}dt$. Hence, based on (13) and (14), we can finally get the expression as

$$P_d = Q\left(\frac{Q^{-1}\left(P_{fa}\right) - \sqrt{(N/2)\sum_{i=1}^{M}\alpha_i r_i}}{\sqrt{\sum_{i=1}^{M}\alpha_i^2\left(1 + 2r_i\right)}}\right), \tag{15}$$

where $\alpha_i = w_i/\sqrt{\sum_{i=1}^{M} w_i^2}$ and $\sum_{i=1}^{M}\alpha_i^2 = 1$. Since the SNR of spectrum sensing is rather low (−20 dB), which leads to $r_i \ll 1$, we can get $\sum_{i=1}^{M}\alpha_i^2(1 + 2r_i) \approx 1$. Hence, (15) can be approximated as

$$P_d \approx Q\left(Q^{-1}\left(P_{fa}\right) - \sqrt{\frac{N}{2}\sum_{i=1}^{M}\alpha_i r_i}\right). \tag{16}$$

Therefore, problem (7) can be rewritten as

$$\begin{aligned} \max_{\alpha} \quad & \sum_{i=1}^{M}\alpha_i r_i \\ \text{s.t.} \quad & \sum_{i=1}^{M}\alpha_i^2 = 1. \end{aligned} \tag{17}$$

Note that this problem can be solved by Lagrangian multiplier method and the solution is written as

$$\alpha_i^* = \frac{r_i}{\sqrt{\sum_{i=1}^{M} r_i^2}}. \tag{18}$$

Let $\sum_{i=1}^{M} w_i^2 = 1$ and we can finally get the weighting coefficient:

$$w_i^* = \alpha_i^*, \quad 1 \le i \le M. \tag{19}$$

Note that this weighting scheme is exactly identical to the maximal ratio combination (MRC) weighting scheme in [28, 29] and we call it energy based MRC (EN-MRC) detection. Hence, by studying the idea of MRC weighting scheme, we apply this idea into eigenvalue weighting and finally develop a kind of energy based MRC algorithm. The test statistic can be written as

$$T_{\text{EN-MRC}} = \sum_{i=1}^{M}\frac{r_i}{\sqrt{\sum_{i=1}^{M} r_i^2}}\lambda_i, \tag{20}$$

where $r_i = E|\sum_{j=1}^{D} h_{ij}s_j(k)|^2$ is the power of the PU signals.

3.3. Eigenvalue Weighting Based Detection. Note that the transformation from eigenvalue to energy in (9) is approximately equivalent and the equality holds when N tends to infinite. Hence, the corresponding analysis should be more accurate when the number of samples tends to be very large. On the other hand, the analysis under this case is based on the assumption that the received signals are independent and identically distributed (i.i.d.) for each other, which is not very accurate for the case of highly correlated signals. For example, as for (12), the distribution of a_i under H_1 is considered as a linear combination of Gaussian variables with $(1 + r_i)$-variance, which is based on the assumption that the received signals under H_1 are i.i.d. for each other. However, this assumption is only available under a cooperative spectrum sensing model whose samples are collected from different sensing nodes. Hence, the weighting coefficient in (20) is not an appropriate weighting scheme especially for the case of highly correlated signals and thus it needs to be improved for better catching the signals' correlation.

Motivated by this, we try to analyze the weighting coefficients from the aspect of eigenvalue directly. Since $r_i = E|h_{ij}s_j(k)|^2$ is the power of the PU signals and $E[|h_{ij}|^2] = 1$, we can then replace the power of the PU signals r_i in (20) with the eigenvalues of signal covariance matrix $\rho_i = [\text{EVD}(\mathbf{H}\mathbf{R}_\mathbf{S}\mathbf{H}^H)]_i$.

In this case, the test statistic can further capture the correlation among signals and may achieve better performance especially when there are highly correlated PU signals. Hence, we propose a signal eigenvalue weighting (SEW) based detection and the test statistic is given as

$$T_{\text{SEW}} = \sum_{i=1}^{M}\frac{\rho_i}{\sqrt{\sum_{i=1}^{M}\rho_i^2}}\lambda_i, \tag{21}$$

where λ_i and ρ_i are the eigenvalues of sample and signals' covariance matrix, respectively. Although the SEW based detection may perform better performance, it is not available in practice as it needs the a priori information of the channel, signal, and noise. Hence, we try to use the maximum likelihood estimation (MLE) of these parameters to design semi-blind detection, in which only noise power is needed. Hence, we will analyze and derive the MLE of eigenvalues of the PU signals' covariance matrix in the following.

According to the analysis in [23], the MLE of signals' covariance matrix $\mathbf{R}_\mathbf{s}$ can be expressed as

$$\begin{aligned} \widehat{\mathbf{R}}_\mathbf{s} = \mathbf{U}_\mathbf{x}\text{Diag}\Big(&\left(\lambda_1 - \sigma_n^2\right)^+, \left(\lambda_2 - \sigma_n^2\right)^+, \ldots, \\ &\left(\lambda_M - \sigma_n^2\right)^+\Big)\mathbf{U}_\mathbf{x}^H, \end{aligned} \tag{22}$$

where $\mathbf{U}_\mathbf{x}$ is the eigenvector of sample covariance $\mathbf{R}_\mathbf{x}(N)$ and $(x)^+ = \max(0, x)$ represents the maximum between x and 0. Hence, the MLE of eigenvalues of PU signals' covariance matrix can be written as

$$\widehat{\rho}_i = \left(\lambda_i - \sigma_n^2\right)^+. \tag{23}$$

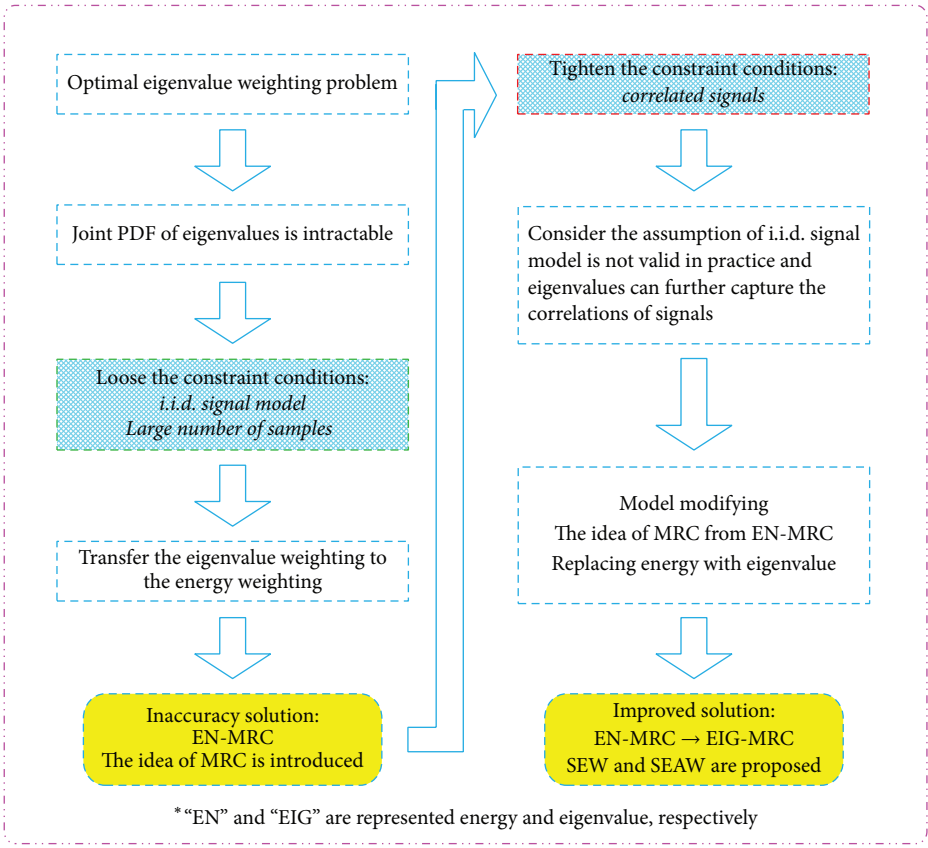

Figure 2: Illustration of how to obtain the eigenvalue weighting schemes.

Substituting the MLE of signal eigenvalue into (21) we can obtain the test statistic of signal eigenvalue approximation weighting (SEAW) based detection as

$$T_{\text{SEAW}} = \sum_{i=1}^{M} \frac{\left(\lambda_i - \sigma_n^2\right)^+}{\sqrt{\sum_{j=1}^{M} \left(\left(\lambda_j - \sigma_n^2\right)^+\right)^2}} \lambda_i. \tag{24}$$

As a summary, we propose three weighting schemes: one is traditional MRC based detection (i.e., EN-MRC) and the other two are improvement eigenvalue weighting schemes, that is, SEW based detection and SEAW based detection. For the convenience of comparison, we summarize these three methods in Table 1.

Remark. Since eigenvalue weighting problem can not be solved directly, we first loose the constraint conditions and assume that the PU signals follow the i.i.d. model and the number of samples is very large. In this case, we can obtain an inaccuracy solution: EN-MRC. Based on the MRC weighting scheme, we then tighten the constraint conditions and modify the assumption to make it satisfy the requirements of the practical system, that is, correlated signal model. Considering the eigenvalues can further capture the correlations of signals, we finally replace the energies with eigenvalues and design the eigenvalue based MRC (EIG-MRC) schemes: SEW and SEAW based detection. The corresponding illustration is shown in Figure 2.

4. Simulations and Discussions

This section provides some simulation results for multi-antenna cognitive radio systems in the MATLAB environment. Since this paper focuses the eigenvalue weighting schemes for spectrum sensing, we will compare the proposed EN-MRC, SEW, and SEAW based detection with eigenvalue based methods, including MED, MME, and AGM detection. We assume there is 1 PU or 2 PUs transmitting signal over the Nakagami-m ($m = 1$) channel in presence of AWGN. The SUs are equipped with 4-element antenna array. The stopping criterion set is at 10 000 iterations and the P_{fa} is set as 0.1 (this has been specified as the maximum allowable P_{fa} by the WRAN 802.22 working group).

The simulation results of detection performance in terms of number of samples $N = 100$ with 1 PU and 2 PUs are presented in Figures 3 and 4, respectively. It is shown that when compared with eigenvalue based methods, such as MED, MME, and AGM, the proposed SEW and SEAW based detection perform much higher probability of detection with different SNRs, while the EN-MRC performs a relatively lower detection probability when compared with MED, MME, and AGM detection. It is because algorithms SEW and SEAW are regarded as "EIG-MRC" weighting scheme and MED and

Table 1: Promotion schemes of eigenvalue weighting based spectrum sensing algorithm.

Algorithm	Test statistic	Priori conditions
Energy based maximum ratio combination (EN-MRC)	$T_{\text{EN-MRC}} = \sum_{i=1}^{M} \frac{r_i}{\sqrt{\sum_{i=1}^{M} r_i^2}} \lambda_i$, where λ_i and r_i are the eigenvalues of sample and the power of the PU signals, respectively.	PU signals' energy and noise power
Signal eigenvalue weighting (SEW) based detection	$T_{\text{SEW}} = \sum_{i=1}^{M} \frac{\rho_i}{\sqrt{\sum_{i=1}^{M} \rho_i^2}} \lambda_i$, where λ_i and ρ_i are the eigenvalues of sample and PU signals' covariance matrix, respectively.	Eigenvalues of PU signals' covariance matrix and noise power
Signal eigenvalue approximation weighting (SEAW) based detection	$T_{\text{SEAW}} = \sum_{i=1}^{M} \frac{(\lambda_i - \sigma_n^2)^+}{\sqrt{\sum_{j=1}^{M} ((\lambda_j - \sigma_n^2)^+)^2}} \lambda_i$, where λ_i is the eigenvalues of sample covariance matrix; σ_n^2 is the noise power at receiver.	Noise power at receiver

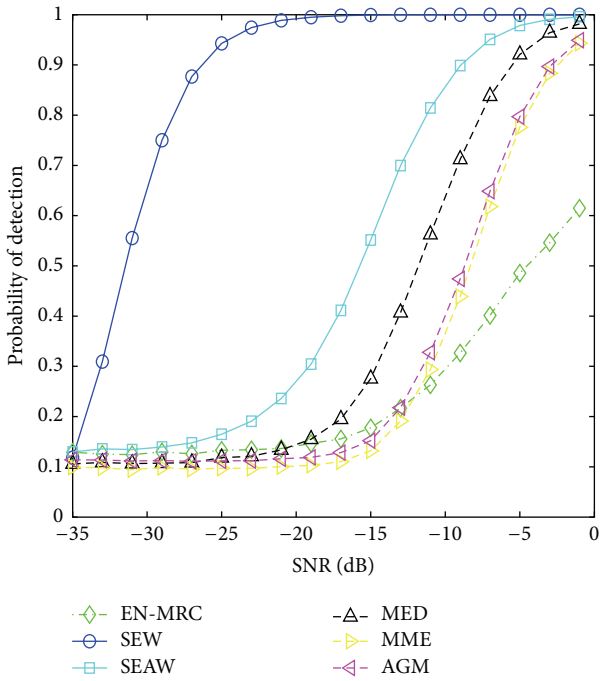

Figure 3: Detection performance under $N = 100$ with 1 PU.

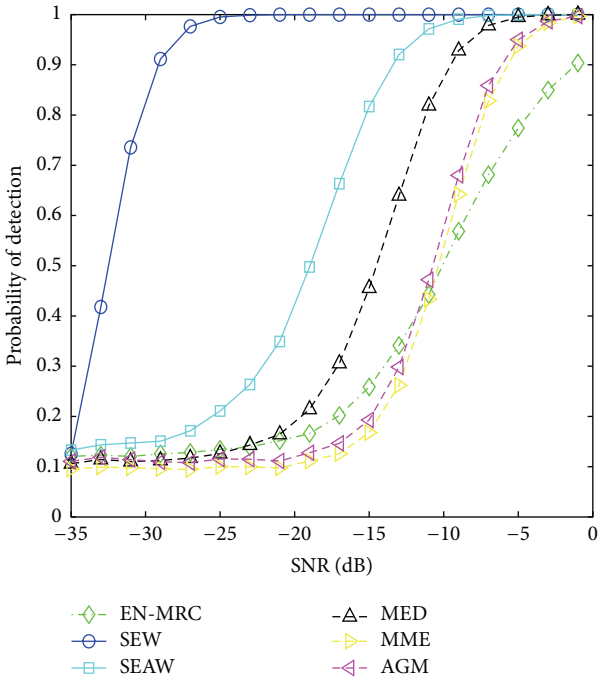

Figure 4: Detection performance under $N = 100$ with 2 PUs.

AGM belong to the selection combination (SC) and equal gain combination (EGC) weighting schemes for eigenvalues, respectively. As for EN-MRC, it is the energy based weighting coefficients, which can not fully capture the correlations. In addition, the MME is just a kind of partial eigenvalue based nonweighting detection and thus it has limited detection performance. However, since low SNR approximation has been adopted to derive the EN-MRC scheme, the EN-MRC is able to achieve a relatively higher detection probability. For example, the EN-MRC is slightly better than MME and AGM when the SNR is ranging from −35 dB to −13 dB. On the other hand, when the SNR increases, the probability of detection of EN-MRC drops a little and presents a slightly worse performance (since the number of eigenvalues for the simulation is very small, the advantages of making detection by using all the eigenvalues or the energies are not obvious, which means the AGM or EN-MRC may not achieve a better performance than MME). When comparing Figure 3 with Figure 4, we can find that the performance increases with the increasing number of PUs, such as a nearly 30% detection probability improvement in terms of −15 dB.

Similarly, Figures 5 and 6 present the simulation results of probability of detection in terms of number of samples $N = 1000$ with 1 PU and 2 PUs. Again, the proposed SEW and SEAW methods achieve a higher detection performance and the EN-MRC outperforms MME and AGM under low SNRs. Hence, the simulation results can further verify that it is just

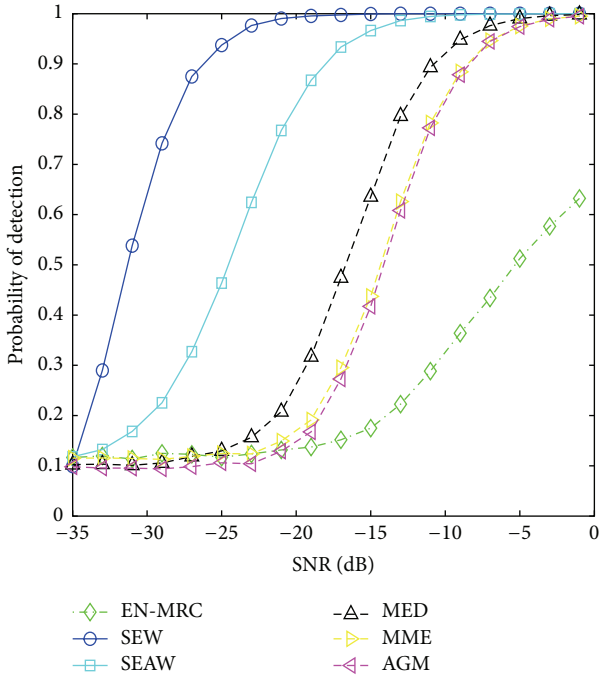

Figure 5: Detection performance under $N = 1000$ with 1 PU.

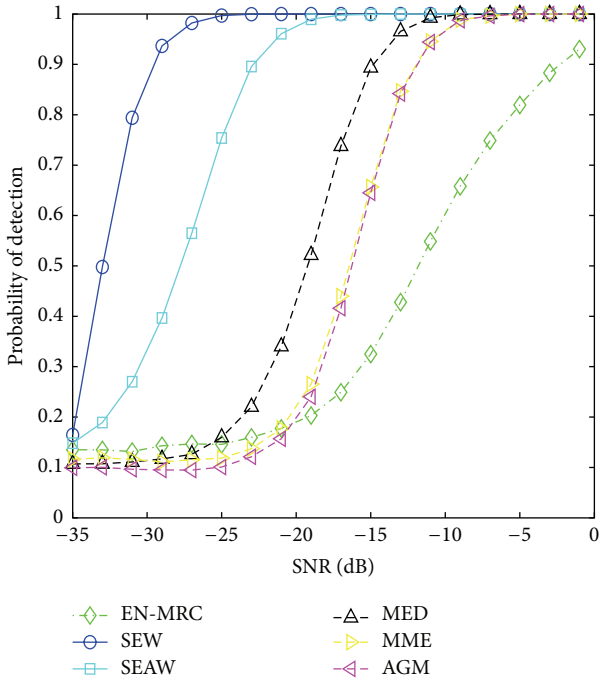

Figure 6: Detection performance under $N = 1000$ with 2 PUs.

the replacement of energy with eigenvalue that leads to the high improvements in terms of detection probability.

In addition, as for the three new methods, we can find that SEW performs the best among these proposed methods, EN-MRC performs the worst, and the performance of SEAW is between these two methods. For example, the probability of detection of SEAW with 2 PUs (i.e., SEAW in Figure 3) is 0.5 in terms of SNR = −15 dB, which is in the middle of P_d of SEW (i.e., 1) and P_d of EN-MRC (i.e., 0.2).

According to Figures 3–6, a more interesting phenomenon can be found; that is, the SEAW's performance shifts from the lower P_d area (close to EN-MRC) to a higher P_d area (close to SEW) with the increasing of number of samples and number of PUs, which is like a kind of lower and upper bounds of the performance of SEAW. If we consider the performance-complexity tradeoff, the proposed SEAW can be selected as an alternative for its low complexity and relatively better performance. Hence, the SEAW may be more suitable for the application in reality.

5. Conclusion

This paper focuses on the problem of the eigenvalue weighting based spectrum sensing in multiantenna cognitive radio system. Through the analysis of system model, we transfer the eigenvalue weighting issue to the energy based weighting problem and derive the theoretical expression of detection threshold and probability of false alarm and finally obtain the close form expression. Considering the case of correlated signals is common in applications, we then design the signal eigenvalue based detection methods and they can achieve more higher detection probability. Simulation results verify the efficiency of the proposed algorithms.

Competing Interests

The authors declare that they have no competing interests.

Acknowledgments

This research was supported by the MSIP (Ministry of Science, ICT and Future Planning), Korea, under the ITRC (Information Technology Research Center) support program (IITP-2016-H8501-16-1019) supervised by the IITP (Institute for Information & Communications Technology Promotion).

References

[1] Federal Communications Commission, "Notice of proposed rule making and order: facilitating opportunities for flexible, efficient, and reliable spectrum use employing cognitive radio technologies," ET Docket 03-108, Federal Communications Commission, Washington, Wash, USA, 2005.

[2] J. Mitola III and G. Q. Maguire Jr., "Cognitive radio: making software radios more personal," *IEEE Personal Communications*, vol. 6, no. 4, pp. 13–18, 1999.

[3] T. Yücek and H. Arslan, "A survey of spectrum sensing algorithms for cognitive radio applications," *IEEE Communications Surveys and Tutorials*, vol. 11, no. 1, pp. 116–130, 2009.

[4] E. Axell, G. Leus, E. G. Larsson, and H. V. Poor, "Spectrum sensing for cognitive radio: state-of-the-art and recent advances," *IEEE Signal Processing Magazine*, vol. 29, no. 3, pp. 101–116, 2012.

[5] M. T. Masonta, M. Mzyece, and N. Ntlatlapa, "Spectrum decision in cognitive radio networks: a survey," *IEEE Communications Surveys and Tutorials*, vol. 15, no. 3, pp. 1088–1107, 2013.

[6] H. Sun, A. Nallanathan, C.-X. Wang, and Y. Chen, "Wideband spectrum sensing for cognitive radio networks: a survey," *IEEE Wireless Communications*, vol. 20, no. 2, pp. 74–81, 2013.

[7] X. Huang, T. Han, and N. Ansari, "On green-energy-powered cognitive radio networks," *IEEE Communications Surveys and Tutorials*, vol. 17, no. 2, pp. 827–842, 2015.

[8] Y. Zeng, Y.-C. Liang, A. T. Hoang, and R. Zhang, "A review on spectrum sensing for cognitive radio: challenges and solutions," *EURASIP Journal on Advances in Signal Processing*, vol. 2010, Article ID 381465, 15 pages, 2010.

[9] S. M. Kay, *Fundamentals of Statistical Signal Processing: Detection Theory*, Prentice Hall, 1998.

[10] W. A. Gardner, "Exploitation of spectral redundancy in cyclostationary signals," *IEEE Signal Processing Magazine*, vol. 8, no. 2, pp. 14–36, 1991.

[11] N. Han, S. H. Shon, J. O. Joo, and J. M. Kim, "Spectral correlation based signal detection method for spectrum sensing in IEEE 802.22 WRAN systems," in *Proceedings of the 8th International Conference Advanced Communication Technology*, pp. 1765–1770, Dublin, Ireland, February 2006.

[12] A. Sahai and D. Cabric, "Spectrum sensing: fundamental limits and practical challenges," in *Proceedings of the IEEE International Symposium on New Frontiers in Dynamic Spectrum Access Networks (DySPAN '05)*, Baltimore, Md, USA, November 2005.

[13] H.-S. Chen, W. Gao, and D. G. Daut, "Signature based spectrum sensing algorithms for IEEE 802.22 WRAN," in *Proceedings of the IEEE International Conference on Communications (ICC '07)*, pp. 6487–6492, Glasgow, UK, June 2007.

[14] H. Urkowitz, "Energy detection of unknown deterministic signals," *Proceedings of the IEEE*, vol. 55, no. 4, pp. 523–531, 1967.

[15] Y. Zeng, C. L. Koh, and Y.-C. Liang, "Maximum eigenvalue detection: theory and application," in *Proceedings of the IEEE International Conference on Communications (ICC '08)*, pp. 4160–4164, Beijing, China, May 2008.

[16] R. Tandra and A. Sahai, "SNR walls for signal detection," *IEEE Journal on Selected Topics in Signal Processing*, vol. 2, no. 1, pp. 4–17, 2008.

[17] Y. Zeng and Y. C. Liang, "Covariance based signal detections for cognitive radio," in *Proceedings of the 2nd IEEE International Symposium on New Frontiers in Dynamic Spectrum Access Networks (DySPAN '07)*, pp. 202–207, Dublin, Ireland, April 2007.

[18] C. Liu, M. Li, and M.-L. Jin, "Blind energy-based detection for spatial spectrum sensing," *IEEE Wireless Communications Letters*, vol. 4, no. 1, pp. 98–101, 2015.

[19] C. Liu and M. Jin, "Maximum-minimum spatial spectrum detection for cognitive radio using parasitic antenna arrays," in *Proceedings of the IEEE/CIC International Conference on Communications in China (ICCC '14)*, pp. 365–369, Shanghai, China, October 2014.

[20] C. Liu, H. Li, and M. Jin, "Blind central symmetry-based feature detection for spatial spectrumsensing," *IEEE Transactions on Vehicular Technology*, 2016.

[21] C. Liu, S. S. Ali, R. Zhang, S.-Y. Li, J. Wang, and M.-L. Jin, "Spatial spectrum based blind spectrum sensing for multi-antenna cognitive radio system," *Journal on Communications*, vol. 36, no. 4, Article ID 2015087, 10 pages, 2015.

[22] Y. Zeng and Y.-C. Liang, "Eigenvalue-based spectrum sensing algorithms for cognitive radio," *IEEE Transactions on Communications*, vol. 57, no. 6, pp. 1784–1793, 2009.

[23] R. Zhang, T. J. Lim, Y.-C. Liang, and Y. Zeng, "Multi-antenna based spectrum sensing for cognitive radios: a GLRT approach," *IEEE Transactions on Communications*, vol. 58, no. 1, pp. 84–88, 2010.

[24] C. G. Tsinos and K. Berberidis, "Decentralized adaptive eigenvalue-based spectrum sensing for multiantenna cognitive radio systems," *IEEE Transactions on Wireless Communications*, vol. 14, no. 3, pp. 1703–1715, 2015.

[25] Z. Li, D. Wang, P. Qi, and B. Hao, "Maximum eigenvalue based sensing and power recognition for multi-antenna cognitive radio system," *IEEE Transactions on Vehicular Technology*, 2015.

[26] A. M. Tulino and S. Verd, *Random Matrix Theory and Wireless Communivations*, Now Publishers, Hanover, Mass, USA, 2004.

[27] I. M. Johnstone, "On the distribution of the largest eigenvalue in principal components analysis," *The Annals of Statistics*, vol. 29, no. 2, pp. 295–327, 2001.

[28] Y.-C. Liang, Y. Zeng, E. C. Y. Peh, and A. T. Hoang, "Sensing-throughput tradeoff for cognitive radio networks," *IEEE Transactions on Wireless Communications*, vol. 7, no. 4, pp. 1326–1337, 2008.

[29] J. Ma, G. Zhao, and Y. Li, "Soft combination and detection for cooperative spectrum sensing in cognitive radio networks," *IEEE Transactions on Wireless Communications*, vol. 7, no. 11, pp. 4502–4507, 2008.

Hindawi Publishing Corporation
Mobile Information Systems
Volume 2016, Article ID 2152538, 11 pages
http://dx.doi.org/10.1155/2016/2152538

Research Article

Rank-Constrained Beamforming for MIMO Cognitive Interference Channel

Duoying Zhang, Yao Zhang, Zujian Wu, and Huiqin Du

College of Information Science and Technology, Jinan University, Guangzhou 510632, China

Correspondence should be addressed to Huiqin Du; duhq518@gmail.com

Received 29 January 2016; Revised 14 April 2016; Accepted 5 May 2016

Academic Editor: Yunfei Chen

This paper considers the spectrum sharing multiple-input multiple-output (MIMO) cognitive interference channel, in which multiple primary users (PUs) coexist with multiple secondary users (SUs). Interference alignment (IA) approach is introduced that guarantees that secondary users access the licensed spectrum without causing harmful interference to the PUs. A rank-constrained beamforming design is proposed where the rank of the interferences and the desired signals is concerned. The standard interferences metric for the primary link, that is, *interference temperature*, is investigated and redesigned. The work provides a further improvement that optimizes the dimension of the interferences in the cognitive interference channel, instead of the power of the interference leakage. Due to the nonconvexity of the rank, the developed optimization problems are further approximated as convex form and are solved via choosing the transmitter precoder and receiver subspace iteratively. Numerical results show that the proposed designs can improve the achievable degree of freedom (DoF) of the primary links and provide the considerable sum rate for both secondary and primary transmissions under the rank constraints.

1. Introduction

Cognitive radio (CR) network is a potential solution to enhance spectrum utilization by allowing coexistence with licensed networks. The concurrent transmissions are allowed in the spectrum sharing cognitive radio networks by keeping the CR interferences to the primary user receivers (PU-Rxs) under an acceptable level. Hence, an effective approach to control the interference level is of critical importance to underlay CR networks.

Recently, interference alignment (IA) has been developed to achieve the maximum spatial degrees of freedom in the K user interference channel, which guarantees an interference-free received signal by forcing interferences into a reduced-dimensional receiver subspace [1–13]. Considering its potential to mitigate the interference, the IA is widely introduced to multiple-input multiple-output (MIMO) cognitive radio system [14–19], MIMO relay system [20], multihop MIMO networks [21], and the simultaneous wireless information and power transfer (SWIPT) system [22]. In the MIMO CR networks, the upper bound and lower bound of achievable degrees of freedom (DoF) have been studied with global channel information [1, 23], and the CR interferences to the PUs are nulled in [14–16]. However, the global channel state information usually is not available, which may lead to severe CR interferences to PU. As a result, the practical algorithm is developed that minimizes the interference leakage power by selecting the precoding and receiving beamforming matrices alternatively [16, 23–25]. In [16], the active IA and success interference cancelation (SIC) techniques are combined to transmit data over MIMO underlay CR network. Moreover, an efficient antenna selection IA algorithm based on discrete stochastic optimization (DSO) is proposed to improve the received signal-to-interference-and-noise ratio (SINR) of each user in IA-based CR networks with low complexity [17]. In the abovementioned works, the interference temperature is considered as a standard interference *metric* that suppresses the CR interferences and guarantees the quality of service (QoS) of the primary transmission. Considering the available eigenmodes distributed among the SUs and PUs, the adaptive number of eigenmodes beamforming (ANEB) algorithm for the PU is developed which adjusts the number of PU's eigenmodes to meet its rate requirement [26]. It suggests that the DoF of the receiving eigenspace is of crucial

importance to the system performance, which motivates us to revise the standard interference *metric*, that is, interference temperature, in the underlay CR networks.

In this paper, the rank-constrained beamforming design is developed for underlay MIMO CR network. Instead of using the standard interference metric, *interference temperature*, the CR interferences to the PU-Rxs are controlled by a rank constraint that aligns the CR interferences into a reduced-dimensional subspace. As a result, the CR interferences are suppressed in a low-dimensional subspace, rather than an acceptable low level of the received power; consequently the achievable DoF of the intended primary signal is guaranteed. The optimal transmit precoding and receiving beamforming are selected by minimizing the total interference of the secondary transmission subject to the rank constraint on the CR interferences. Different from those designs based on Cadambe-Jafar scheme [14–16], the proposed design strives to null the CR interferences at the PU-Rxs without the global channel state information. Considering the benefits of the multiplexing gain/DoF, we further maximize the achievable DoF of the secondary links by minimizing the dimension of the interferences of the secondary transmission while maintaining the full rank of the desired signal matrix and the low rank of the CR interferences to PUs. Due to the nonconvexity of the rank, the proposed optimization problem can be approximated as convex form and efficiently solved via alternating minimization. Simulation results show that the proposed scheme can improve the sum rate of both PU and SUs due to the effective rank constraint on the CR interferences.

This paper is organized as follows. The system model is introduced in Section 2. Section 3 presents the rank-constrained interference minimization algorithm, followed by further improvement in Section 4. Simulation results are presented and discussed in Section 5. Concluding remarks are given in Section 6.

Notations. Matrices and vectors are type-faced using slanted bold uppercase and lowercase letters, respectively. Conjugate transpose of the matrix $\mathbf{A}$ is denoted as $\mathbf{A}^H$. Positive semidefiniteness of the matrix $\mathbf{A}$ is depicted using $\mathbf{A} \succeq 0$, and $\mathbf{I}_d$ is an identity matrix with the dimension equal to d. $\mathbb{C}^{m\times n}$ is used to describe the complex space of $m \times n$ matrices, and $\mathcal{CN}(\mathbf{m}, \mathbf{\Sigma})$ denotes a complex Gaussian distribution with mean $\mathbf{m}$ and covariance $\mathbf{\Sigma}$. Finally, mathematical expectation is described as $\mathsf{E}[\cdot]$. The trace, nuclear norm, and Frobenius norm of a matrix/vector are denoted by $\mathrm{tr}\{\cdot\}$, $\|\cdot\|_*$, and $\|\cdot\|_F$, respectively.

2. System Model

Consider a MIMO cognitive radio network with L PU and K SUs, shown in Figure 1. The secondary transmitter (SU-Tx) is equipped with N_k transmit antennas and M_k receiving antennas at the kth SU. The transmission of all K users is synchronized such that each simultaneously begins and ends each transmission, and no frequency or timing offsets exist in the network [2, 6]. In the primary links, there are N_p transmit antennas and M_p receiving antennas equipped at each PU.

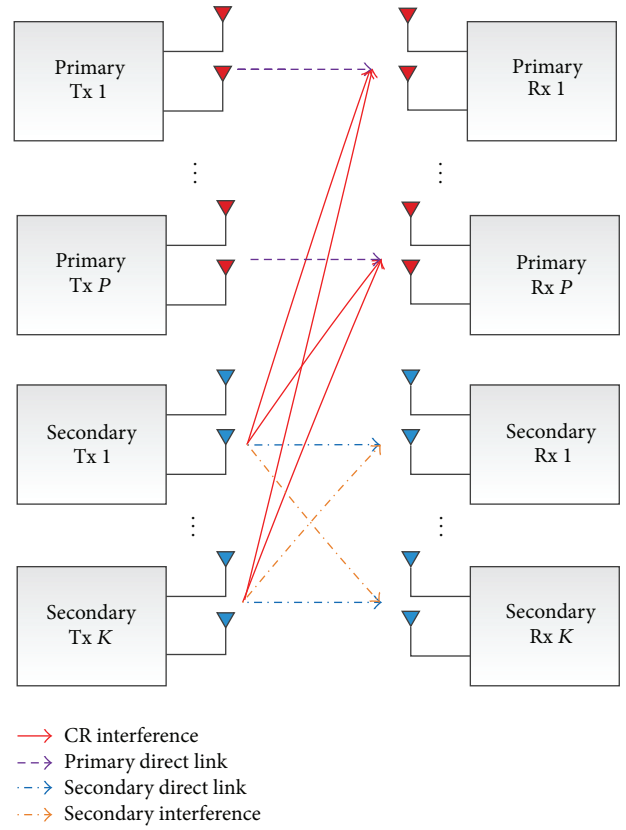

Figure 1: MIMO underlay cognitive radio network with single primary link and K secondary pairs.

Without any loss of generality, we assume that the users are indexed so that users $1, \ldots, K$ are SUs and the users $1, \ldots, L$ are the PUs. The total signal received at the kth secondary user receiver (SU-Rx) can be expressed as

$$\mathbf{y}_k = \mathbf{H}_{kk}\mathbf{V}_k\mathbf{x}_k + \sum_{l=1, l\neq k}^{K} \mathbf{H}_{kl}\mathbf{V}_l\mathbf{x}_l + \mathbf{n}_k, \quad k = 1, \ldots, K, \tag{1}$$

where $\mathbf{x}_k \in \mathbb{C}^{d_k\times 1}$ represents the transmitted signal from the kth SU-Tx with equally loaded power and $\mathbf{H}_{kl} \in \mathbb{C}^{M_k\times N_k}$ denote the flat-fading channel from the lth SU-Tx to the kth SU-Rx receiver. The columns of the precoding matrix $\mathbf{V}_k \in \mathbb{C}^{N_k\times d_k}$ are orthonormal basis of the kth transmitted signal where $\mathbf{V}_k^H\mathbf{V}_k = \mathbf{I}$ (for all k), and the receiver thermal noise $\mathbf{n}_k \in \mathbb{C}^{N_k\times 1}$ is assumed as the complex additive white Gaussian noise with covariance $\sigma_k^2\mathbf{I}$; that is, $\mathbf{n}_k \sim \mathcal{CN}(\mathbf{0}, \sigma_k^2\mathbf{I})$. Note that any interference from the PU-Tx is assumed to be neglected. (This can be possible if the PU-Tx is located far away from the secondary users, or the interference is represented by the noise under an assumption that the PU-Tx's signal is generated by random Gaussian codebooks [27]. In IEEE 802:22 standard, the secondary wireless regional area network (WRAN) is located far away from the primary TV transmitter and hence the interference from the primary TV

transmitter can be neglected at the receiver.) Similarly, the received signal $\mathbf{y}_p$ at the pth PU-Rx can be expressed as

$$\mathbf{y}_p = \mathbf{H}_{pp}\mathbf{V}_p\mathbf{x}_p + \sum_{p=1,p\neq q}^{L}\mathbf{H}_{pq}\mathbf{V}_q\mathbf{x}_q + \sum_{k=1}^{K}\mathbf{H}_{pk}\mathbf{V}_k\mathbf{x}_k + \mathbf{n}_p, \quad p = 1,\ldots,L, \tag{2}$$

where $\mathbf{x}_p \in \mathbb{C}^{d_p\times 1}$ represents the transmitted signal from the pth PU-Tx with equally loaded power, $\mathbf{H}_{pq} \in \mathbb{C}^{M_p\times N_p}$ denote the channel from the qth PU-Tx to the pth PU-Rx, and $\mathbf{H}_{pk} \in \mathbb{C}^{M_p\times N_k}$ is the channel from the kth SU-Tx to the pth PU-Rx. The columns of the precoding matrix $\mathbf{V}_p \in \mathbb{C}^{N_p\times d_p}$ are orthonormal basis of the transmitted signal from the pth PU-Tx, and the receiver thermal noise $\mathbf{n}_p \in \mathbb{C}^{N_p\times 1}$ is assumed as the complex additive white Gaussian noise with covariance $\sigma_p^2\mathbf{I}$; that is, $\mathbf{n}_p \sim \mathcal{CN}(\mathbf{0}, \sigma_p^2\mathbf{I})$. Note that the first term in (2) is the received intended signal of the pth primary link, the second term is the interferences from other primary links, and the third term is the CR interferences to the corresponding PU-Rx.

In the underlay CR network, the secondary base stations are allowed to concurrently transmit data as long as the interference metric has been satisfied. Previous researches nulled the CR interferences at the PU-Rxs with global channel state information, in which the CR interferences can be completely aligned in the receiver subspace of the primary user [14–16]. However, the global channel state information is usually not available in practice, in which the CR interferences at the PU-Rxs may be difficultly eliminated, leading to the performance degradation of the primary links. Without the global channel state information, the well-known interference *metric* that is used to control the CR interferences is named as interference temperature; that is,

$$\mathbf{IT}_{pk} = \left\|\mathbf{U}_p^H\mathbf{H}_{pk}\mathbf{V}_k\right\|_F, \tag{3}$$

where $\mathbf{U}_p \in \mathbb{C}^{M_p\times d_p}$ is the receiver beamforming matrix of the pth PU. Note that the interference temperature is used to suppress the CR interferences under an acceptable power level, rather than a reduced-dimensional subspace. However, the standard IA techniques suggest that the interference-free subspace can provide high DoF of the desired signal and provide considerable average sum rate at that moderate and high signal-to-noise ratio (SNR) [28, 29], which motivates us to further investigate another interference *metric* that can provide more dimensions of the interference-free receiver subspace.

3. Rank-Constrained Interference Minimization Beamforming

The CR interference *metric* is of critical importance to the secondary transmission in the underlay CR network. It works as admission control; that is, the secondary transmission is allowed once the QoS of the primary links is satisfied; otherwise, it will be prohibited to transmit. The ideal scenario is that the CR interference is completely aligned and that there are no CR interferences to each PU-Rx, as suggested in [14–16]. With respect to the dimension of the receiver subspace, the ideal scenario that CR interference is canceled can be expressed in the following equation; that is,

$$\operatorname{rank}\left(\mathbf{J}_p\right) = \operatorname{rank}\left(\mathbf{U}_p^H\left\{\mathbf{H}_{pk}\mathbf{V}_k\right\}_{k=1}^{K}\right) = 0, \tag{4}$$

where $\mathbf{J}_p$ is defined as the CR interferences to the pth PU-Rx; that is, $\mathbf{J}_p = \mathbf{U}_p^H[\mathbf{H}_{p1}\mathbf{V}_1,\ldots,\mathbf{H}_{pk}\mathbf{V}_k,\ldots,\mathbf{H}_{pK}\mathbf{V}_K]$. Supposing that the interferences coming from other primary links are perfectly aligned, the achievable multiplexing gain per PU can be expressed as

$$\mathrm{DoF}_p = \left[\operatorname{rank}\left(\mathbf{U}_p^H\mathbf{H}_{pp}\mathbf{V}_p\right) - \operatorname{rank}\left(\mathbf{J}_p\right)\right]^+, \tag{5}$$

where $\operatorname{rank}(\mathbf{U}_p^H\mathbf{H}_{pp}\mathbf{V}_p) \geq \operatorname{rank}(\mathbf{J}_p)$, or else $\mathrm{DoF}_p = 0$. To minimize the DoF degradation of the pth primary link caused by the CR interferences, the effective approach is to force the CR interferences from the SU-Txs to share a reduced-dimensional subspace at the PU-Rxs, leading to an interference-free receiver subspace for the primary transmission.

Without global channel state information (in this work, the local channel information is followed by the definition in [6], where each of the transmitters is assumed to know only the channel to its desired transmitter and the covariance matrix of its effective noise (consisting of the AWGN and the interference from all other users), e.g., the local channel information of the kth link including the direct channel $\mathbf{H}_{kk}$ and desired link $\{\mathbf{H}_{lk}\}_{l=1,l\neq k}^{K}$, while the global channel information is defined as that in [1] where each node has to know all the channels $\{\{\mathbf{H}_{lk}\}_{l=1}^{K}\}_{k=1}^{K}$), each secondary link primarily can adjust its precoding and receiver subspaces to minimize the interference leaked to unintended SU-Rxs. More specifically, the precoder matrices $\{\mathbf{V}_l\}_{l=1}^{K}$ and interference receiving matrices $\{\mathbf{U}_k\}_{k=1}^{K}$ are chosen such that each SU-Rx can decode its own signal by minimizing the interference leakage while forcing the CR interferences to share a reduced-dimensional subspace at the PU-Rxs. The underlying optimization problem can be mathematically described as follows:

$$\underset{\mathbf{U}_k,\mathbf{V}_l}{\text{minimize}} \quad \sum_{k=1}^{K}\sum_{l=1,l\neq k}^{K}\left\|\mathbf{U}_k^H\mathbf{H}_{kl}\mathbf{V}_l\right\|_F^2, \tag{6}$$

$$\text{subject to} \quad \operatorname{rank}\left(\mathbf{J}_p\right) = 0, \tag{7}$$

$$\operatorname{rank}\left(\mathbf{U}_k^H\mathbf{H}_{kk}\mathbf{V}_k\right) = d_k, \tag{8}$$

where $\mathbf{U}_k \in \mathbb{C}^{M\times d_k}$ presents the receiving beamforming matrix whose columns are the orthonormal basis of the kth SU receiver. The objective function (6) minimizes the total interference leakage of the secondary transmission, and the full rank of the desired signals of the secondary links is guaranteed in (8). However, the rank constraints in (7) and (8) are not convex, and possible approximations are required.

In order to minimize the performance degradation from the secondary links, it is reasonable to approximate the rank constraint (7) as a nuclear norm with a prespecified small value ε; that is,

$$\left\|\mathbf{J}_p\right\|_* \leq \varepsilon, \tag{9}$$

which can align the CR interferences into a low-dimensional subspace, where $\|\mathbf{A}\|_*$ is denoted as nuclear norm of the matrix $\mathbf{A}$. Such approximation has been well studied in compressive sensing and sparse matrix completion problems, such as [30, 31] and references therein. Moreover, the rank constraint (9) on the desired signal can be replaced by Hermitian positive semidefinite matrix; that is,

$$\sigma_{\min}\left(\mathbf{U}_k^H\mathbf{H}_{kk}\mathbf{V}_k\right) \geq \epsilon, \quad \mathbf{U}_k^H\mathbf{H}_{kk}\mathbf{V}_k \succeq 0, \tag{10}$$

where $\sigma_{\min}(\mathbf{A})$ denotes the minimum singular value of the matrix $\mathbf{A}$. Note that the closed set, $\sigma_{\min}(\mathbf{U}_k^H\mathbf{H}_{kk}\mathbf{V}_k) \geq \epsilon$ and $(\mathbf{U}_k^H\mathbf{H}_{kk}\mathbf{V}_k) \succeq 0$, is a subset of Hermitian positive definite matrix; that is, $\mathbf{U}_k^H\mathbf{H}_{kk}\mathbf{V}_k = (\mathbf{U}_k^H\mathbf{H}_{kk}\mathbf{V}_k)^H$ and $\sigma_{\min}(\mathbf{U}_k^H\mathbf{H}_{kk}\mathbf{V}_k) > 0$. As ϵ gets closer to 0, the two sets asymptotically overlap [28]. As a result, the underlying rank-constrained problem can be approximated as

$$\begin{aligned}
&\underset{\mathbf{U}_k,\mathbf{V}_l}{\text{minimize}} \quad \sum_{k=1}^{K}\sum_{l=1,l\neq k}^{K}\left\|\mathbf{U}_k^H\mathbf{H}_{kl}\mathbf{V}_l\right\|_F^2, && (11)\\
&\text{subject to} \quad \left\|\mathbf{J}_p\right\|_* \leq \varepsilon, && (12)\\
&\qquad \sigma_{\min}\left(\mathbf{U}_k^H\mathbf{H}_{kk}\mathbf{V}_k\right) \geq \epsilon, \quad \mathbf{U}_k^H\mathbf{H}_{kk}\mathbf{V}_k \succeq 0. && (13)
\end{aligned}$$

The remaining problem is still nonconvex due to simultaneously optimizing the precoding matrix $\mathbf{V}_k$ and the receiving beamforming matrix $\mathbf{U}_k$; therefore, the alternating minimization is introduced; that is, temporarily holding the receiver matrices fixed, we can optimize the objective function for the remaining variables, alternating between which variables are held fixed and which are updated. More specifically, with fixed $\{\mathbf{U}_l\}_{l=1}^K$, the precoders $\{\mathbf{V}_k\}_{k=1}^K$ are obtained by solving the following problem:

$$\begin{aligned}
&\underset{\mathbf{V}_k}{\text{minimize}} \quad \sum_{k=1}^{K}\sum_{l=1,l\neq k}^{K}\left\|\mathbf{U}_l^H\mathbf{H}_{lk}\mathbf{V}_k\right\|_F^2,\\
&\text{subject to} \quad \sum_{k=1}^{K}\left\|\mathbf{U}_p^H\mathbf{H}_{pk}\mathbf{V}_k\right\|_* \leq \varepsilon, && (14)\\
&\qquad \sigma_{\min}\left(\mathbf{U}_k^H\mathbf{H}_{kk}\mathbf{V}_k\right) \geq \epsilon, \quad \mathbf{U}_k^H\mathbf{H}_{kk}\mathbf{V}_k \succeq 0.
\end{aligned}$$

Then, the receiver matrices $\{\mathbf{U}_k\}_{k=1}^K$ are achieved by using the solutions $\{\mathbf{V}_l\}_{l=1}^K$ as an input, such as

$$\begin{aligned}
&\underset{\mathbf{U}_k}{\text{minimize}} \quad \sum_{k=1}^{K}\sum_{l=1,l\neq k}^{K}\left\|\mathbf{U}_k^H\mathbf{H}_{kl}\mathbf{V}_l\right\|_F^2, && (15)\\
&\text{subject to} \quad \sigma_{\min}\left(\mathbf{U}_k^H\mathbf{H}_{kk}\mathbf{V}_k\right) \geq \epsilon, \quad \mathbf{U}_k^H\mathbf{H}_{kk}\mathbf{V}_k \succeq 0.
\end{aligned}$$

Given: $\varepsilon \geq 0$, and $\epsilon \geq 0$, $\mathbf{U}_0$, and $\mathbf{U}_k^{(0)}$
repeat
(1) Solve the subproblem (14) with fixed $\mathbf{U}_k^{(i-1)}$,
Output $\mathbf{V}_k^i$
(2) Solve the subproblem (15) with fixed $\mathbf{V}_k^{(i)}$,
Output $\mathbf{U}_k^i$
until objective function $\|\text{Obj}^{(i)} - \text{Obj}^{(i-1)}\| \leq \varsigma$
Output: $\mathbf{U}_k^{\text{opt}}$, and $\mathbf{V}_k^{\text{opt}}$

Algorithm 1: Rank-constrained beamforming design.

Now, each optimization problem is convex which can be solved by using CVX toolbox [32]. We continue by iterating this process until it converges in terms of the cost function or stop it when the iteration number achieves the maximum prespecified number. Note that the constraint on the CR interferences to the PU is not included when selecting the receiving beamforming. The step-by-step algorithm is presented in Algorithm 1.

Proposition 1. *Under the same prespecified interference threshold, the nuclear norm constraint (12) is equal to or tighter than the interference temperature constraint (3) in terms of power.*

Proof. Supposing the matrix $\mathbf{A} \in \mathbb{C}^{m\times n}$ with rank r, the matrix norm inequality is held [33]; that is,

$$\|\mathbf{A}\|_F \leq \|\mathbf{A}\|_*, \tag{16}$$

where the Frobenius norm $\|\mathbf{A}\|_F = \sqrt{\text{tr}\{\mathbf{A}^H\mathbf{A}\}} = \sqrt{\sum_{i=1}^{\min\{m,n\}}\sigma_i^2}$ and the nuclear norm $\|\mathbf{A}\|_* = \text{tr}\{\sqrt{\mathbf{A}^H\mathbf{A}}\} = \sum_{i=1}^{\min\{m,n\}}\sigma_i$ (σ_i is the ith singular value of the matrix $\mathbf{A}$). Once the optimum solution is achieved, we have

$$\begin{aligned}
&\left\|\mathbf{U}_p^H\mathbf{H}_{pk}\mathbf{V}_k^{*^{\text{IM}}}\right\|_F = \varepsilon,\\
&\left\|\mathbf{U}_p^H\mathbf{H}_{pk}\mathbf{V}_k^{*^{\text{RCIM}}}\right\|_F \leq \left\|\mathbf{U}_p^H\mathbf{H}_{pk}\mathbf{V}_k^{*^{\text{RCIM}}}\right\|_* = \varepsilon,
\end{aligned} \tag{17}$$

under the same prespecified interference threshold, where $\mathbf{V}_k^{*^{\text{IM}}}$ is defined as the optimal precoding under the standard interference temperature and $\mathbf{V}_k^{*^{\text{RCIM}}}$ is the optimal precoding under the nuclear norm constraint. It leads to the result straightforwardly obtained. □

Remark 1. Since the nuclear norm is a surrogate approximation of the rank, the optimization problem under the rank constraint (7) leaks fewer CR interferences to the PU-Rx in terms of power, compared with that under the standard interference temperature.

Remark 2. It is worth emphasizing the key difference between the optimization problem with the proposed rank constraint and that with standard interference temperature [16, 17, 23–25]. Although it seems simple to replace the rank constraint

on the CR interferences with the standard interference temperature, the proposed constraint actually provides a new way to investigate the interference *metric* of the CR network. Section 5 shows that the higher DoF of the primary links can be achieved under the new interference *metric* compared with that under the standard one.

Remark 3. Each iteration reduces the objective function $\sum_{k=1}^{K}\sum_{l=1,l\neq k}^{K}\|\mathbf{U}_k^H\mathbf{H}_{kl}\mathbf{V}_l\|_F^2$, which is the nonnegative function. As a result, it is clear that the objective function decreases monotonically. Moreover, the objective function is not jointly convex on $\mathbf{U}_k$ and $\mathbf{V}_k$. Hence, although each step of the proposed algorithms finds the minimum of the objective function over the optimized variables, the proposed algorithm is not guaranteed to converge to the global optimum; only local optimum is guaranteed. More details are presented in Section 5.

Remark 4. In this work, the precoders and receiving beamformers are iteratively optimized via the centralized approach which is difficult to implement for distributed SUs. Minimization of the interference subspace can be an alternative algorithm where the interference subspace of the kth SU can be expressed as $\mathbf{R}_k = [\mathbf{H}_{k1}\mathbf{V}_1,\ldots,\mathbf{H}_{k,k-1}\mathbf{V}_{k-1}, \mathbf{H}_{k,k+1}\mathbf{V}_{k+1},\ldots,\mathbf{H}_{kK}\mathbf{V}_K]$, and the optimization problem can be solved by following the process in [13].

4. Rank-Constrained Interference Rank Minimization Beamforming

Due to its effective interference elimination, the IA scheme has been introduced in CR network. Most recent works cancel the interferences of the secondary links in terms of power, such as interference leakage minimization [16, 23–25] and SINR maximization [17]. However, the key concept of the IA is to select precoder matrices $\{\mathbf{V}_k\}_{k=1}^K$ and receiver subspaces spanned by $\{\mathbf{U}_k\}_{k=1}^K$ such that each receiver can decode its own signal by forcing interfering users to share a reduced-dimensional subspace [1]

$$\begin{aligned}\operatorname{rank}\left(\mathbf{U}_k^H\mathbf{H}_{k,k}\mathbf{V}_k\right) &= d_k,\\ \mathbf{U}_k^H\mathbf{H}_{k,l}\mathbf{V}_l &= 0.\end{aligned} \tag{18}$$

In other words, the IA approach strives to maximize the achievable multiplexing gain per user. The interference-free subspace optimization framework can lead to better performance compared with the power optimizations, as suggested in [28, 29]. It motivates us to investigate the rank optimization framework in CR networks.

In order to understand the dimension optimization framework, we follow the definition of the *signal* and *interference* matrices of the secondary transmission [28, 29]:

$$\begin{aligned}&\mathbf{S}_k\left(\mathbf{U}_k,\mathbf{V}_k\right) \triangleq \mathbf{U}_k^H\mathbf{H}_{k,k}\mathbf{V}_k,\\ &\mathbf{J}_k\left(\mathbf{U}_k,\{\mathbf{V}_l\}_{l=1}^K\right)\\ &\quad\triangleq \mathbf{U}_k^H\left[\mathbf{H}_{k,1}\mathbf{V}_1,\ldots,\mathbf{H}_{k,l}\mathbf{V}_l,\ldots,\mathbf{H}_{k,K}\mathbf{V}_K\right],\end{aligned} \tag{19}$$

where the dimensions of signal and interference matrices are $\mathbf{S}_k \in \mathbb{C}^{d_k\times d_k}$ and $\mathbf{J}_k \in \mathbb{C}^{d_k\times[(K-1)d_k]}$. For simplicity, we refer to $\mathbf{S}_k(\mathbf{U}_k,\mathbf{V}_k)$ and $\mathbf{J}_k(\mathbf{U}_k,\{\mathbf{V}_l\}_{l=1}^K)$ as $\mathbf{S}_k$ and $\mathbf{J}_k$. Consequently, the achievable multiplexing gain of the kth SU can be expressed as

$$\mathrm{DoF}_k = \left[\operatorname{rank}\left(\mathbf{S}_k\right) - \operatorname{rank}\left(\mathbf{J}_k\right)\right]^+, \tag{20}$$

where $\operatorname{rank}(\mathbf{S}_k) \geq \operatorname{rank}(\mathbf{J}_k)$, or else $\mathrm{DoF}_k = 0$. To aim for d_k interference-free dimensions per SU, proper precoding and receiving beamforming matrices are selected to maximize the achievable DoF in (20) while maintaining the full rank of the desired signal of secondary user and aligning the CR interferences to a reduced-dimensional subspace of the primary receiver; that is,

$$\underset{\mathbf{V}_k,\{\mathbf{U}_k\}_{k=1}^K}{\text{minimize}} \quad \operatorname{rank}\left(\mathbf{J}_k\right), \tag{21}$$

$$\text{subject to} \quad \operatorname{rank}\left(\mathbf{S}_k\right) = d_k, \tag{22}$$

$$\operatorname{rank}\left(\mathbf{J}_p\right) = 0, \tag{23}$$

due to

$$\begin{aligned}&\underset{\mathbf{U}_k,\mathbf{V}_k}{\text{maximize}}\left[\operatorname{rank}\left(\mathbf{S}_k\right) - \operatorname{rank}\left(\mathbf{J}_k\right)\right]\\ &\Longleftrightarrow \underset{\mathbf{U}_k,\mathbf{V}_k}{\text{maximize}}\left[d_k - \operatorname{rank}\left(\mathbf{J}_k\right)\right]\\ &\Longleftrightarrow \underset{\mathbf{U}_k,\mathbf{V}_k}{\text{minimize}}\operatorname{rank}\left(\mathbf{J}_k\right).\end{aligned} \tag{24}$$

However, it is difficult to solve the K optimization problem in parallel, which can be reformulated as the sum of the interference dimension minimizations subject to the rank constraints instead. Moreover, the rank function is nonconvex and intractable, and hence, the underlying problem can be further approximated as

$$\begin{aligned}&\underset{\mathbf{V}_k,\{\mathbf{U}_k\}_{k=1}^K}{\text{minimize}} \quad \sum_{k=1}^{K}\left\|\mathbf{J}_k\right\|_*,\\ &\text{subject to} \quad \left\|\mathbf{J}_p\right\|_* \leq \varepsilon,\\ &\qquad \sigma_{\min}\left(\mathbf{U}_k^H\mathbf{H}_{kk}\mathbf{V}_k\right) \geq \epsilon, \quad \mathbf{U}_k^H\mathbf{H}_{kk}\mathbf{V}_k \geq 0.\end{aligned} \tag{25}$$

The optimal precoding and receiving beamforming can be selected by alternating minimization algorithm, and the subproblems can be efficiently solved via CVX toolbox [34].

Remark 5. The objective function (21) can be approximated as the reweighted nuclear norm which uses the sum of log surrogate functions with a weight matrix. It can provide better approximation compared with the standard nuclear norm approximation, leading to an improvement of the sum rate and the achievable DoF, especially when the perfect IA is not feasible, suggested in [28]. In this work, we investigate the difference between the dimension optimization and the power optimization. Therefore, the further improvement of the objective function is beyond our discussion and will be presented in future work.

5. Simulations

We consider the MIMO cognitive radio network where the $(4 \times 4, 3)^2$ MIMO cognitive interference channel is considered, which follows the same manner $(M \times N, d)^K$ for the K-user MIMO cognitive interference channel [35]. The channel is assumed as a flat-fading channel, where each channel element is drawn independently identically distributed (i.i.d) from a complex Gaussian distribution with mean zero and variance 1, and each link has the unit variance of white Gaussian noise. The transmit power is equally allocated to each column of the precoding matrices, that is, $10^{P/10}/d_k$; consequently, the SNR per user is P dB. The algorithms stop once the difference of the objective functions that obtained the two iterations is less than 0.001. Note that, in order to illustrate the effect of the CR interferences on primary transmission, single primary transmission is considered, in which the interferences from its own link are perfectly aligned. Three IA approaches are presented, that is, the interference minimization algorithm subject to the standard constraint, *interference temperature* [25, 36], the proposed rank-constrained interference minimization design, and the developed rank-constrained interference rank minimization approach. For simplicity, we abbreviate the standard approach as IM and the proposed algorithms as *rank-constrained IM* and *rank-constrained IRM*, respectively. Each point is based on 200 Monte Carlo iterations on National Super Computing Center in Guangzhou Tianhe II supercomputer.

5.1. Performance with respect to Fixed Interference Threshold. In this subsection, we present the system performances under the interference temperature and the interference rank constraint and demonstrate the difference between the standard and new metrics, where the thresholds of the interference *metrics* are set equally to $\varepsilon = 1.5$.

The performance of the average sum rate and the achievable multiplexing gain of secondary links is illustrated in Figures 2 and 3, respectively. The proposed rank-constrained IRM approach achieves the highest sum rate due to its highest achievable multiplexing gain, as shown in Figure 3. Meanwhile, compared with the standard IM algorithm, the proposed rank-constrained IM design obtains higher average sum rate. Due to $\|\mathbf{A}\|_F \leq \|\mathbf{A}\|_*$, the nuclear norm surrogate is tighter than the Frobenius norm constraint under the same interference threshold, leading to less interference leaking to the PU-Rx. Consequently, more power would be concentrated on the cognitive transmission, resulting in the improvement on the sum rate of the secondary links. Taking the multiplexing gain as optimization objective, the rank-constrained IM design achieves the highest DoF, followed in order by the proposed rank-constrained IM design and the standard IM design. These two figures clearly demonstrate the key difference between the power minimization approach and the dimension minimization framework (including the two proposed algorithms): the interference minimization focuses on the power minimization with low energy of interference achieved, and the rank minimization designs reduce the dimensions of the subspace spanned by interference

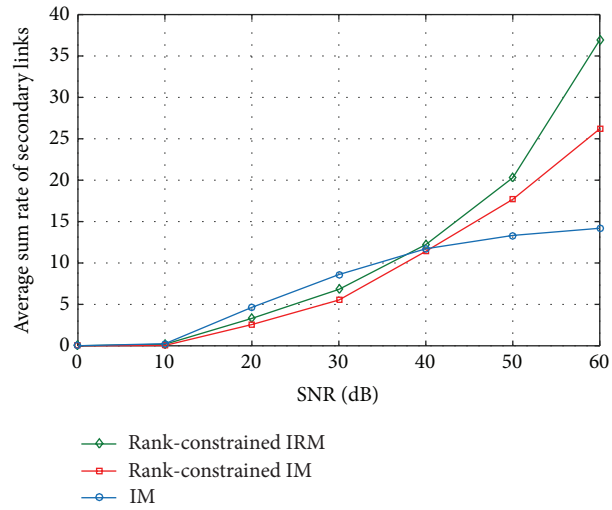

Figure 2: Average sum rate of secondary transmissions versus SNR ($\varepsilon = 0.9$).

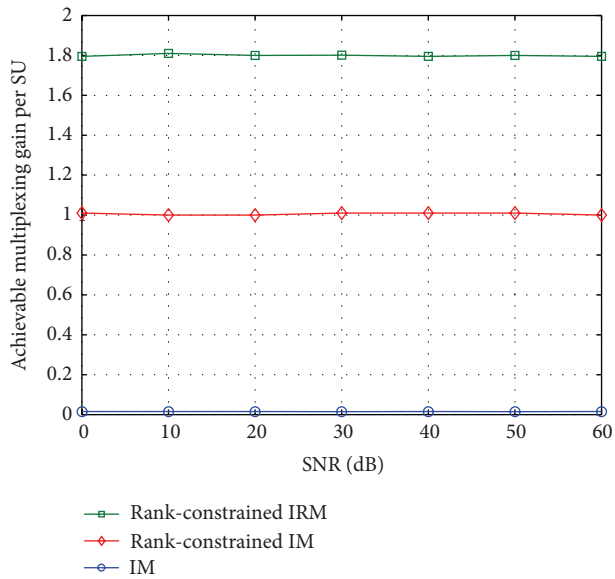

Figure 3: Achievable multiplexing gain of secondary transmissions versus SNR.

matrices. The latter one can provide more interference-free subspace for the indented signal, compared with the former one.

To further investigate the effect of the dimension constraint and the power constraint, the performance of the average sum rate and the achievable multiplexing gain of primary link is also presented. In Figure 4, the sum rate of the primary link tends to be a constant, which is caused by CR interferences, even though the rank-constrained IRM approach still obtains the highest sum rate among three algorithms. Figure 5 presents the advantage of the dimension constraint: the CR interferences under standard IM approach contaminate all receiver signal subspaces of the PU, while the interference-free subspace provided by the rank-constrained

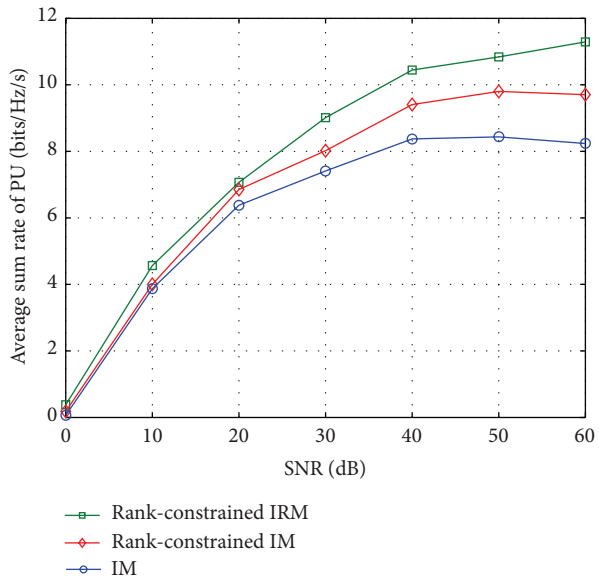

Figure 4: Average sum rate of primary link versus SNR ($\varepsilon = 0.9$).

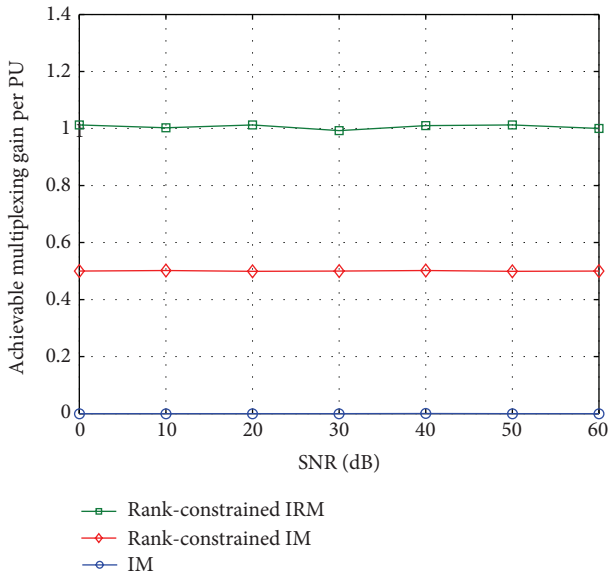

Figure 5: Achievable multiplexing gain of primary link versus SNR.

framework is larger than zero. Both figures show that the dimension constraint could be an effective interference *metric* in the underlay CR network, which can provide higher sum rate and interference-free subspace for the primary transmission.

Furthermore, Figure 6 presents the convergence of the objective function with SNR = 0 dB. As we expected, the objective functions of all three distributed algorithms converge monotonically. The proposed rank-constrained IRM approach has the fastest convergence speed, and the standard IM approach has the slowest one. Figure 7 further investigates the CR interferences to the PU-Rx under the rank-constrained IM, rank-constrained IRM, and IM algorithms. For fair comparison, the power of the CR interferences

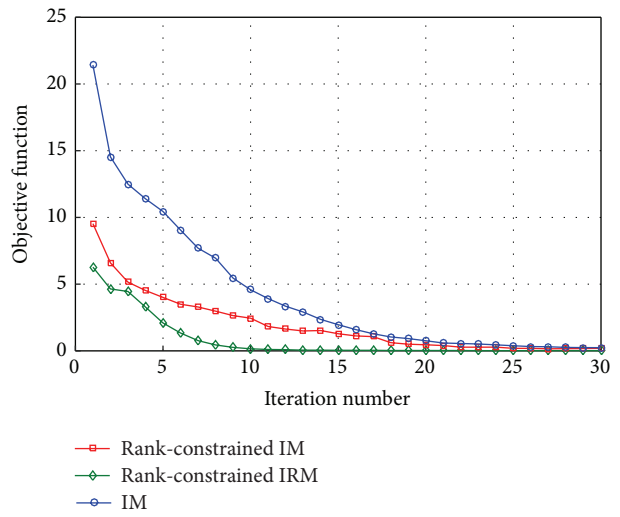

Figure 6: Convergence of the alternating algorithms (SNR = 0 dB).

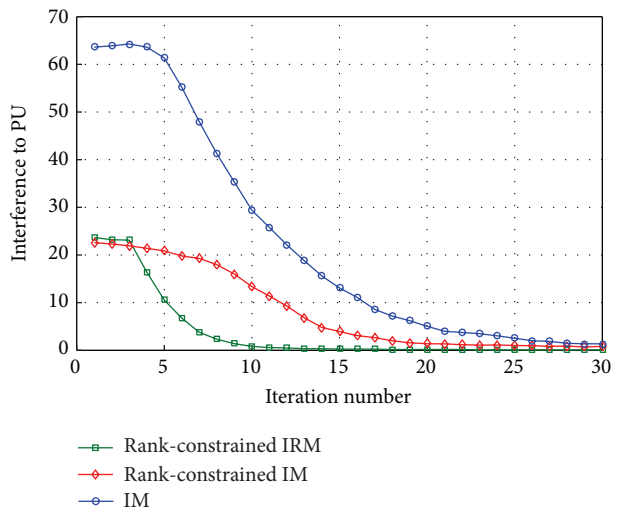

Figure 7: Convergence of the CR interference to PU (SNR = 0 dB).

is taken into account. It is clear that the converged CR interferences under the rank-constrained designs are lower than that under the interference temperature, which on the other hand confirms that the nuclear norm constraint is tighter than the Frobenius norm constraint.

5.2. Performance with respect to Varied Interference Threshold. In this subsection, we investigate the effect of different interference metrics. The SNRs of the cognitive links and primary link are equal to $P = 40$ dB, and the length of the transmitted signals in the primary link is $d_p = d_k = 3$.

Figures 8 and 9 present the performance of the sum rate and the achievable multiplexing gain of the secondary transmission, respectively. In Figure 8, the increased threshold of the interference *metrics* indicates that more power from the secondary links is allowed to leak into the primary transmission, leading to less power transmitting the secondary signals. As a result, the increased threshold degrades the performance

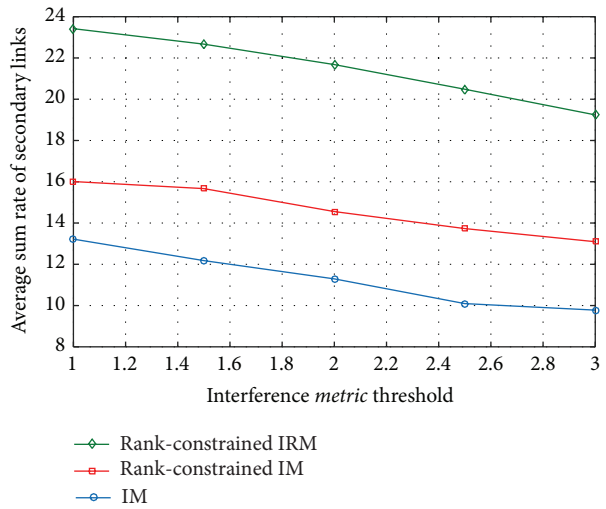

Figure 8: Average sum rate per SU under varied interference threshold.

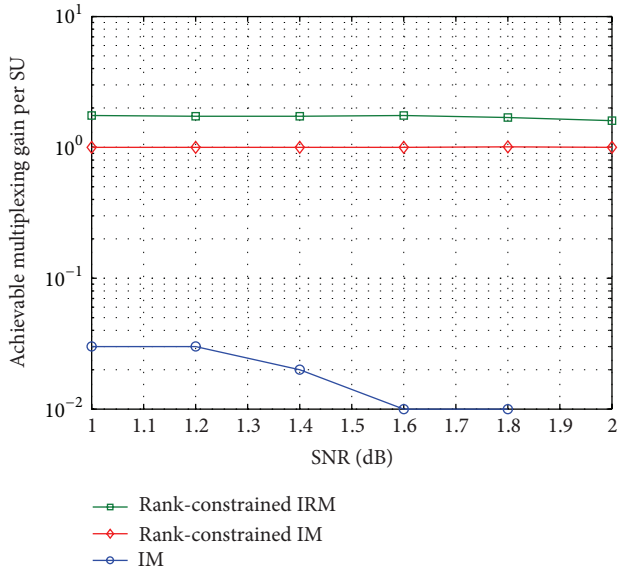

Figure 9: Achievable multiplexing gain per SU under varied interference threshold.

of the sum rate of the secondary links provided by all three algorithms. In terms of the average achievable multiplexing gain of the secondary links, Figure 9 demonstrates the advantage of the dimension maximization of the interference-free receiver subspace. The proposed rank-constrained IRM algorithm provides the best performance among all considered algorithms, followed by the proposed rank-constrained IM algorithm, while the traditional IM algorithm achieves the lowest interference-free subspace. The rank-constraint designs are less sensitive to the varied threshold since the dimensions of the CR interferences are limited to 2 due to $\lceil \varepsilon_i \rceil = 1$ ($i = 1, \ldots, 6$ and $\lfloor x \rfloor$ is the element of x to the nearest integer towards infinity). Compared with the proposed design, the standard IM is very sensitive to the varied threshold, where the achievable DoF becomes zero

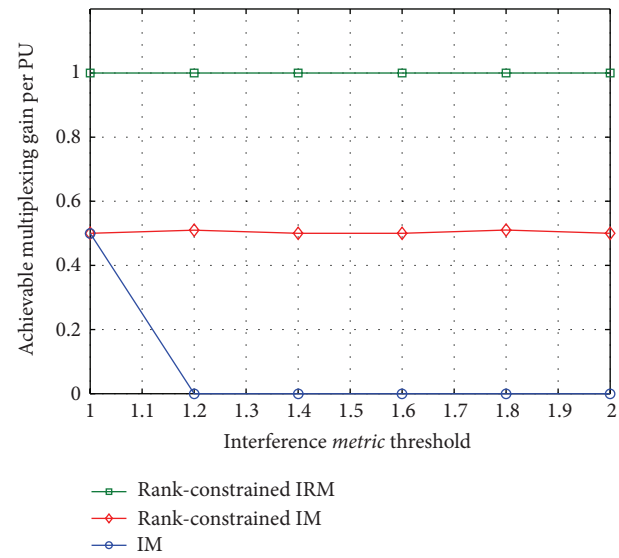

Figure 10: Achievable multiplexing gain per PU under varied interference threshold.

as long as $\varepsilon \geq 1.6$. Both Figures 8 and 9 indicate that the consideration of the dimension optimization is reasonable and effective.

Figure 10 presents the advantage of the developed framework in terms of the average achievable multiplexing gain of the primary link, which provides overall better performance than the IM approach. More specifically, when the threshold increases to 2, the IM designs cannot obtain any multiplexing gain at PU-Rx, while the proposed framework achieves $\mathrm{DoF}_p = 0.5$ (in rank-constrained IM) and $\mathrm{DoF}_p = 1$ (in rank-constrained IRM), respectively. It is because the developed algorithms strive to align the CR interferences into a reduced-dimensional subspace at PU-Rx that only low-dimensional signal subspace would be contaminated by the CR interferences, even if perfect alignment is not achievable at PU-Rx.

In addition, Figure 11 illustrates the iteration number under the varied interference threshold. Interestingly, we find that the rank-constrained IRM algorithm has the lowest computation complexity, and the IM algorithm has the highest complexity, which suggests that the proposed algorithm is practicable.

5.3. Performance with respect to Implicit Advantages. In the subsection, we further explore the implicit advantages of the proposed algorithms in terms of the robustness against imperfect CSI and varied feasibility conditions, shown in Figures 12, 13, and 14, respectively. The imperfect channel state information (CSI) is modeled as $\widehat{\mathbf{H}} = \sqrt{1-\delta}\mathbf{H} + \sqrt{\delta}\mathbf{E}$, where $\delta^2 = 0.15$. Figure 12 shows that the proposed RCRM algorithm has the potential robustness against the imperfections, since the RCRM framework strives to minimize the dimension of the interferences rather than the power.

Moreover, two different feasibility conditions are considered, that is, $(4 \times 4, 2)^3$ and $(4 \times 4, 3)^2$ with single PU ($M_p = N_p = 2$, $d_p = 2$, $P = 1$). When the perfect IA cannot be

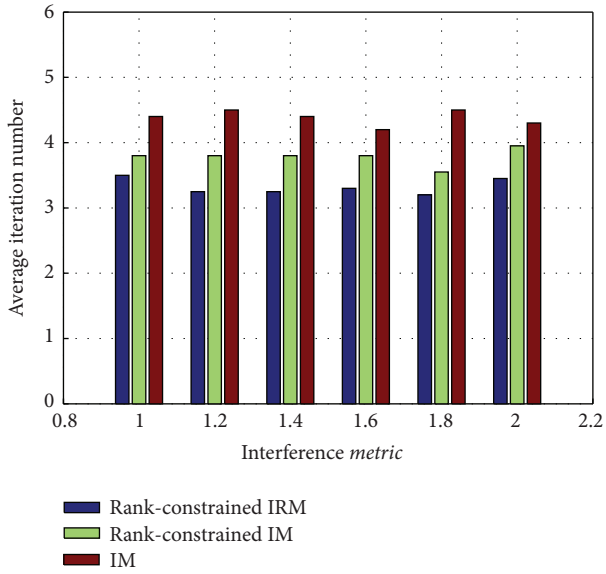

Figure 11: Iteration number under the varied interference threshold.

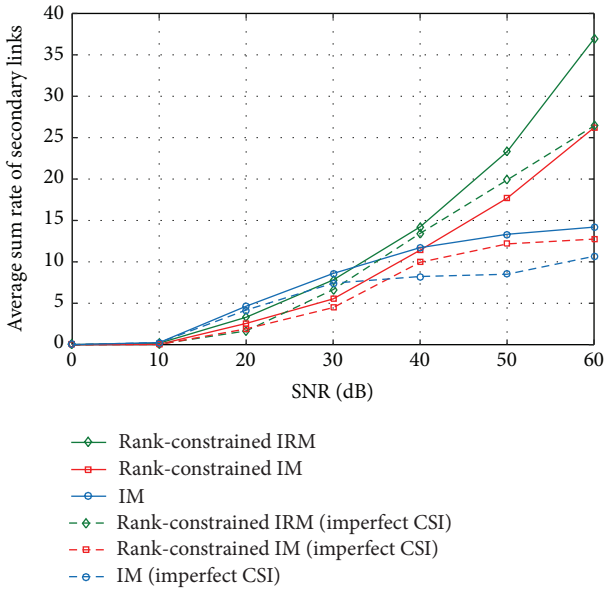

Figure 12: Robustness of the proposed algorithm with respect to average sum rate of secondary transmissions.

achieved, the proposed algorithm still can achieve reasonable performance with no limitation on the number of transmit antennas, receiving antennas, and secondary users and the length of transmit data. In Figures 13 and 14, the higher sum rate of the secondary transmission can be achieved under the configuration of $(4 \times 4, 2)^3$, compared with that under $(4 \times 4, 3)^2$ system in the low and moderate SNR region. However, the curves of the sum rate become flat, which indicates that the interference increases with the increase of SNR, leading to the degradation of the sum rate of primary transmission.

Finally, the scenario that the multiple PUs coexist with multiple SUs is presented in Figure 15. In multiple primary

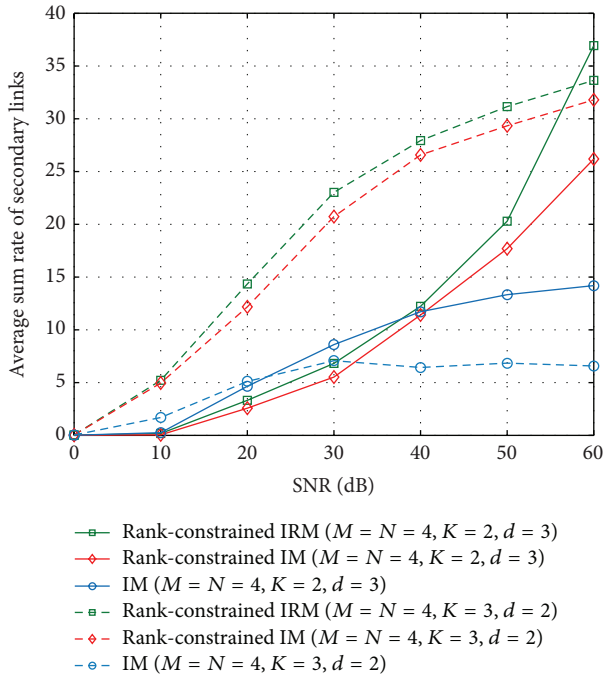

Figure 13: Average sum rate of secondary transmissions with two feasible conditions.

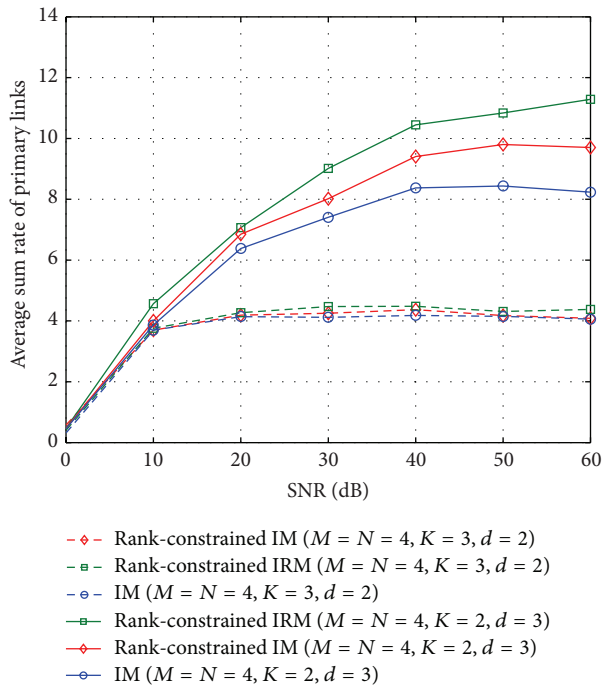

Figure 14: Average sum rate of primary transmissions with two feasible conditions.

links, we assume that there might exist interferences between multiple primary links by generating the primary receiving beamforming randomly. The sum rate of the secondary links is limited by the multiple CR interference constraints, and its performance of the sum rate is degraded especially in high SNR region. However, the rank-constrained IRM

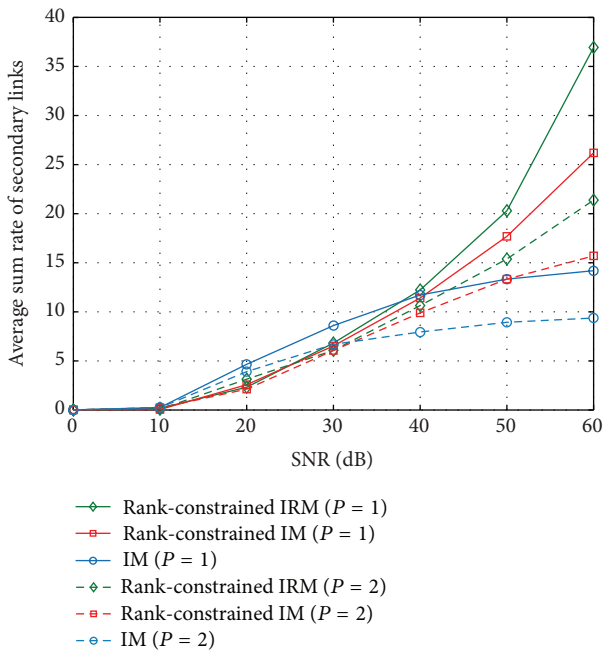

Figure 15: Single PU versus multi-PUs in terms of average sum rate of secondary transmissions.

still achieves the best performance compared with rank-constrained IM and standard IM, due to the rank minimization. The numerical simulation results motivate us to explore the corresponding mathematical background in our future work.

6. Conclusion

In this paper, we developed a rank-constrained beamforming algorithm for MIMO cognitive radio network. Instead of using the *interference temperature*, a rank constraint on CR interferences to the PU-Rxs is proposed, which aligns the CR interferences into a reduced-dimensional subspace. The optimal precoding and receiving beamforming matrices are designed by minimizing the total interferences of the cognitive interference channel subject to the rank constraints on CR interferences and SUs and achieved iteratively via alternating minimization. The rank-constrained design is further improved to minimize the dimension of the interference of the cognitive interference channel. Numerical results show that the proposed algorithm and its development not only improve the achievable average sum rate of the SUs and PU, but also provide more DoF of the interference-free subspace for the primary transmission, under the help of the rank constraint on CR interferences.

Competing Interests

The authors declare that there is no conflict of interests regarding the publication of this paper.

Acknowledgments

The work of Zujian Wu is supported by the Fundamental Research Funds for the Central Universities (no. 21615316) and Special Program for Applied Research on Super Computation of the NSFC-Guangdong Joint Fund (the second phase). The work of Huiqin Du is supported by the Fundamental Research Funds for the Central Universities and National Natural Science Foundation of China (no. 61401178).

References

[1] V. R. Cadambe and S. A. Jafar, "Interference alignment and spatial degrees of freedom of the K-user interference channel," in *Proceedings of the IEEE International Conference on Communications (ICC '08)*, pp. 971–975, May 2008.

[2] S. W. Peters and R. W. Heath Jr., "Interference alignment via alternating minimization," in *Proceedings of the IEEE International Conference on Acoustics, Speech, and Signal Processing (ICASSP '09)*, pp. 2445–2448, April 2009.

[3] K. R. Kumar and F. Xue, "An iterative algorithm for joint signal and Interference Alignment," in *Proceedings of the IEEE International Symposium on Information Theory (ISIT '10)*, pp. 2293–2297, Austin, Tex, USA, June 2010.

[4] B. Nosrat-Makouei, J. G. Andrews, and R. W. Heath Jr., "A simple SINR characterization for linear interference alignment over uncertain MIMO channels," in *Proceedings of the IEEE International Symposium on Information Theory (ISIT '10)*, pp. 2288–2292, Austin, Tex, USA, June 2010.

[5] E. Chiu, V. K. N. Lau, H. Huang, T. Wu, and S. Liu, "Robust transceiver design for K-pairs quasi-static MIMO interference channels via semi-definite relaxation," *IEEE Transactions on Wireless Communications*, vol. 9, no. 12, pp. 3762–3769, 2010.

[6] K. Gomadam, V. R. Cadambe, and S. A. Jafar, "Approaching the capacity of wireless networks through distributed interference alignment," in *Proceedings of the IEEE Global Telecommunications Conference (GLOBECOM '08)*, pp. 4260–4265, New Orleans, La, USA, December 2008.

[7] H. Sung, S.-H. Park, K.-J. Lee, and I. Lee, "Linear precoder designs for K-user interference channels," *IEEE Transactions on Wireless Communications*, vol. 9, no. 1, pp. 291–301, 2010.

[8] H. Huang, V. K. Lau, Y. Du, and S. Liu, "Robust lattice alignment for K-user MIMO interference channels with imperfect channel knowledge," *IEEE Transactions on Signal Processing*, vol. 59, no. 7, pp. 3315–3325, 2011.

[9] H. Yu and Y. Sung, "Least squares approach to joint beam design for interference alignment in multiuser multi-input multi-output inferference channels," *IEEE Transactions on Signal Processing*, vol. 58, no. 9, pp. 4960–4966, 2010.

[10] H. Shen, B. Li, M. Tao, and X. Wang, "MSE-based transceiver designs for the MIMO interference channel," *IEEE Transactions on Wireless Communications*, vol. 9, no. 11, pp. 3480–3489, 2010.

[11] M. Guillaud and D. Gesbert, "Interference alignment in the partially connected K-user MIMO interference channel," in *Proceedings of the 19th European Signal Processing Conference (EUSIPCO '11)*, pp. 1095–1099, Barcelona, Spain, September 2011.

[12] M. Guillaud and D. Gesbert, "Interference alignment in partially connected interfering multiple-access and broadcast channels," in *Proceedings of the IEEE Global Telecommunications*

Conference (GLOBECOM '11), pp. 1–5, IEEE, Houston, Tex, USA, December 2011.

[13] G. Sridharan and W. Yu, "Linear beamformer design for interference alignment via rank minimization," *IEEE Transactions on Signal Processing*, vol. 63, no. 22, pp. 5910–5923, 2015.

[14] F. Negro, S. P. Shenoy, D. T. M. Slock, and I. Ghauri, "Interference alignment limits for K-user frequency-flat MIMO interference channels," in *Proceedings of the 17th European Signal Processing Conference (EUSIPCO '09)*, pp. 2445–2449, Glasgow, Scotland, August 2009.

[15] H. Zhou and T. Ratnarajah, "A novel interference draining scheme for cognitive radio based on interference alignment," in *Proceedings of the IEEE Symposium on New Frontiers in Dynamic Spectrum (DySPAN '10)*, pp. 6–9, April 2010.

[16] J.-M. Wu, T.-F. Yang, and H.-J. Chou, "MIMO active interference alignment for underlay cognitive radio," in *Proceedings of the IEEE International Conference on Communications Workshops (ICC '10)*, pp. 1–5, Cape Town, South Africa, May 2010.

[17] X. Li, N. Zhao, Y. Sun, and F. R. Yu, "Interference alignment based on antenna selection with imperfect channel state information in cognitive radio networks," *IEEE Transactions on Vehicular Technology*, 2015.

[18] L. Sboui, H. Ghazzai, Z. Rezki, and M. S. Alouini, "On achievable rate of two-way relaying cognitive radio with space alignment," in *Proceedings of the IEEE International Conference on Communications (ICC '15)*, pp. 7628–7632, June 2015.

[19] A. Alizadeh, H. R. Bahrami, M. Maleki, and S. Sastry, "Spatial sensing and cognitive radio communication in the presence of a K-user interference primary network," *IEEE Journal on Selected Areas in Communications*, vol. 33, no. 5, pp. 741–754, 2015.

[20] Z. Cheng, N. Devroye, and T. Liu, "The degrees of freedom of full-duplex bidirectional interference networks with and without a MIMO relay," *IEEE Transactions on Wireless Communications*, vol. 15, no. 4, pp. 2912–2924, 2016.

[21] H. Zeng, Y. Shi, Y. T. Hou, W. Lou, S. Kompella, and S. F. Midkiff, "An analytical model for interference alignment in Multi-Hop MIMO networks," *IEEE Transactions on Mobile Computing*, vol. 15, no. 1, pp. 17–31, 2016.

[22] N. Zhao, F. R. Yu, and V. C. M. Leung, "Opportunistic communications in interference alignment networks with wireless power transfer," *IEEE Wireless Communications*, vol. 22, no. 1, pp. 88–95, 2015.

[23] M. Amir, A. El-Keyi, and M. Nafie, "Constrained interference alignment and the spatial degrees of freedom of mimo cognitive networks," *IEEE Transactions on Information Theory*, vol. 57, no. 5, pp. 2994–3004, 2011.

[24] P.-J. Chung, H. Du, and J. Gondzio, "A probabilistic constraint approach for robust transmit beamforming with imperfect channel information," *IEEE Transactions on Signal Processing*, vol. 59, no. 6, pp. 2773–2782, 2011.

[25] S. Ma, H. Du, T. Ratnarajah, and L. Dong, "Robust joint signal and interference alignment in cognitive radio networks with ellipsoidal channel state information uncertainties," *IET Communications*, vol. 7, no. 13, pp. 1360–1366, 2013.

[26] W. Guo, W. Xu, J. Lin, and L. Fu, "Adaptive eigenmodes beamforming and interference alignment in underlay and overlay cognitive networks," in *Proceedings of the IEEE 26th Annual International Symposium on Personal, Indoor, and Mobile Radio Communications (PIMRC '15)*, pp. 798–802, Hong Kong, August 2015.

[27] J. Lee, H. Wang, J. G. Andrews, and D. Hong, "Outage probability of cognitive relay networks with interference constraints," *IEEE Transactions on Wireless Communications*, vol. 10, no. 2, pp. 390–395, 2011.

[28] H. Du, T. Ratnarajah, M. Sellathurai, and C. B. Papadias, "Reweighted nuclear norm approach for interference alignment," *IEEE Transactions on Communications*, vol. 61, no. 9, pp. 3754–3765, 2013.

[29] D. S. Papailiopoulos and A. G. Dimakis, "Interference alignment as a rank constrained rank minimization," *IEEE Transactions on Signal Processing*, vol. 60, no. 8, pp. 4278–4288, 2012.

[30] E. J. Candes, M. B. Wakin, and S. P. Boyd, "Enhancing sparsity by reweighted l1 minimization," *The Journal of Fourier Analysis and Applications*, vol. 14, no. 5-6, pp. 877–905, 2008.

[31] M. Fazel, *Matrix rank minimization with applications [Ph.D. thesis]*, Stanford University, Stanford, Calif, USA, 2002.

[32] M. Grant and S. Boyd, "Matlab software for disciplined convex programming (web page and software)," http://arxiv.org/pdf/0909.4017.

[33] R. A. Horn and C. R. Johnson, *Matrix Analysis*, Cambridge Univeristy Pres, Cambridge, UK, 1985.

[34] S. Boyd and L. Vandenberghe, *Convex Optimization*, Cambridge University Press, Cambridge, UK, 2004.

[35] C. M. Yetis, T. Gou, S. A. Jafar, and A. H. Kayran, "Feasibility conditions for interference alignment," in *Proceedings of the IEEE Global Telecommunications Conference (GLOBECOM '09)*, pp. 1–6, Honolulu, Hawaii, USA, December 2009.

[36] H. Du, T. Ratnarajah, H. Zhou, and Y. C. Liang, "Interference alignment for peer-to-peer underlay MIMO cognitive radio network," in *Proceedings of the 45th Asilomar Conference on Signals, Systems and Computers (ASILOMAR '11)*, pp. 349–353, Pacific Grove, Calif, USA, November 2011.

Hindawi Publishing Corporation
Mobile Information Systems
Volume 2016, Article ID 1051632, 10 pages
http://dx.doi.org/10.1155/2016/1051632

Research Article

The Effect of Misdetection Probability on the Performance of Cooperative-Relaying-Based Cognitive Radio Systems

Ning Cao, Yuchang Ye, and Minghe Mao

School of Computer and Information, Hohai University, Nanjing 210098, China

Correspondence should be addressed to Yuchang Ye; ye_yuchang@163.com

Received 29 December 2015; Accepted 18 April 2016

Academic Editor: Chao Chen

Cognitive radio (CR) is a promising solution to address the more and more congested radio spectrum. Cooperative relaying can provide a better transmission performance for the secondary user (SU), while the performance of the primary user (PU, also named licensed user) should be preferentially protected especially when there is misdetection probability. In this paper, in order to keep the PU away from outage caused by the interference from the SU under a certain signal-to-noise ratio (SNR), the maximum SNR for the SU can be derived by using the rate decaying factor (RDF). Then, based on the maximum channel gain and the maximum SNR, the outage probability is analyzed using decode-and-forward (DF) relaying and amplify-and-forward (AF) relaying schemes. Numerical results show that the outage probability decreases when the power allocation factor increases for DF strategy, while the outage probability has error floor when the power allocation factor increases for AF strategy. And the relaying scheme based on the maximum channel gain outperforms that based on the maximum SNR when the power allocation factor and detection probability are small, while the relaying scheme based on the maximum SNR outperforms that based on the maximum channel gain when the power allocation factor is large. What is more, AF relaying has better outage performance in the practical implementation.

1. Introduction

In the CR system, the SUs share the PU bands. Therefore, it is a great challenge for CR systems to protect the PU signal away from the interference caused by the SU signal [1]. How to deal with the interference which is caused by the misdetection probability in the CR sensing period is a critical issue. In other words, on one hand, the performance of the SU transmission should be improved; on the other hand, the PU's transmission quality should be guaranteed. This requires the cooperative relaying with perfect sensing ability. In [2] the ideal sensing result is assumed on the PU's bands, and SUs only can communicate with each other through the common existing bands when they are not occupied by the PUs. Therefore, there will be no direct communication link which can be performed if there is no common band. The concept of cooperative relaying has been incorporated into cognitive radio system when there is no direct transmission link between two cognitive users. Cooperative transmission can maintain the SU's average throughput. The reason is that the cooperative relaying nodes provide additional spatial and spectrum diversity which improves the performance of the transmission between the source and the destination [3].

The cooperative relay has two main strategies: DF relaying and AF relaying. Cooperative communication is an efficient strategy that overcomes most of the limitations in wireless communications systems [4, 5]. Using cooperation, the users require less total power to achieve a certain throughput [4]. DF relaying uses relays to demodulate and decode the transmitted signal from the source before reencoding and retransmitting to the destination.

Related Work. In [6], a closed-form solution for the outage probability of DF relaying when the statistics of the channels between the source, relays, and destination are assumed to be independent and identically distributed was presented, while an exact closed-form expression for the outage probability of DF relaying in independent but not identically distributed dissimilar Rayleigh fading channels was derived in [7]. As a low-cost strategy, the AF relaying boosts the coverage and capacity of cellular networks, particularly in regions with signal shadowing [8]. The outage probability is a criterion

of the performance evaluation for cooperative relaying. The outage probability for AF relaying using variable gain nodes is accurately calculated in [9, 10]. Variable gain relay is a kind of common AF strategy which compensates the signal fading with the instantaneous channel state information (CSI). The fixed relay is another strategy which is analyzed in [11], while the instantaneous CSI in the fixed relay is not required compared with the variable gain relay.

The capacity theorems of DF relaying and AF relaying are proposed in [12]. Reference [13] analyzes and compares the performances of AF, DF, selection DF, and incremental AF strategies. The optimal resource allocation is researched for the Gaussian parallel fading relay channel under both full duplex and half duplex where the source and relay nodes are subject to separate power constraints [14]. The power allocation is investigated in a three-node CR network after the cooperative relay in direct, dual-hop, and relay channels is studied to acquire optimal throughput [15]. In [16], in the case that the Rayleigh instantaneous channel gain is exponentially distributed and available, the optimal outage probability is achieved using power allocation under source node and select nodes. In [17], the authors derive the optimal power allocation scheme using selection amplify-and-forward (S-AF) relay nodes to maximize the capacity in Rayleigh fading channel with known complete CSI and channel statistics. The outage probabilities of DF relaying and AF relaying with different power allocation factors were analyzed in [18], while [19] analyzes the outage probability of DF relaying and AF relaying using channel gain and signal-to-noise ratio (SNR) with different time duration allocation factors. However the impact of misdetection (one is the case in which the PU occupies the bands and is detected to be busy and another is the case in which the PU occupies the bands but is detected to be free; only the second midsection can cause interference to PU) probability in spectrum sensing period on the data transmission has not been discussed.

In this paper, we propose the concept of rate decaying factor (RDF). Using RDF, the SUs maximum SNR is derived in the premise of PU transmission link without interruption under the right PUs SNR. Then, using maximum channel gain and maximum SNR schemes, we analyze and calculate the outage probabilities of DF relaying and AF relaying for the relay node under the maximum SUs SNR with different power allocation factors.

2. System Model

The failure of spectrum sensing causes the SU signal to interfere with the PU on certain spectrum bands. As depicted in Figure 1, The PU's signal is truncated by the SU's signal when the bands are occupied but detected to be free. The SU's signal is the same as PU: one is from the SU's base station and another is from the relay nodes. The SU's signal is truncated by the PU's signal when the bands are occupied but detected to be free. So the SU and PU may interfere with each other when the bands are misdetected. g_0 represents the PU direct transmission link; f_0 and f_1 represent the interference links to the PU caused by the SU signal. On the other hand, the SU may be interfered with by the PU signal when it starts to

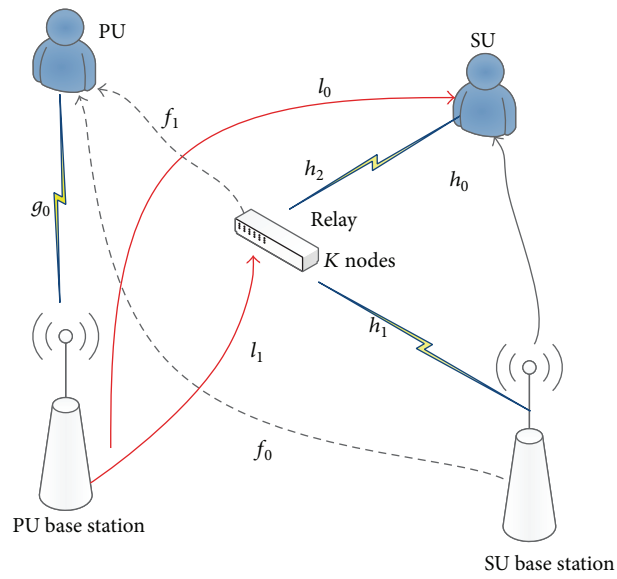

Figure 1: The system model.

utilize the PU spectrum bands in the case in which the PU is actually busy but is detected to be free; h_0 represents the SU direct transmission link, h_1 and h_2 represent the relaying links of the SU, and l_0 and l_1 represent the interference links to the SU caused by the PU. Furthermore, we assume the system is a full duplex system.

2.1. Decode-and-Forward Relaying Strategy. For DF strategy, there is the case that the PU is detected (P_D: PU is absent and is detected to be absent; PU is busy and is detected to be busy) or misdetected ($\overline{P_D}$; PU is absent but is detected to be busy; PU is busy but is detected to be absent). The received PU signal can be divided into two cases: one is the case in which the PU occupies bands and is detected to be busy; therefore the noise is the channel noise; the other is the case in which the PU occupies the bands but is detected to be free; thus the noises consist of not only the channel noise but also the SU signal. Considering these two cases, the received signal of PU (y_{pu}) can be represented as

$$y_{\text{pu}} = \begin{cases} g_0\sqrt{P_{\text{pu}}}x_{\text{pu}} + n_{\text{pu}}, & P_D, \\ g_0\sqrt{P_{\text{pu}}}x_{\text{pu}} + f_0\sqrt{\xi P_{\text{su}}}x_{\text{su}} + f_1\sqrt{(1-\xi)P_{\text{su}}}x_{\text{su}} + n_{\text{pu}}, & \overline{P_D}, \end{cases} \quad (1)$$

where P_{pu} is the PU transmitting power, P_{su} is the SU total transmitting power which contains the power of source node and relay nodes, x_{pu} is the PU transmitting signal, x_{su} is the SU transmitting signal, and we assume that $E\{|x_{\text{pu}}|^2\} = E\{|x_{\text{su}}|^2\} = 1$, g_0 is the average channel gain of the PU link, f_0 and f_1 are the average channel gains of interference link to the PU, n_{pu} is the PU noise, P_D is the detection probability in spectrum sensing period, and $\overline{P_D} = 1 - P_D$ is misdetection probability.

The received SU signal contains two main parts. The first part is the transmitted signal from the SU when the PU signal is absent and is actually detected to be free (P_D); the noise is only the channel noise. The second part contains not only the channel noise but also the PU signal when the PU signal is present but detected to be free ($\overline{P_D}$). Take all cases into account; the received signal from the direct link of SU (y_{su}) can be represented as

$$y_{\mathrm{su}} = \begin{cases} \widetilde{h_0}\sqrt{\xi P_{\mathrm{su}}}x_{\mathrm{su}} + n_{\mathrm{su}}, & P_D, \\ \widetilde{h_0}\sqrt{\xi P_{\mathrm{su}}}x_{\mathrm{su}} + l_0\sqrt{P_{\mathrm{pu}}}x_{\mathrm{pu}} + n_{\mathrm{su}}, & \overline{P_D}, \end{cases} \tag{2}$$

where $\widetilde{h_0}$ is the instantaneous channel gain of the SU direct link, l_0 is the average channel gain of interference link to the SU, ξ is the SU base station (BS) power allocation factor, and n_{su} is the SU noise.

When multihop relaying is performed the received signal of the kth node (r_k) is

$$r_k = \begin{cases} \widetilde{h_1^k}\sqrt{\xi P_{\mathrm{su}}}x_{\mathrm{su}} + n_{h_1}, & P_D, \\ \widetilde{h_1^k}\sqrt{\xi P_{\mathrm{su}}}x_{\mathrm{su}} + l_1\sqrt{P_{\mathrm{pu}}}x_{\mathrm{pu}} + n_{h_1}, & \overline{P_D}, \end{cases} \tag{3}$$

where $\widetilde{h_1^k}$ is the instantaneous channel gain of the relay link of the SU BS-to-relay nodes, l_1 is the average channel gain value of interference link to the SU, and n_{h_1} is the receiver noise.

The received signal from the relaying link of the SU ($y_{k-\mathrm{su}}$) is

$$y_{k-\mathrm{su}} = \begin{cases} \widetilde{h_2}\sqrt{(1-\xi)P_{\mathrm{su}}}x_{\mathrm{su}} + n_{h_2}, & P_D, \\ \widetilde{h_2}\sqrt{(1-\xi)P_{\mathrm{su}}}x_{\mathrm{su}} + \widetilde{h_2}l_1\sqrt{P_{\mathrm{pu}}}x_{\mathrm{pu}} + l_0\sqrt{P_{\mathrm{pu}}}x_{\mathrm{pu}} + n_{h_2}, & \overline{P_D}, \end{cases} \tag{4}$$

where $\widetilde{h_2}$ is the instantaneous channel gain of relay link from relay node to the SU and n_{h_2} is the channel noise of relay to the SU.

2.2. Amplify-and-Forward Relaying Strategy. For AF strategy, the channel noise introduced from the relay in the receiver is not considered for simplicity; in the case in which the PU is detected (P_D) or misdetected ($\overline{P_D}$) when it is actually present, the received signal of the PU (y_{pu}) can be represented as

$$y_{\mathrm{pu}} = \begin{cases} g_0\sqrt{\xi P_{\mathrm{pu}}}x_{\mathrm{pu}} + n_{\mathrm{pu}}, & P_D, \\ g_0\sqrt{\xi P_{\mathrm{pu}}}x_{\mathrm{pu}} + f_0\sqrt{\xi P_{\mathrm{su}}}x_{\mathrm{su}} + \alpha f_1\sqrt{(1-\xi)P_{\mathrm{su}}}x_{\mathrm{su}} + n_{\mathrm{pu}}, & \overline{P_D}, \end{cases} \tag{5}$$

where $\alpha = 1/h_1$ is the relay scale of AF relaying. The received signal for the kth relay node of the relay link is the same as (2).

The SU received signal of the relay link in the condition that the spectrum bands are detected and misdetected for the AF strategy can be represented as

$$y_{k-\mathrm{su}} = \begin{cases} \alpha\widetilde{h_2}\sqrt{(1-\xi)P_{\mathrm{su}}}x_k + n_{h_2}, & P_D, \\ \alpha\widetilde{h_2}\sqrt{(1-\xi)P_{\mathrm{su}}}x_k + \alpha\widetilde{h_2}l_1\sqrt{P_{\mathrm{pu}}}x_{\mathrm{pu}} + l_0\sqrt{P_{\mathrm{pu}}}x_{\mathrm{pu}} + n_{h_2}, & \overline{P_D}. \end{cases} \tag{6}$$

The Scheme for Selecting Node. (1) The maximum channel gain scheme: the maximum channel gain node is selected from the relay nodes through comparing the received signals; when the maximum channel gain is larger than the direct link channel gain, the relay link is selected to transmit the signal; otherwise the direct link is selected.

(2) The maximum SNR scheme: the maximum SNR node is selected from the relay nodes through comparing the received signals; when the maximum SNR is larger than the direct link SNR, the relay link is selected to transmit the signal; otherwise the direct link is selected.

The remainder of the paper is organized as follows. The system model and the relay nodes selected scheme are proposed in Section 2. In Section 3, the SUs' maximum SNR is derived through RDF in the premise of keeping PUs away from interruption under a certain PUs' SNR; then the outage probabilities of DF relaying and AF relaying based on the selected relay node using maximum channel gain and maximum SNR with different power allocation factors are analyzed. In Section 4, numerical results are discussed. In Section 5, we draw the conclusion.

3. System Analysis

3.1. Decode-and-Forward Relaying

3.1.1. Max Channel Gain. The average SNR of the PU when using the DF strategy can be written as

$$\gamma_{\mathrm{DF_{aver}}} = E\{\mathrm{SNR_{DF}}\} = P_D\gamma_{\mathrm{DF}_{P_D}} + (1-P_D)\gamma_{\mathrm{DF}_{\overline{P_D}}}, \tag{7}$$

where we consider n_{pu}, n_{su}, n_{h_2}, and n_{h_1} are the additive white Gaussian noises (AWGN) with zero mean and variance $E\{n_{\mathrm{pu}}, n_{\mathrm{su}}, n_{h_1}, n_{h_2}\} = N_0$, where $E[\cdot]$ denotes the expectation. $\gamma_{\mathrm{DF}_{P_D}}$ is the PU SNR under the probability of detection which can be written as

$$\gamma_{\mathrm{DF}_{P_D}} = \frac{{g_0}^2 P_{\mathrm{pu}}}{N_0} = {g_0}^2\gamma_{\mathrm{pu}}, \tag{8}$$

γ_{su} is the SU SNR, and $\gamma_{\mathrm{DF}_{\overline{P_D}}}$ is the PU SNR under the misdetection probability which can be written as

$$\gamma_{\mathrm{DF}_{\overline{P_D}}} = \frac{{g_0}^2\gamma_{\mathrm{pu}}}{1 + {f_0}^2\xi\gamma_{\mathrm{su}} + {f_1}^2(1-\xi)\gamma_{\mathrm{su}} + f_0f_1\sqrt{\xi(1-\xi)}\gamma_{\mathrm{su}}}. \tag{9}$$

The criterion to keep the PU away from interruption is $(1/2)\log(1+\gamma_{\mathrm{aver}}) > R_{\mathrm{pu}}^{\max}$ (γ_{aver} is the average SNR considering the PU interference signal). The maximum transmission

rate will be changed if the SNR changes; therefore we put forward the concept of rate decaying factor (RDF) and define the RDF as follows:

$$\eta = \frac{R_{\text{pu}}^{\max}}{R_{\text{pu}}}, \tag{10}$$

where $R_{\text{pu}} = (1/2)\log(1 + \gamma_{\text{DF}_{P_D}})$ is the maximum transmission rate without SU interference and $R_{\text{pu}}^{\max}$ is the maximum transmission considering the SU interference. The PU maximum transmission rate will decrease due to the interference from the SU signal.

Define the RDF value for DF strategy:

$$\eta_{\text{DF}} = \frac{1}{1 + P_D(1 - P_D)\left[{f_0}^2\xi + {f_1}^2(1 - \xi) + f_0 f_1\sqrt{\xi(1 - \xi)}\right]}. \tag{11}$$

Then the maximum SU SNR can be derived using (7), (10), and (11) as

$$\gamma_{\text{DF}_{\text{su}}} < \frac{{g_0}^2\gamma_{\text{pu}} - \left[\left(1 + \gamma_{\text{DF}_{P_D}}\right)^{\eta_{\text{DF}}} - 1\right]}{\phi\left[\left(1 + \gamma_{\text{DF}_{P_D}}\right)^{\eta_{\text{DF}}} - 1\right] - P_D{g_0}^2\phi\gamma_{\text{pu}}}, \tag{12}$$

where $\phi = {f_0}^2\xi + {f_1}^2(1 - \xi) + f_0 f_1\sqrt{\xi(1 - \xi)}$. Also, for AF strategy, the RDF value can be defined as

$$\eta_{\text{AF}} = \frac{1}{1 + P_D(1 - P_D)\left[{f_0}^2\xi + \alpha^2{f_1}^2(1 - \xi) + \alpha f_0 f_1\sqrt{\xi(1 - \xi)}\right]}. \tag{13}$$

Then the maximum SU SNR is

$$\gamma_{\text{AF}_{\text{su}}} < \frac{{g_0}^2\gamma_{\text{pu}} - \left[\left(1 + \gamma_{\text{DF}_{P_D}}\right)^{\eta_{\text{AF}}} - 1\right]}{\varphi\left[\left(1 + \gamma_{\text{DF}_{P_D}}\right)^{\eta_{\text{AF}}} - 1\right] - P_D{g_0}^2\varphi\gamma_{\text{pu}}}, \tag{14}$$

where $\varphi = \xi{f_0}^2 + (1 - \xi)\alpha^2{f_1}^2 + \alpha f_0 f_1\sqrt{\xi(1 - \xi)}$. We assume that the channel is a complex Gaussian channel. $\widetilde{h_0}$, $\widetilde{h_1^k}$, and $\widetilde{h_2}$ follow Gaussian distribution, sign as $\widetilde{h_0} \sim \text{CN}(0, \Omega_0)$, $\widetilde{h_1^k} \sim \text{CN}(0, \Omega_1^k)$, and $\widetilde{h_2} \sim \text{CN}(0, \Omega_2)$, where $\text{CN}(\cdot, \cdot)$ means Gaussian distribution. Therefore, $\widetilde{h_0}^2 \sim E(\Omega_0)$, $\widetilde{h_1^k}^2 \sim E(\Omega_1^k)$, and $\widetilde{h_2}^2 \sim E(\Omega_2)$.

The SU SNR of the direct link is

$$\begin{aligned}\gamma_{b-\text{su}} &= E\left\{\text{SNR}_{b-\text{su}}\right\} \\ &= P_D\widetilde{h_0}^2\xi\gamma_{\text{DF}_{\text{su}}} + (1 - P_D)\frac{\widetilde{h_0}^2\xi\gamma_{\text{DF}_{\text{su}}}}{1 + {l_0}^2\gamma_{\text{pu}}}.\end{aligned} \tag{15}$$

The SNR probability density function (PDF) of the direct link for DF strategy is derived in Appendix $Z = X + Y$:

$$f(x) = \frac{\lambda_{h_0^1}\lambda_{h_0^2}}{\lambda_{h_0^2} - \lambda_{h_0^1}}\left(e^{-\lambda_{h_0^1}x} - e^{-\lambda_{h_0^2}x}\right), \tag{16}$$

where $\lambda_{h_0^1} = 1/P_D\xi\gamma_{\text{DF}_{\text{su}}}\Omega_0$ and $\lambda_{h_0^2} = (1 + {l_0}^2\gamma_{\text{pu}})/(1 - P_D)\xi\gamma_{\text{DF}_{\text{su}}}\Omega_0$.

The SNR of SU BS-to-relaying node link for DF strategy is

$$\begin{aligned}\gamma_{b-k} &= E\left\{\text{SNR}_{b-k}\right\} \\ &= P_D\widetilde{h_1^k}^2\xi\gamma_{\text{DF}_{\text{su}}} + (1 - P_D)\frac{\widetilde{h_1^k}^2\xi\gamma_{\text{DF}_{\text{su}}}}{1 + {l_1}^2\gamma_{\text{pu}}}.\end{aligned} \tag{17}$$

The SNR of the relay node-to-SU for DF strategy is

$$\begin{aligned}\gamma_{k-\text{su}} &= E\left\{\text{SNR}_{k-\text{su}}\right\} \\ &= P_D\widetilde{h_2}^2\xi\gamma_{\text{DF}_{\text{su}}} \\ &\quad + (1 - P_D)\frac{\widetilde{h_2}^2(1 - \xi)\gamma_{\text{DF}_{\text{su}}}}{{l_1}^2\widetilde{h_2}^2\gamma_{\text{pu}} + {l_0}^2\gamma_{\text{pu}} + 1}.\end{aligned} \tag{18}$$

Then the SNR PDF of the relay node-to-SU link for DF strategy is derived in Appendix $Z = Z_3 + W$:

$$f(x) = \lambda_{h_2^1}\lambda_{h_2^2}\lambda_{h_2^3}e^{\lambda_{h_2^2}\theta}\frac{xe^{-(\lambda_{h_2^3}/2)x}}{\left(\left(\lambda_{h_2^1}/2\right)x + \lambda_{h_2^2}\right)^2}, \tag{19}$$

where $\lambda_{h_2^1} = 1/(1 - P_D)(1 - \xi)\gamma_{\text{DF}_{\text{su}}}\Omega_2$, $\lambda_{h_2^2} = 1/{l_1}^2\gamma_{\text{pu}}\Omega_2$, $\lambda_{h_2^3} = 1/P_D(1 - \xi)\gamma_{\text{DF}_{\text{su}}}\Omega_2$, and $\theta = {l_0}^2\gamma_{\text{pu}} + 1$. The outage probability of the SU using maximum channel gain for DF strategy is

$$\begin{aligned}P_{\text{out}}^{\text{cg}} &= P_{h_{b-k}^{\max}}P\left\{\widetilde{h_1^{\max}} < \widetilde{h_0}\right\}P\left\{\gamma_{b-\text{su}} < \left(2^{2R_{\text{su}}} - 1\right)\right\} \\ &\quad + P_{h_{b-k}^{\max}}P\left\{\widetilde{h_1^{\max}} > \widetilde{h_0}\right\} \\ &\quad \cdot P\left\{\min\left(\gamma_{b-k}, \gamma_{k-\text{su}}\right) < \left(2^{2R_{\text{su}}} - 1\right)\right\},\end{aligned} \tag{20}$$

and the probability of selecting the maximum channel gain node is

$$\begin{aligned}P_{h_{b-k}^{\max}} &= P\left\{\max\left(\widetilde{h_1^1}, \widetilde{h_1^2}, \ldots, \widetilde{h_1^N}\right)\right\} = \prod_{k=1}^{N}P_k\left(\widetilde{h_1^k}\right. \\ &\quad \left. < \frac{2^{2R_{\text{su}}} - 1}{P_D\xi\gamma_{\text{DF}_{\text{su}}} + (1 - P_D)\xi\left(\gamma_{\text{DF}_{\text{su}}}/\left(1 + {l_0}^2\gamma_{\text{pu}}\right)\right)}\right),\end{aligned} \tag{21}$$

where P_k is the probability of the case when the kth node channel gain is less than the maximum channel gain.

3.1.2. Max Signal-to-Noise Ratio. The SNR PDF of direct link using maximum SNR scheme is the same as (16). The SNR PDF of relay node-to-SU is the same as (19). The SNR PDF of SU BS-to-relay node is

$$f(x) = \frac{\lambda_{h_1^1}\lambda_{h_1^2}}{\lambda_{h_1^2} - \lambda_{h_1^1}}\left(e^{-\lambda_{h_1^1}x} - e^{-\lambda_{h_1^2}x}\right), \tag{22}$$

where $\lambda_{h_1^1} = 1/P_D\xi\gamma_{\mathrm{DF}_{\mathrm{su}}}\Omega_1^k$ and $\lambda_{h_1^2} = (1 + {l_1}^2\gamma_{\mathrm{pu}})/(1 - P_D)\xi\gamma_{\mathrm{DF}_{\mathrm{su}}}\Omega_1^k$. The outage probability of the SU using maximum SNR for DF strategy is

$$\begin{aligned} P_{\mathrm{out}}^{\mathrm{snr}} &= P_{\gamma_{b-k}^{\max}} P\left\{\gamma_{b-\mathrm{su}}^{\max} > \gamma_{b-k}^{\max}\right\} P\left\{\gamma_{b-\mathrm{su}} < \left(2^{2R_{\mathrm{su}}} - 1\right)\right\} \\ &\quad + P_{\gamma_{b-k}^{\max}}\left\{P\left\{\gamma_{b-\mathrm{su}}^{\max} < \gamma_{b-k}^{\max}\right\}\right. \\ &\quad \left.\cdot P\left\{\min\left(\gamma_{b-k}, \gamma_{k-\mathrm{su}}\right) < \left(2^{2R_{\mathrm{su}}} - 1\right)\right\}\right\}, \end{aligned} \tag{23}$$

where selecting maximum SNR relay node probability is

$$P_{\gamma_{b-k}^{\max}} = P\left\{\max\left(\gamma_{b-k}^1, \gamma_{b-k}^2, \ldots, \gamma_{b-k}^N\right)\right\}. \tag{24}$$

3.2. Amplify-and-Forward Relaying

3.2.1. Max Channel Gain. The SU SNR of the direct link for AF strategy can be written as

$$\begin{aligned} \gamma_{b-\mathrm{su}} &= E\left\{\mathrm{SNR}_{b-\mathrm{su}}\right\} \\ &= P_D\widetilde{h_0^2}\xi\gamma_{\mathrm{AF}_{\mathrm{su}}} + (1 - P_D)\frac{\widetilde{h_0^2}\xi\gamma_{\mathrm{AF}_{\mathrm{su}}}}{1 + {l_0}^2\gamma_{\mathrm{pu}}}, \end{aligned} \tag{25}$$

and the SNR PDF of the direct link for AF strategy is

$$f(x) = \frac{\lambda_{h_0^1}\lambda_{h_0^2}}{\lambda_{h_0^2} - \lambda_{h_0^1}}\left(e^{-\lambda_{h_0^1}x} - e^{-\lambda_{h_0^2}x}\right), \tag{26}$$

where $\lambda_{h_0^1} = 1/P_D\xi\gamma_{\mathrm{AF}_{\mathrm{su}}}\Omega_0$ and $\lambda_{h_0^2} = (1 + {l_0}^2\gamma_{\mathrm{pu}})/(1 - P_D)\xi\gamma_{\mathrm{AF}_{\mathrm{su}}}\Omega_0$. The SNR of SU BS-to-relay nodes is

$$\begin{aligned} \gamma_{b-k} &= E\left\{\mathrm{SNR}_{b-k}\right\} \\ &= P_D\xi\widetilde{h_1^k}^2\gamma_{\mathrm{AF}_{\mathrm{su}}} + (1 - P_D)\frac{\widetilde{h_1^k}^2\xi\gamma_{\mathrm{AF}_{\mathrm{su}}}}{1 + {l_1}^2\gamma_{\mathrm{pu}}}. \end{aligned} \tag{27}$$

The SNR of the selected relay node-to-SU is

$$\begin{aligned} \gamma_{k-\mathrm{su}} &= E\left\{\mathrm{SNR}_{k-\mathrm{su}}\right\} \\ &= P_D\alpha^2\widetilde{h_2}^2(1 - \xi)\gamma_{\mathrm{AF}_{\mathrm{su}}} \\ &\quad + (1 - P_D)\frac{\alpha^2\widetilde{h_2}^2(1 - \xi)\gamma_{\mathrm{AF}_{\mathrm{su}}}}{\alpha^2{l_1}^2\widetilde{h_2}^2\gamma_{\mathrm{pu}} + {l_0}^2\alpha^2\gamma_{\mathrm{pu}} + 1}. \end{aligned} \tag{28}$$

Then the SNR PDF of the selected relay node-to-SU is

$$f(x) = \lambda_{h_2^1}\lambda_{h_2^2}\lambda_{h_2^3}e^{\lambda_{h_2^2}\theta}\frac{xe^{-(\lambda_{h_2^3}/2)x}}{\left(\left(\lambda_{h_2^1}/2\right)x + \lambda_{h_2^2}\right)^2}, \tag{29}$$

where $\lambda_{h_2^1} = 1/(1 - P_D)(1 - \xi)\gamma_{\mathrm{AF}_{\mathrm{su}}}\Omega_2$, $\lambda_{h_2^2} = 1/{l_1}^2\gamma_{\mathrm{pu}}\Omega_2$, $\lambda_{h_2^3} = 1/P_D(1 - \xi)\gamma_{\mathrm{AF}_{\mathrm{su}}}\Omega_2$, and $\theta = {l_0}^2\gamma_{\mathrm{pu}} + 1$. The outage probability of the SU using maximum channel gain for AF strategy is the same as (20); the probability of selecting the maximum channel gain relay node is

$$\begin{aligned} P_{h_{b-k}^{\max}} &= P\left\{\max\left(\widetilde{h_1^1}, \widetilde{h_1^2}, \ldots, \widetilde{h_1^N}\right)\right\} = \prod_{k=1}^{N} P_k\left(\widetilde{h_1^k}\right. \\ &\quad \left. < \frac{2^{2R_{\mathrm{su}}} - 1}{P_D\xi\gamma_{\mathrm{AF}_{\mathrm{su}}} + (1 - P_D)\xi\left(\gamma_{\mathrm{AF}_{\mathrm{su}}}/\left(1 + {l_0}^2\gamma_{\mathrm{pu}}\right)\right)}\right). \end{aligned} \tag{30}$$

3.2.2. Max Signal-to-Noise Ratio. The SNR PDF of direct link using max SNR scheme is the same as (26). The SNR PDF of the selected node-to-SU using max SNR scheme is the same as (29). The SNR PDF of SU BS-to-relay nodes using max SNR scheme is

$$f(x) = \frac{\lambda_{h_1^1}\lambda_{h_1^2}}{\lambda_{h_1^2} - \lambda_{h_1^1}}\left(e^{-\lambda_{h_1^1}x} - e^{-\lambda_{h_1^2}x}\right), \tag{31}$$

where $\lambda_{h_1^1} = 1/P_D\xi\gamma_{\mathrm{AF}_{\mathrm{su}}}\Omega_1^k$ and $\lambda_{h_1^2} = (1 + {l_1}^2\gamma_{\mathrm{pu}})/(1 - P_D)\xi\gamma_{\mathrm{AF}_{\mathrm{su}}}\Omega_1^k$. The outage probability of the SU using maximum SNR for AF strategy is the same as (23).

4. Simulation and Performance Analysis

In this section, the numerical simulations are performed using the analysis of outage probability which is obtained in the previous section. We assume that $R_{\mathrm{pu}} = 1$ bps/Hz and relay nodes $N = 8$, the average channel gain value is $1/d^{\varepsilon}$, where d is the channel distance of each link, and ε is pass loss exponent ($\varepsilon = 2$ assumed). We also assume that $d_{f0} = 2.5$, $d_{f1} = 1.5$, $d_{g0} = 1$, $d_{f0} = 2.5$, $d_{f1} = 1.5$, $d_{h0} = 2.5$, $d_{h1} = 1.5$, $d_{h2} = 1$, $d_{l0} = 2.5$, and $d_{l1} = 1.5$. For all the simulations, we make the assumption that the distributions of the noise parts of the received PU or SU signals are Gaussian.

Figure 2 shows the SU outage probability versus power allocation factor ξ with different values of PU SNR when the detection probability is set to 0.9. One sees that the SU outage probability decreases when PU SNR increases and the power allocation factor increases.

Figure 3 shows the SU outage probability versus detection probability P_D and SU BS power allocation factor ξ when PU SNR is set to 20 dB. One sees that the SU outage probability decreases when the detection probability increases and SU BS power allocation factor increases.

Figure 4 shows the SU outage probability versus power allocation factor ξ with different values of PU SNR when the detection probability is set to 0.9. One observes that the SU outage probability decreases when PU SNR increases and the detection probability increases. Compared with Figure 2, the performance of using maximum channel gain is better than using maximum SNR when the SU BS power allocation factor $\xi \sim [0\text{–}0.1]$, while it is worse when the SU BS power allocation factor $\xi \sim [0.1\text{–}1]$.

Figure 5 shows the SU outage probability versus detection probability P_D and power allocation factor ξ when the PU SNR is set to 20 dB. One sees that the SU outage probability decreases when the detection probability increases and SU BS

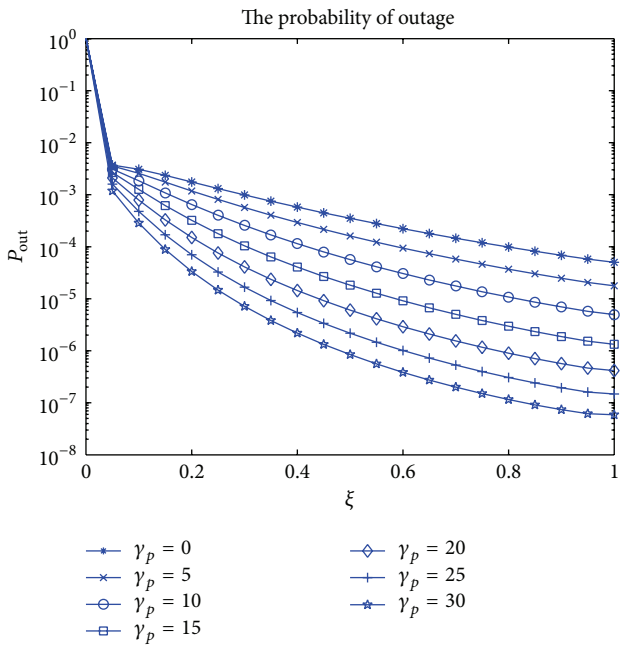

FIGURE 2: Max channel gain node with different ξ and γ_p using DF.

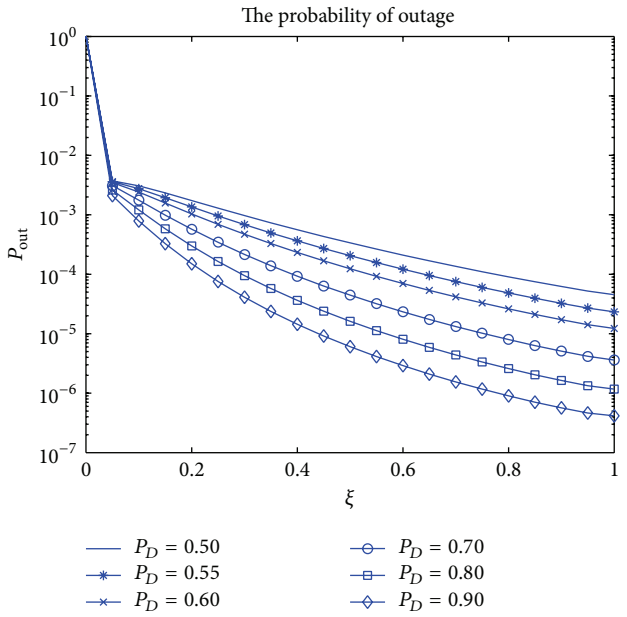

FIGURE 3: Max channel gain node with different ξ and P_D using DF.

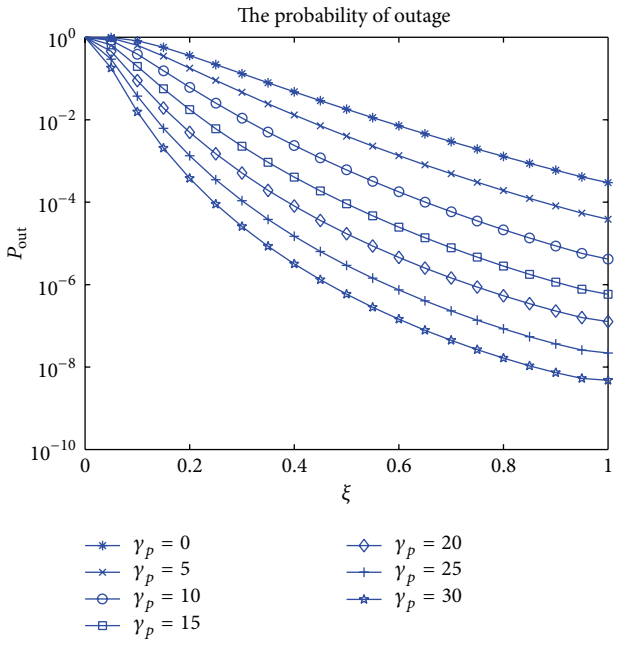

FIGURE 4: Max SNR with different ξ and γ_p using DF.

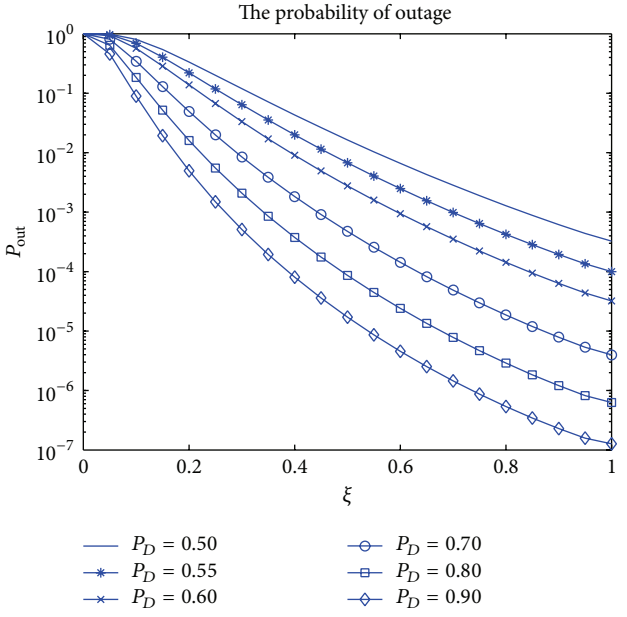

FIGURE 5: Max SNR with different ξ and P_D using DF.

power allocation factor increases. Compared with Figure 3, the performance of using maximum channel gain is better than using maximum SNR when the detection probability $P_D < 0.60$, while it is worse when the detection probability $P_D > 0.60$. The performance of using maximum channel gain is better than using maximum SNR when the SU BS power allocation factor $\xi \sim [0\text{–}0.1]$, while it is worse when the SU BS power allocation factor $\xi \sim [0.1\text{–}1]$.

Figure 6 shows the SU outage probability versus power allocation factor ξ with different values of PU SNR when the detection probability is set to 0.9. When SNR $\leq$ 10 dB, the SU outage probability decreases while the BS power allocation factor increases. When the SU power allocation factor $\xi \sim [0\text{–}0.55]$ the SU outage probability decreases. The SU outage probability increases when the SU power allocation factor $\xi \sim [0.55\text{–}0.1]$ and PU SNR is 30 dB. On the other hand, the larger the PU SNR is the smaller the SU BS power allocation factor corresponding to the minimum outage probability will be.

Figure 7 shows the SU outage probability versus detection probability P_D and power allocation factor ξ when

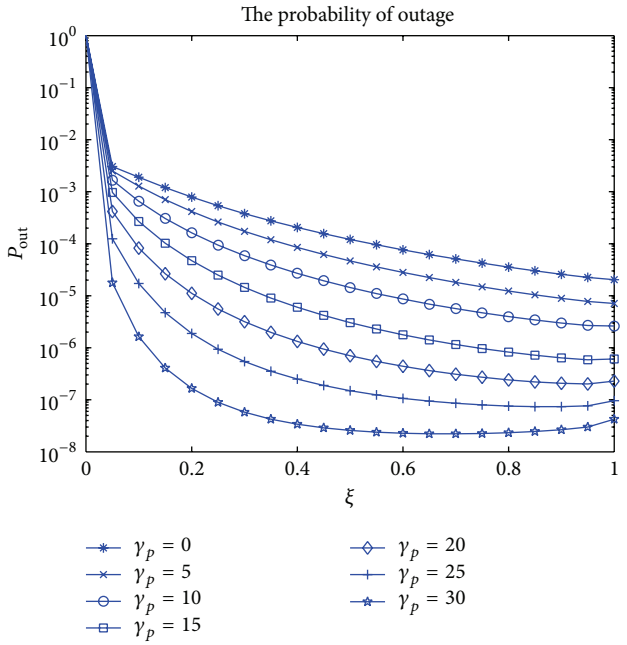

Figure 6: Max channel gain node with different ξ and γ_p using AF.

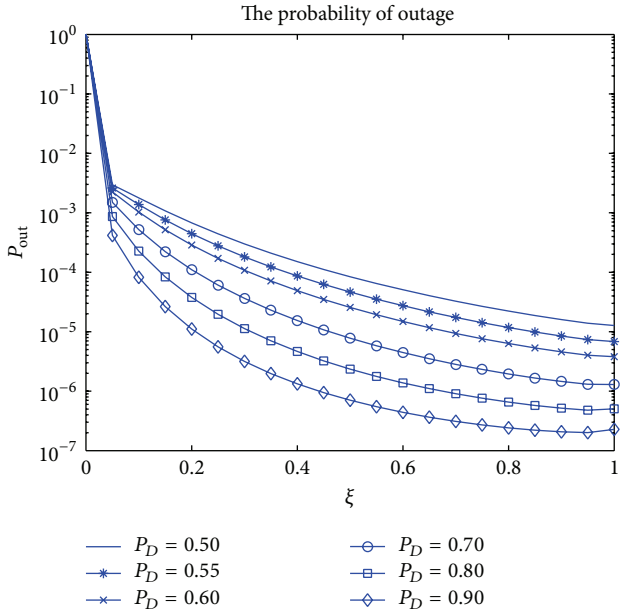

Figure 7: Max channel gain node with different ξ and P_D using AF.

the PU SNR is 20 dB. In Figure 7, one sees that the SU outage probability decreases when the detection probability increases; one also observes that the SU outage probability can reach an error floor when the SU BS power allocation factor changes with different detection probability. Moreover, the larger the detection probability is, the smaller the SU BS power allocation factor corresponding to the minimum outage probability will be.

Figure 8 shows the SU outage probability versus power allocation factor ξ with different values of PU SNR when

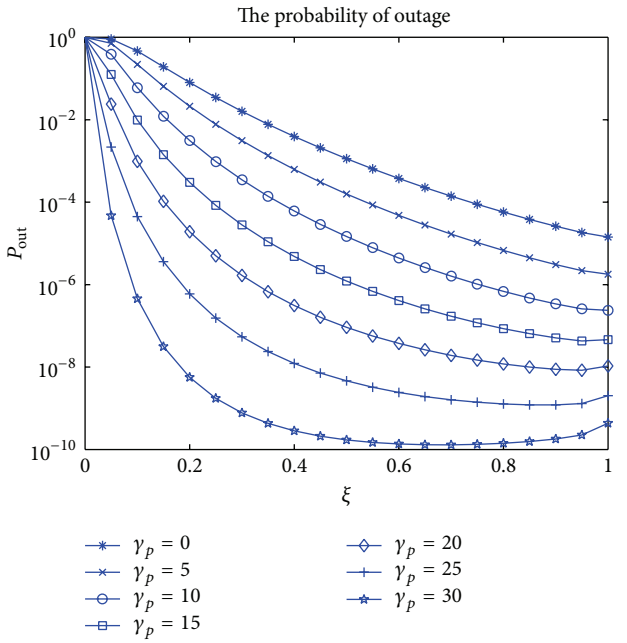

Figure 8: Max SNR with different ξ and γ_p using AF.

the detection probability is set to 0.9. One observes that the SU outage probability decreases when the BS power allocation factor increases and the SU power allocation factor $\xi \sim [0–0.55]$, while the SU outage probability increases when the SU power allocation factor $\xi \sim [0.55–0.1]$ and PU SNR is 30 dB. On the other hand, the larger the PU SNR is, the smaller the SU BS power allocation factor corresponding to the minimum outage probability will be. Compared with Figure 6, the performance of using maximum channel gain is better than using maximum SNR when the SU BS power allocation factor $\xi \sim [0–0.1]$, while it is worse when the SU BS power allocation factor $\xi \sim [0.1–1]$.

Figure 9 shows the SU outage probability versus detection probability P_D and power allocation factor ξ when the PU SNR is set to 20 dB. One observes that SU outage probability can reach an error floor when the SU BS power allocation factor changes with different detection probability. What is more, the larger the detection probability is, the smaller the SU BS power allocation factor corresponding to the minimum outage probability will be. Otherwise, compared with Figure 7, the performance of using maximum channel gain is better than that using maximum SNR when the detection probability $P_D < 0.60$, while it is worse when the detection probability $P_D > 0.60$. The performance of using maximum channel gain is better than using maximum SNR when the SU BS power allocation factor $\xi \sim [0–0.1]$, while it is worse when the SU BS power allocation factor $\xi \sim [0.1–1]$.

Figure 10 shows the SU outage probability versus detection probability P_D, maximum channel gain, maximum SNR, and power allocation factor ξ when the PU SNR is set to 20 dB. When $P_D = 0.7$, the outage probability of maximum channel gain is better than maximum SNR while $\xi < 0.75$; when $P_D = 0.8$, the outage probability of maximum channel gain is better than maximum SNR in the case of $\xi < 0.45$;

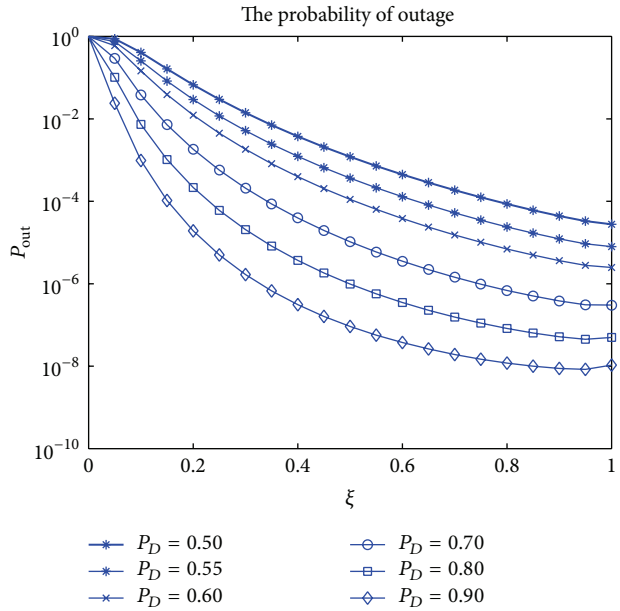

Figure 9: Max SNR with different ξ and P_D using AF.

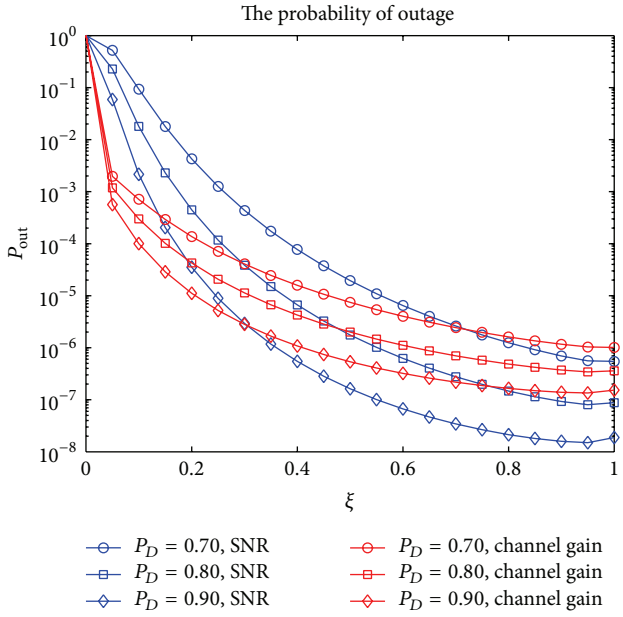

Figure 10: Max SNR and channel gain with different ξ and P_D using AF.

when $P_D = 0.9$, the outage probability of maximum channel gain is better than maximum SNR while $\xi < 0.30$. When $P_D = 0.70$, the outage probability is intersected at $\xi = 0.75$; when $P_D = 0.8$, the outage probability is intersected at $\xi = 0.45$; when $P_D = 0.9$, the outage probability is intersected at $\xi = 0.30$. So maximum channel gain is better than maximum SNR when the SU BS power allocation factor is small; on the contrary, it is worse when the SU BS power allocation factor is big.

Figure 11 shows the SU outage probability versus detection probability PD, AF, DF, and power allocation factor ξ

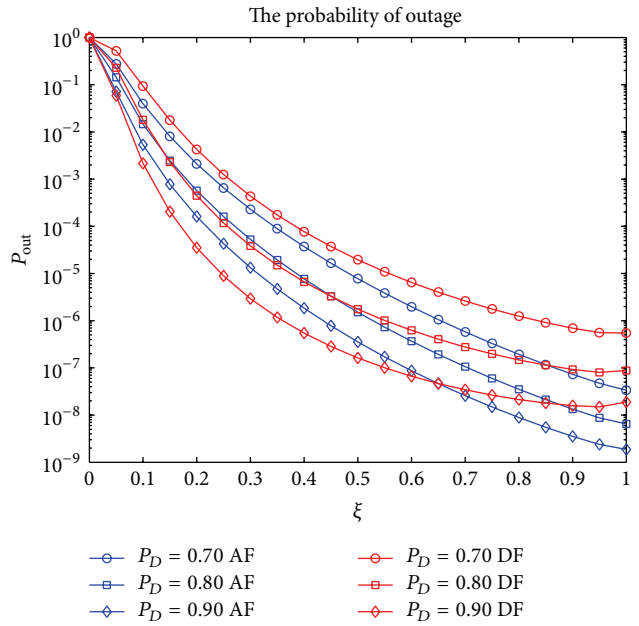

Figure 11: AF and DF ξ and P_D using max SNR.

when the PU SNR is set to 20 dB. When $P_D = 0.7$, the outage probability of AF is better than DF; when $P_D = 0.8$, the outage probability of AF is nearly equal to DF in the case of $\xi < 0.50$ and the outage probability of AF is better than DF while $\xi > 0.50$; when $P_D = 0.9$, the outage probability of AF is better than DF in the case of $\xi < 0.65$. Therefore only when the SU BS power allocation factor is small and detection probability is big can DF be better than AF; in contrast it is different.

5. Conclusions

In DF relaying, the outage probability decreases when the power allocation factor increases. While in AF relaying, the outage probability can reach a minimum value under the right power allocation factor and the right detection probability. In addition, the larger the PU SNR and detection probability are, the smaller the SU base station power allocation factor corresponding to the minimum outage probability that will be required is. The larger the detection probability is, the smaller the SU base station power allocation factor corresponding to the outage probability minimum value that will be required is. Moreover, the relaying scheme based on the maximum channel gain has the better performance based on the maximum SNR when the power allocation factor and detection probability are small, while the relaying scheme based on the maximum SNR has the better performance based on the maximum channel gain when the power allocation factor is large. Compared with DF relaying, AF relaying amplifies the transmitting signal; therefore, what is more, only when the SU BS power allocation factor is small and detection probability is big can the outage performance of DF be better than AF; otherwise the outage performance of AF is better than DF.

Appendix

For the exponential distribution, if $X \sim E(\lambda_1)$, $Y \sim E(\lambda_2)$, $W \sim E(\lambda_3)$.

Consider $Z_1 = X + Y$:

$$\begin{aligned} f_1(z) &= \int_0^z \lambda_1 e^{-\lambda_1(z-x)} \lambda_2 e^{-\lambda_2 x} dx \\ &= \lambda_1 \lambda_2 e^{-\lambda_1 z} \int_0^z e^{-(\lambda_2-\lambda_1)x} dx \\ &= \frac{\lambda_1 \lambda_2}{\lambda_2 - \lambda_1} e^{-\lambda_1 z} \left(1 - e^{-(\lambda_2-\lambda_1)z}\right) \\ &= \frac{\lambda_1 \lambda_2}{\lambda_2 - \lambda_1} \left(e^{-\lambda_1 z} - e^{-\lambda_2 z}\right). \end{aligned} \tag{A.1}$$

Consider $Z_2 = Y + \theta$:

$$f_2(z) = \lambda_2 e^{-\lambda_2(z-\theta)} = \lambda_2 e^{\lambda_2 \theta} e^{-\lambda_2 z}. \tag{A.2}$$

Consider $Z_3 = X/Z_2$:

$$\begin{aligned} f_3(z) &= \int_0^\infty x f(xz) f(x) dx \\ &= e^{\lambda_2 \theta} \int_0^\infty x \lambda_1 e^{-\lambda_1 xz} \lambda_2 e^{-\lambda_2 x} dx \\ &= \frac{\lambda_1 \lambda_2 e^{\lambda_2 \theta}}{(\lambda_1 z + \lambda_2)^2}. \end{aligned} \tag{A.3}$$

Consider $Z = Z_3 + W$:

$$\begin{aligned} f(z) &= \int_0^z f(z-x) f(x) dx \\ &= \int_0^z \frac{\lambda_1 \lambda_2 e^{\lambda_2 \theta}}{(\lambda_1 x + \lambda_2)^2} \lambda_3 e^{-\lambda_3(z-x)} dx \\ &= \lambda_1 \lambda_2 \lambda_3 e^{\lambda_2 \theta} e^{-\lambda_3 z} \int_0^z \frac{e^{\lambda_3 x}}{(\lambda_1 x + \lambda_2)^2} dx \\ &= \lambda_2 \lambda_3 e^{\lambda_2 \theta} e^{-\lambda_3 \lambda_2/\lambda_1} e^{-\lambda_3 z} \int_{\lambda_2}^{z\lambda_1+\lambda_2} \frac{e^{(\lambda_3/\lambda_1)x}}{x^2} dx \\ &= \lambda_2 \lambda_3 e^{\lambda_2 \theta} e^{-(\lambda_3 \lambda_2/\lambda_1)} e^{-\lambda_3 z} \frac{e^{(\lambda_3/\lambda_1)\zeta}}{\zeta^2} z\lambda_1; \\ &\qquad \lambda_2 < \zeta < z\lambda_1 + \lambda_2 \\ &\approx \lambda_2 \lambda_3 e^{\lambda_2 \theta} e^{-\lambda_3 \lambda_2/\lambda_1} e^{-\lambda_3 z} \frac{e^{(\lambda_3/\lambda_1)(z\lambda_1/2+\lambda_2)}}{((\lambda_1/2) z + \lambda_2)^2} z\lambda_1 \\ &= \lambda_1 \lambda_2 \lambda_3 e^{\lambda_2 \theta} \frac{z e^{-(\lambda_3/2)z}}{((\lambda_1/2) z + \lambda_2)^2}. \end{aligned} \tag{A.4}$$

Competing Interests

The authors declare that they have no competing interests.

References

[1] M. Song, C. Xin, Y. Zhao, and X. Cheng, "Dynamic spectrum access: from cognitive radio to network radio," *IEEE Wireless Communications*, vol. 19, no. 1, pp. 23–29, 2012.

[2] B. Wang and K. J. R. Liu, "Advances in cognitive radio networks: a survey," *IEEE Journal on Selected Topics in Signal Processing*, vol. 5, no. 1, pp. 5–23, 2011.

[3] Q. Zhang, J. Jia, and J. Zhang, "Cooperative relay to improve diversity in cognitive radio networks," *IEEE Communications Magazine*, vol. 47, no. 2, pp. 111–117, 2009.

[4] A. Sendonaris, E. Erkip, and B. Aazhang, "User cooperation diversity—part i: system description," *IEEE Transactions on Communications*, vol. 51, no. 11, pp. 1927–1938, 2003.

[5] A. Sendonaris, E. Erkip, and B. Aazhang, "User cooperation diversity—part II: implementation aspects and performance analysis," *IEEE Transactions on Communications*, vol. 51, no. 11, pp. 1939–1948, 2003.

[6] Y. Zhao, R. Adve, and T. J. Lim, "Outage probability at arbitrary SNR with cooperative diversity," *IEEE Communications Letters*, vol. 9, no. 8, pp. 700–702, 2005.

[7] N. C. Beaulieu and J. Hu, "A closed-form expression for the outage probability of decode-and-forward relaying in dissimilar Rayleigh fading channels," *IEEE Communications Letters*, vol. 10, no. 12, pp. 813–815, 2006.

[8] S. Berger, M. Kuhn, A. Wittneben, T. Unger, and A. Klein, "Recent advances in amplify-and-forward two-hop relaying," *IEEE Communications Magazine*, vol. 47, no. 7, pp. 50–56, 2009.

[9] H. Min, S. Lee, K. Kwak, and D. Hong, "Effect of multiple antennas at the source on outage probability for amplify-and-forward relaying systems," *IEEE Transactions on Wireless Communications*, vol. 8, no. 2, pp. 633–637, 2009.

[10] R. H. Y. Louie, Y. Li, H. A. Suraweera, and B. Vucetic, "Performance analysis of beamforming in two hop amplify and forward relay networks with antenna correlation," *IEEE Transactions on Wireless Communications*, vol. 8, no. 6, pp. 3132–3141, 2009.

[11] D. B. da Costa and S. Aissa, "Cooperative dual-hop relaying systems with beamforming over Nakagami-m fading channels," *IEEE Transactions on Wireless Communications*, vol. 8, no. 8, pp. 3950–3954, 2009.

[12] G. Kramer, M. Gastpar, and P. Gupta, "Cooperative strategies and capacity theorems for relay networks," *IEEE Transactions on Information Theory*, vol. 51, no. 9, pp. 3037–3063, 2005.

[13] J. N. Laneman, D. N. C. Tse, and G. W. Wornell, "Cooperative diversity in wireless networks: efficient protocols and outage behavior," *IEEE Transactions on Information Theory*, vol. 50, no. 12, pp. 3062–3080, 2004.

[14] Y. Liang, V. V. Veeravalli, and H. Vincent Poor, "Resource allocation for wireless fading relay channels: max-min solution," *IEEE Transactions on Information Theory*, vol. 53, no. 10, pp. 3432–3453, 2007.

[15] G. Zhao, C. Yang, G. Y. Li, D. Li, and A. C. K. Soong, "Power and channel allocation for cooperative relay in cognitive radio networks," *IEEE Journal on Selected Topics in Signal Processing*, vol. 5, no. 1, pp. 151–159, 2011.

[16] J. Luo, R. S. Blum, L. J. Cimini, L. J. Greenstein, and A. M. Haimovich, "Decode-and-forward cooperative diversity with power allocation in wireless networks," *IEEE Transactions on Wireless Communications*, vol. 6, no. 3, pp. 793–799, 2007.

[17] Y. Zhao, R. Adve, and T. J. Lim, "Improving amplify-and-forward relay networks: optimal power allocation versus selection," *IEEE Transactions on Wireless Communications*, vol. 6, no. 8, pp. 3114–3123, 2007.

[18] A. Bletsas, H. Shin, and M. Z. Win, "Cooperative communications with outage-optimal opportunistic relaying," *IEEE Transactions on Wireless Communications*, vol. 6, no. 9, pp. 3450–3460, 2007.

[19] D. K. Verma and S. Prakriya, "Performance of a cooperative downlink multiplexing scheme using dynamic spectrum access principles," *IET Communications*, vol. 9, no. 2, pp. 258–270, 2015.

Hindawi Publishing Corporation
Mobile Information Systems
Volume 2016, Article ID 7107103, 17 pages
http://dx.doi.org/10.1155/2016/7107103

Research Article

Cognitive Privacy for Personal Clouds

Milena Radenkovic

School of Computer Science, University of Nottingham, Nottingham NG8 1BB, UK

Correspondence should be addressed to Milena Radenkovic; milena.radenkovic@nottingham.ac.uk

Received 24 December 2015; Accepted 3 April 2016

Academic Editor: Chao Chen

This paper proposes a novel Cognitive Privacy (CogPriv) framework that improves privacy of data sharing between Personal Clouds for different application types and across heterogeneous networks. Depending on the behaviour of neighbouring network nodes, their estimated privacy levels, resource availability, and social network connectivity, each Personal Cloud may decide to use different transmission network for different types of data and privacy requirements. CogPriv is fully distributed, uses complex graph contacts analytics and multiple implicit novel heuristics, and combines these with smart probing to identify presence and behaviour of privacy compromising nodes in the network. Based on sensed local context and through cooperation with remote nodes in the network, CogPriv is able to transparently and on-the-fly change the network in order to avoid transmissions when privacy may be compromised. We show that CogPriv achieves higher end-to-end privacy levels compared to both noncognitive cellular network communication and state-of-the-art strategies based on privacy-aware adaptive social mobile networks routing for a range of experiment scenarios based on real-world user and network traces. CogPriv is able to adapt to varying network connectivity and maintain high quality of service while managing to keep low data exposure for a wide range of privacy leakage levels in the infrastructure.

1. Introduction

We live in the era when people expect seamless connectivity for everyone and to everything everywhere. For the majority, this means that potentially personal and sensitive data may get transferred by the networks which can compromise user privacy in different ways [1]. Even though some users may use VPN overlays to improve privacy of their traffic, they will often face difficulties when being mobile or in the areas of intermittent connectivity. This paper addresses the problem of end-to-end privacy in the face of possibly unreliable and mobile networks. We argue that continuously decreasing control that users have on their data needs to be addressed across multiple layers (i.e., not only the application or not only the radio level) and we propose the idea of Personal Cloud architecture that improves privacy of storage as well as sharing of user data. This paper describes an open-source distributed virtual platform that allows adaptive privacy for sharing multiple kinds of data via different routing protocols and networks. In particular, we build on and expand our early work on light weight Personal Clouds demonstration proposed in [2] to allow adaptive and dynamic transfer mechanisms for different types of user traffic based on different traffic privacy levels required. Recent research [3] has shown the wide spread use of transparent middleboxes in cellular networks that actively analyse, monitor, and modify individual's traffic without the knowledge of the individuals and thus compromise their privacy. We propose Cognitive Privacy (CogPriv) which allows different application services (hosted in different virtual containers within Personal Cloud (PC)) to route traffic via most suitable networks in order to avoid network segments that may compromise user privacy and redirect user communication towards more secure networks. For example, if the Cognitive Privacy module in the user's Personal Cloud detects that user's cellular network is likely to spy on them, highly private traffic will be on-the-fly and transparently redirected to local ad hoc networks and follow the more trusted opportunistic ad hoc route to the destination. We propose to integrate several metrics to allow CogPriv routing protocol to probe cellular network trustworthiness and to estimate local ad hoc wireless nodes social dynamics, nodes' trust levels, and resources' availability.

The paper is organised as follows. Section 2 describes the state-of-the-art work on privacy-aware user data

communication in mobile networks. Section 3 begins with describing the architecture and design of our light weight Raspberry Pi Personal Cloud testbed. We then move to proposing an opportunistic disconnection tolerant network framework for data forwarding that can on-the-fly adapt to dynamic properties of access points/links and different privacy requirements of user application. The Cognitive Privacy module (CogPriv) of user's Personal Cloud can monitor the local network access points and individually or though collaboration make decisions on the network interface via which to send the data (and whether to send the data) depending on the privacy level required by the application. Section 4 describes CogPriv decision making algorithm and heuristics in more detail. Section 5 provides description of the real world cellular data traces and Facebook users connectivity traces used in our experiments and then moves to describing experiment scenarios and discussing the results. CogPriv shows that it outperform cellular network and mobile social ad hoc network forwarding across a range of metrics. Section 6 gives summary and future work directions.

2. Related Work

In [2], we propose the design and architecture of a low cost Personal Cloud testbed demonstration which uses Raspberry Pi computer and a range of heterogeneous sensors (RasPiPCloud). RasPiPCloud supports multiple on demand virtual containers to host different services and applications that can collect, store and share data with varying different levels of privacy. RasPiPCloud utilizes opportunistic networks communication among itself, heterogeneous sensors and other devices. Figure 1 shows the architecture of the RasPiPCloud with three example LXC containers [4] Healthcare, Finance, and Social Network (with a fourth container template ready for rapid on demand deployment). Each container gets installed and runs its purpose specific applications to ensure secure data fencing and protection.

In [5], the authors identify the widespread use of transparent middleboxes such as HTTP and DNS proxies that are able to analyse and actively modify user traffic and thus compromise user privacy and security. The authors argue that it is very important to consider higher-layer relationships when seeking to analyse mobile traffic and illustrates how mobile operators can enforce the use of HTTP proxies and gateways through preconfigured APN (Access Point Name) settings on a device. They identify that typical users lack the mechanisms and knowledge to prevent operator-enforced proxies from performing header injection and to stop online services from collecting their information. The reliance on VPN is limiting in cases of mobile or disconnection prone scenarios. Our paper addresses these scenarios by proposing a way how our combined intelligent routing may exploit maximally trusted routes based on the real time probes and collaboration with the infrastructure or ad hoc local nodes.

In [3], authors consider cellular networks where the growth of capacity provision is still behind the user and application demands [6]. Because of this, mobile network operators increasingly use auxiliary networks (e.g., WiFi networks) to offload mobile traffic for additional capacity. In

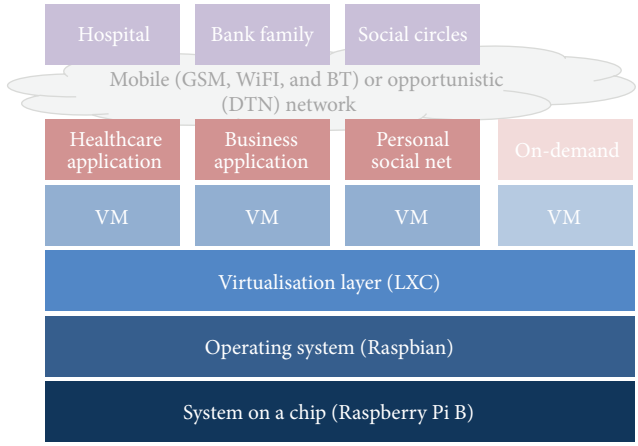

Figure 1: RasPiPCloud architecture.

recent years, WiFi offloading has been rapidly emerging as the preferred technique to meet the needs. Other research has addressed WiFi offloading efficiency [7, 8], energy efficiency [9, 10], user incentives [11] and operator support [12, 13]. Reference [3] focuses on improving the balanced control of WiFi offloading and avoid poor network utilization and undesirable user experience [9, 14] by proposing SoftOffload that aims to enhance deployability and collaboration among mobile network operators, WiFi providers and mobile users. SoftOffload employs collaborative hierarchical design between its central controller and local agents in order to balance between global control and responsiveness at the network edge.

In [15] authors propose cognitive testbed for wireless sensor networks as an emerging technology with a vast potential to avoid traditional wireless problems such as reliability, interferences and spectrum scarcity in wireless sensor networks. In addition to the testbed, [15] also proposes the design of a cognitive simulator for networks with a high number of nodes and the implementation of a new platform with three wireless interfaces and cognitive software for extracting real data.

State of the art work in [16] proposes Haystack system which aims to allow unobtrusive and comprehensive monitoring of network communications on mobile phones entirely from user space. Haystack correlates disparate contextual information such with specific traffic flows destined to illuminate mobile phone app performance, privacy and security.

Authors in [5] use data collected by the Netalyzr network service over 16 months to identify and characterize HTTP header enrichment in modern mobile networks. They present an overview of HTTP header usage for 299 mobile service providers from 112 countries to show three main categories: unique user and device identifiers, headers related to advertising programs, and headers associated with network operations which present significant compromise to user privacy. In our paper, we use traces of 17 mobile service providers of one country provided in this dataset with real world social network connectivity traces.

Reference [17] identify that typical privacy preserving solutions for data analysis which utilise cryptographic algorithms introduce high computation costs or restrict the possible range of values due to the need of discrete logarithm computation. Reference [18] propose a solution with a fully trusted dealer which may not be suitable for real world applications due to increased communication overheads necessary for their static key management scheme. Emerging work in [19] proposes to eliminate the need for key redistribution following a user join or leave as well as the need for fully trusted key dealer thus moving to a more P2P paradigm which is core to our approach too.

In [20, 21] we propose a new P2P adaptive anonymity technique for mobile opportunistic networks that improves traditional competitive research which is not well suited to sparse and disconnection prone networks. Reference [22] propose opportunistic, adaptive, fully localized reputation aware obfuscation mechanism that comprises of collaborative testing of nodes' obfuscation behaviour (OCOT) and multidimensional adaptive anonymisation (AA). We show that OCOT-AA is very efficient in terms of achieving high levels of node identity obfuscation and managing low delays while enabling fast detection and avoidance of malicious nodes. This paper moves beyond this to propose Cognitive Privacy for Personal Clouds with multiple application domains.

3. Cognitive Privacy and Personal Clouds

3.1. Personal Cloud: Prototype Testbed and Architectural Overview. Increasing demand for using a range of applications with different privacy requirements on mobile handheld devices raises challenges of how to choose the network (i.e., network interface) with the most suitable levels of privacy. We argue that handheld cognitive devices with several heterogeneous network interfaces (e.g., cellular networks, wireless networks, ad hoc wireless, and Bluetooth) are core for supporting a range of applications with different privacy requirements hosted in different virtual containers [2]. For example, consider a user who can be running a social network that allows them to stay in contact with their friends at the same time as regularly monitoring their long-term medical condition and being in contact with the hospital. These two types of applications have different privacy requirements and need their data to be stored and shared in different ways that can adapt to the required privacy requirements dynamically. We refer to this as Personal Cloud [2] which is in line with the proposals described in [23, 24]. Figure 2 shows deployment of a Personal Cloud prototype demo on a Raspberry Pi device equipped with Xtrinsic sensor board comprising temperature, pressure, and acceleration sensors. Figure 3 shows Raspberry Pi device that captures, stores, and processes a range of user and environment data such as heart rate and pedometer. Figure 4 shows a dashboard visualisation of the heart rate sensor readings and Figure 5 shows a social network hosted by the user and displayed on the user's handheld device.

This paper expands on the idea in [2, 23] in several ways in order to enable reliable and adaptive data sharing.

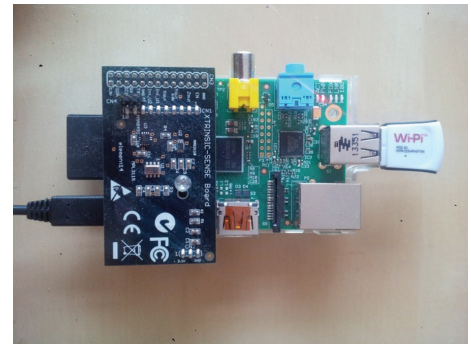

Figure 2: Raspberry Pi B with Xtrinsic sensor board and a WiPi wireless adapter.

Figure 3: Raspberry Pi with Suunto and WiPi USB module, Garmin heartrate sensor, and smartphone displaying readings.

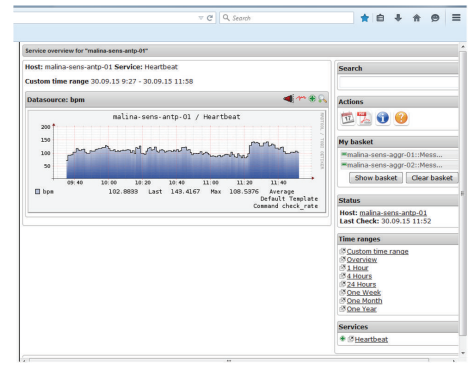

Figure 4: Visualisation of heart rate readings from the Garmin sensor.

While some social media data can be transferred via cellular network independently of whether there are middleboxes present in transit, medical personal data requires higher level of privacy that should not be compromised nor should it be allowed that the frequency and patterns of communication to the hospital are gathered by the cellular network provider infrastructure. Figure 6 shows a Personal Cloud

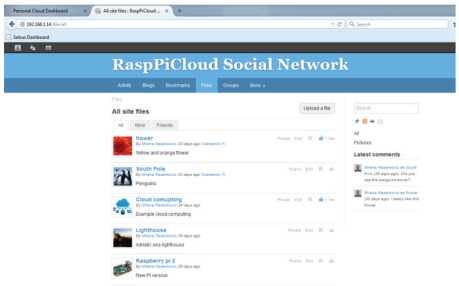

Figure 5: RasPiPCloud personal social network.

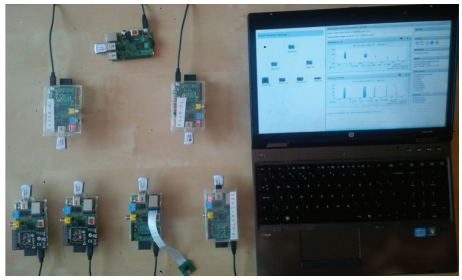

Figure 6: Testbed architecture and visualisation.

prototype demo utilising multiple Raspberry Pis where the leaf Raspberry Pis with heterogeneous sensors aim to send their data (camera and heart rate) to the hub destination node via different routes. Intermediary nodes may have different privacy levels associated with them. Nodes are configured so that leaf nodes have connectivity to intermediary nodes but not directly to destinations. This is important as it allows us to test multiple Personal Clouds communications over variable network conditions and topologies. Note that all nodes are equipped with WiPi wireless adapters that support both infrastructure and ad hoc mode.

3.2. Cognitive Privacy. In this section, we describe how we extend our early work on Personal Cloud testbed [2] to include transparent, efficient, and adaptive Cognitive Privacy (CogPriv) which negotiates access to various networks in real time to suit the privacy requirements of the applications. One of the core building modules of the Cognitive Privacy framework is Intelligent Forwarder which is a P2P DTN module. We extend the DTN bundle protocol (RFC 5050 [25–27]) which provides API for DTN applications with intelligent P2P forwarding. More specifically, our P2P DTN intelligent forwarding module provides multiflow real time bundle forwarding based on a range of criteria such as source ID, Virtual Machine (VM) ID, application privacy requirements, and destination ID so that different incoming bundles can be matched to the appropriate network interface in real time. Additionally, CogPriv comprises the following multiple stages: it probes local cellular network to identify the likelihood of any middleboxes that may compromise user traffic, requests the remote destination nodes to provide their estimations of the cellular network privacy levels, and collaborates and cooperates with the local network nodes. In this way, CogPriv can range dynamically and adaptively from providing fully cellular single hop end-to-end communication to fully localised multihop mobile opportunistic communication.

Intelligent Forwarder makes the decision on the choice of the next forwarding node and network interface based on multiple criteria and objectives: (1) it aims to either maximise end-to-end privacy for a particular application or meet the requirements of the application, (2) it aims to minimise end-to-end delays, and (3) it aims to be resource aware and adaptively avoid congestion. In this way, Intelligent Forwarder manages privacy requirements while being aware and adaptive to the dynamic quality of service challenges.

Through collaborations and cooperation in the local neighbourhoods, each node aims to understand its environment better and learn about its neighbours. More specifically, each node exchanges the following: (1) their own cellular network privacy statistics and predictions to negotiate feasibility of using cellular network for a particular application, (2) predictive analytics of their resources, and (3) mobile social graph network connectivity analytics. Social connectivity analytics is important as it keeps directionality of the data to be routed for ad hoc opportunistic communication. Resource considerations are important as they enable higher reliability of ad hoc opportunistic routing. More specifically, CogPriv builds on implicit heuristics on predictive in-network storage and delays we proposed in [28–31].

Each node's privacy level estimations are important to consider as they are the core criteria for choosing the interface to use for forwarding the data for privacy-aware applications; that is, neighbouring nodes may communicate via WiFi, GSM, or Bluetooth each having different privacy levels. More specifically, each interface will have different probabilities and utilities associated with it (described in Section 4) so that each bundle can be forwarded via the most appropriate interface. Towards this goal, we extend simple static (interface and bundle) forwarding paradigm to the more dynamic (interface, bundle, and forwarding probability) paradigm. Figure 7 shows Personal Cloud extended with the CogPriv framework.

3.3. An Overview of Cognitive Privacy Distributed Decision-Making. Depending on the level of privacy an application requires, the Cognitive Privacy (CogPriv) module in the Personal Cloud will send the data via either cellular network (e.g., default for mobile phones) or WiFi (e.g., default for laptops) when privacy is not required; on the other hand, it will run probes on its local area network and communicate with the destination about the remote cellular network privacy levels, as well as collaborating with the nearby nodes before deciding via which network and next hop to send the data as shown in Figure 8.

These steps are described in more detail as follows:

(i) If the desired privacy level is high, the Personal Cloud first checks its cellular network by running probes to identify possible presence of middleboxes. If it discovers any, it does not use cellular network.

(ii) If the cellular network of the sender does not detect presence of middleboxes, the sender contacts

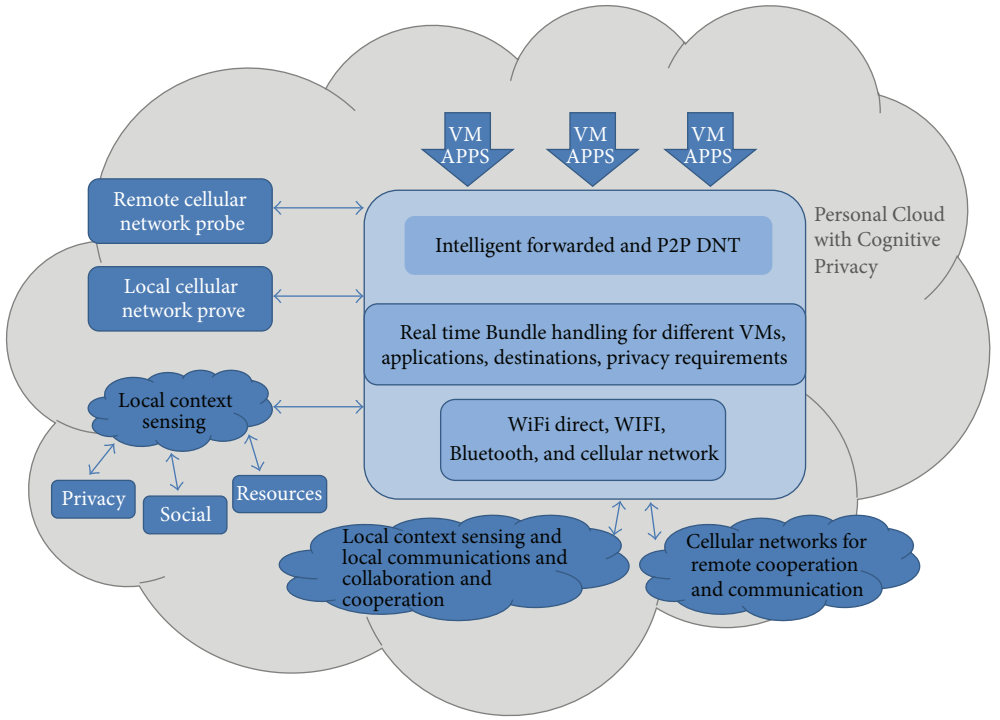

Figure 7: Cognitive Privacy design for Personal Clouds.

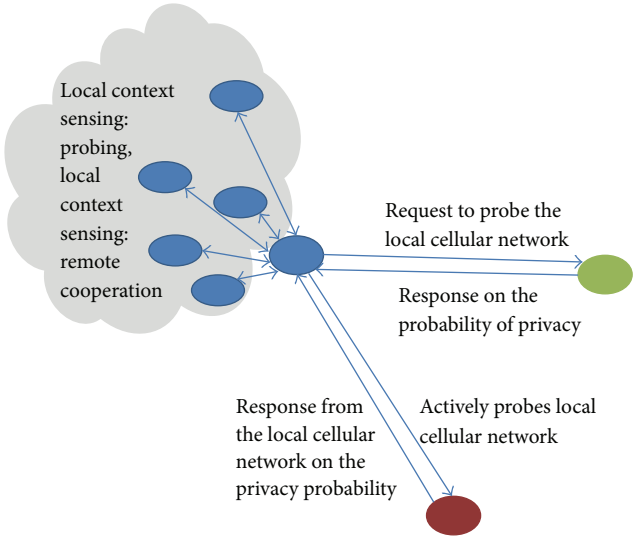

Figure 8: Functional overview of the probing and local collaboration stages.

the destination to enquire if the destination can detect any middleboxes at their end.

(iii) If both the destination and the sender are clear of the middleboxes or the level of middleboxes privacy meets the application requirements, the data gets communicated via the cellular networks.

(iv) If either the destination or the sender is not clear of infrastructure middleboxes, the sender checks its local neighbourhood using ad hoc networks and local contacts with trusted nodes only (for high levels of privacy requirements) and WiFi for medium levels of privacy requirements.

(v) If the next hop node gets a bundle with high level of privacy requirements, it will first probe its cellular network and send the bundle via it only if its cellular network does not have any middleboxes detected. Otherwise, it will scan opportunistically its local nodes and will exchange its social, resource, and privacy matrix in order to determine which node may be the most suitable bundle carrier to the particular destination.

(vi) For each bundle carrier, the same set of steps gets preformed in a fully distributed manner at every node.

Figure 9 illustrates combined, diverse communication approaches that comprise CogPriv and Figure 10 gives architectural overview of CogPriv.

A key challenge that CogPriv solves regarding cellular-local switching is that valuable middlebox and contextual information are distributed across local and remote users. The irregular distribution means that the contextual information possessed by any node alone is not sufficient to guide the switching process. Cellular network infrastructure can vary with the location of access and times users use the network so that different middleboxes may be present or removed without user's knowledge. For example, a Vodafone user in Karsruhe can send traffic without it being intercepted by a middlebox, while a Vodafone user in Berlin might pass via a web cache middlebox. Similarly, a T-Mobile user at a given

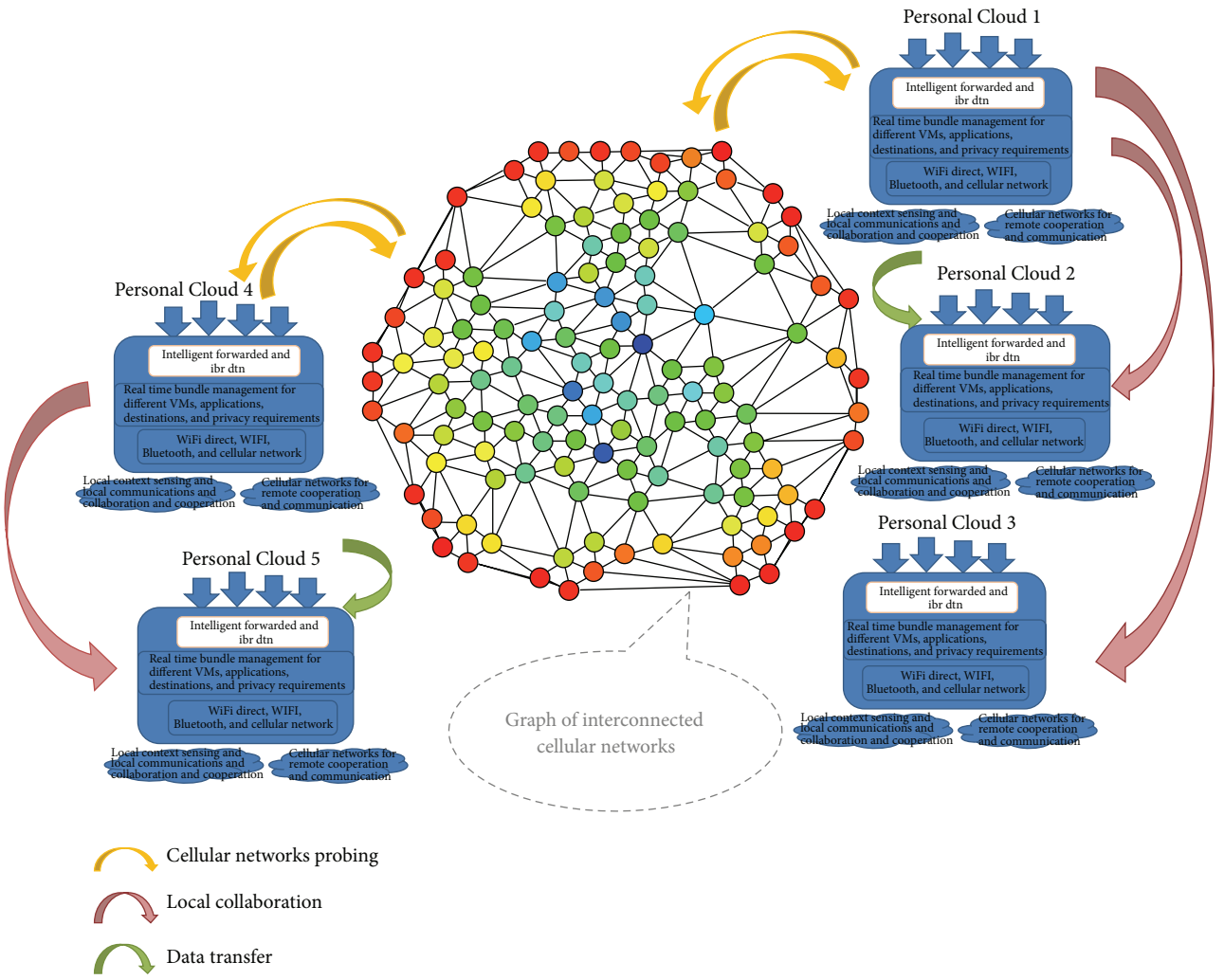

Figure 9: Cellular network interactions with local Personal Clouds.

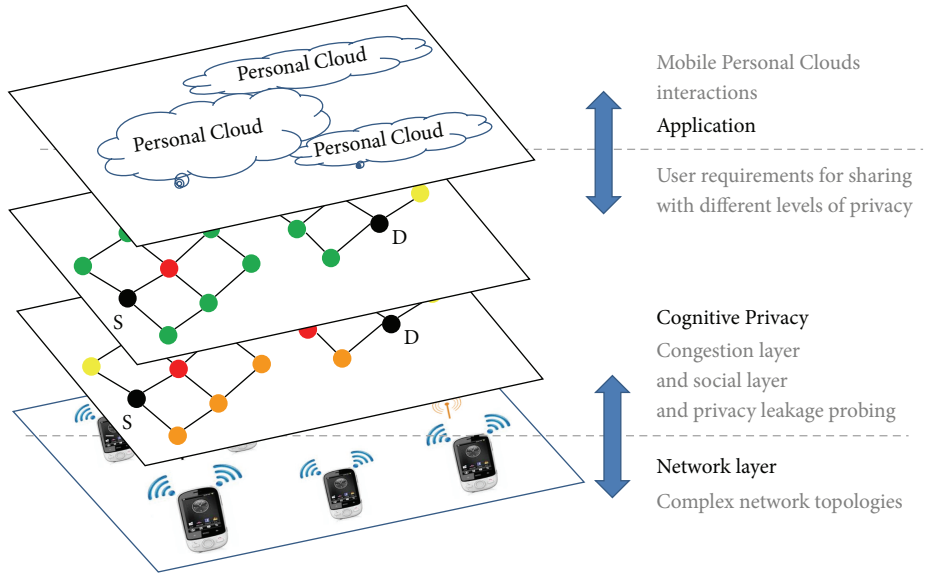

Figure 10: Architectural overview of Cognitive Privacy.

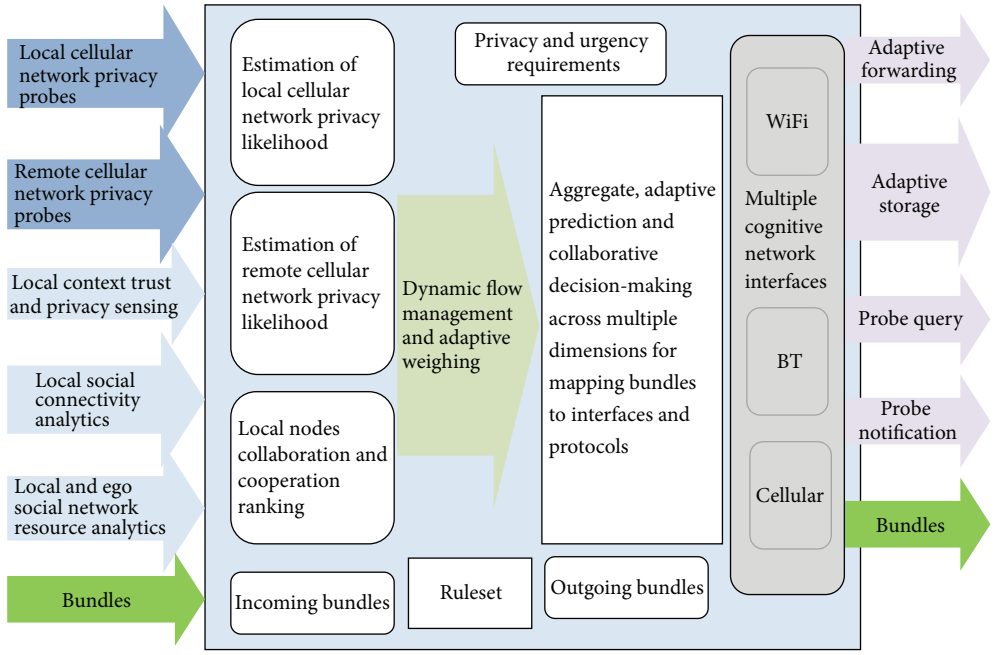

Figure 11: Architectural overview of the decision-making in the Personal Cloud Cognitive Privacy module.

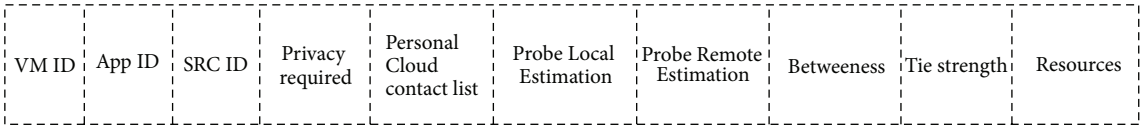

Figure 12: Extended CogPriv bundle header format.

location using 4G might detect a web middlebox, while a T-Mobile user on 3G could identify a DNS middlebox.

Because both the number and the location as well as the functionality of the middleboxes in cellular networks can change randomly, the cellular network probes need to be performed either before each data transfer (which may increase control traffic especially for real time multimedia traffic) or each sensible time interval (e.g., every day or half a day). Based on the statistical and temporal analysis of the probes each node performs for different cellular networks, nodes can adjust their time intervals differently so that they perform probes for some networks more frequently than for others.

In Figure 11, we show that after estimating the privacy levels of local and remote nodes they get ranked via the Ruleset as well as privacy and urgency requirements. Each flow is dynamically managed to enable adaptive weightings of the input parameters. CogPriv then maps the incoming bundles to suitable outgoing interfaces and protocols. Possible decisions that CogPriv can take include adaptive forwarding (choosing the best hop), adaptive storing (choosing to retain the bundle), probe query (issuing the query on behalf of another node), responding to query when being asked.

4. Cognitive Privacy Algorithm and Decision Heuristics

In this section, we propose and describe several new heuristics for driving local collaborative decisions and discuss in detail cooperative probing mechanism as integral and complementary parts of CogPriv.

Cooperative CogPriv module includes intelligent dynamic probing of the local cellular network for any privacy threatening middleboxes and cooperation with the destination about its cellular network. The results of these probes are stored in two fields (Probe Local Estimation and Probe Remote Estimation) as part of extension of the bundle header format referred to as Extended CogPriv bundle header format shown in Figure 12.

Collaborative CogPriv module uses several metrics for heuristics and analytics of ad hoc neighbours privacy levels in order to predict the level of privacy each node can provide. More specifically, each node generates information on its estimated privacy level and exchanges it with its neighbours. The Extended CogPriv bundle header contains information on node social and resource metrics: betweenness, tie strength, and resources as shown in Figure 12.

Adaptive forwarding decision (InfrastructureprivUtil) is a function of estimated local and remote privacy as well as collaboration involving message exchange on these estimations (formula (1)). In addition to the exchange of measurements of local privacy levels (LocalProbUtil) collaboration involves QoS metrics in order to achieve maximum quality of service in terms of minimal delays and minimal resource overload while achieving maximum required privacy. This is shown in formula (2). Consider

$$\text{InfrastructureprivUtil} = f\left(\text{local\_cell\_probe, remote\_cell\_probe}\right), \tag{1}$$

$$\text{LocalProbUtil} = f\left(\text{local\_cell\_probe, social analytics, resource analytics, cooperation}\right). \tag{2}$$

Therefore, the headers need to include in-network delays prediction, in-network storage, social betweenness, centrality, and tie strengths with the destination in order to allow bundles to keep directionality of the sent bundles, as shown in the following:

$$h \in H = \left\{w_1 * \text{Priv}, w_2 * (\text{Ret, Rec}), w_3 * \text{social}\right), \tag{3}$$

where w_1 is weight that depends on the privacy requirements identified for this traffic type, w_2 is the weight of the local resource estimation, and w_3 is the weight of the local social estimation.

When a forwarding node (X) meets contacts on its way, it exchanges relevant heuristics and calculates the CogPrivUtil of each contact. This is shown in formulas (4) and (5). The CogPrivUtil allows the node X to detect how well connected its contact Y is and how available Y is in terms of estimated privacy levels it supports, storage, delay, and social connectivity parameters.

Formula (5) proposes new metric ($\text{Util}_{\text{Priv}}$) for calculating relative utility of the infrastructure privacy ($\text{Infrastructure}_{\text{priv}}$) when compared to the local privacy ($\text{Local}_{\text{priv}}$):

$$\text{CogPrivUtil}_D(X) = \sum_{h \in H} w_h \text{Util}_h(X), \tag{4}$$

$$\text{Util}_{\text{Priv}}(X) = \frac{h\left(\text{Infrastructure}_{\text{priv}}(X)\right)}{h\left(\text{Infrastructure}_{\text{priv}}(X)\right) + h\left(\text{Local}_{\text{priv}}(X)\right)}. \tag{5}$$

Retentiveness (Ret) [28–31] refers to the node's available storage for the new bundles that are sent to them. Retentiveness is an important attribute to consider because of the store and forward nature of opportunistic DTN networks [32]. Nodes with limited storage, either due to popularity or simply due to Personal Cloud hardware constraints, are more susceptible to bundle loss. Retentiveness is calculated as an exponentially weighted moving average of a Personal Cloud remaining storage. Formula (6) shows that retentiveness of X is calculated as the sum of all bundle occupancy subtracted from the node's buffer capacity ($B_c(X)$):

$$\text{Ret}(X) = B_c(X) - \sum_{i=1}^{N} b^i_{\text{size}}(X). \tag{6}$$

Receptiveness (Rec) [28–31] refers to the Personal Clouds' ability to receive bundles and forward them on. This is an important observation as increasing in-network delays is an indication that the volume of traffic a node or region is receiving is greater than the bandwidth available to it for offloading. The delay between receiving a bundle and forwarding a bundle is constrained by the size of the buffer and the bandwidth available for a node to offload the bundles. Nodes with large size of storage are more susceptible to receiving more bundles than being capable of offloading. Formula (7) shows that receptiveness is the total current bundle delay, calculated as the sum of differences between the current time (T_{now}) and the time each bundle was received (M_{received}):

$$\text{Rec}(X) = \sum_{i=1}^{N} \left(T_{\text{now}} - b^i_{\text{received}}(X)\right). \tag{7}$$

Each node keeps track of its centrality degree defined as the number of its encounters during predefined time and betweenness defined as the existing indirect links between each pair of its neighbours.

Degree is computed as total number of direct links to a given user n:

$$C_D(n_0) = \sum_{k=1}^{N} a(n_0, n_k). \tag{8}$$

Related work on online social networks [33] presents large-scale study of fine grained privacy preferences for Facebook users which provides the information on how users specify social access control lists (SACL) on a social networking service. They show that SACL membership has little correlation with profile information and online social network links; and making recent SACLs available to users is more promising as users tend to reuse SACLs. We expand on these findings and propose to use the recency, betweenness, and frequency social metrics for choosing the more trusted data carriers as suitable for mobile (disconnection prone) social networks.

We define betweenness in line with [34] by building and processing adjacency matrix. The adjacency matrix is updated based on the application requirements:

$$C_B(p_i) = \sum_{j=1}^{N} \sum_{k=1}^{j-1} \frac{g_{jk}(p_i)}{g_{jk}}. \tag{9}$$

Frequency refers to the number of times a given user n encounters a destination d. Frequency graph of user n to the destination d is calculated as follows:

$$F_n(d) = \frac{f(d)}{F(n) - f(d)}, \tag{10}$$

where $f(d)$ is the number of times destination d has been encountered and $F(n)$ is the total time that user n has encountered d from the beginning of the simulation.

Recency is defined as how recently a user n last met a destination d shown in the following:

$$\text{Recency}_n(d) = \frac{\text{recency}(d)}{T(n) - \text{recency}(d)}. \tag{11}$$

Tie Predictor. Once a user encounters destination, it computes the similarity to the destination and updates. More specifically, the similarity refers to the number of direct neighbours and indirect encounters. The higher the number of common neighbours is, the higher the probability that a given user moves regularly to this destination is. To account for more synchronous communication, we use similarity as a core metric for calculating tie prediction:

$$\begin{aligned} \text{TsUtil}_n(m) &= \frac{\text{TS}_m(d)}{\text{TS}_m(d) + \text{TS}_n(d)}, \\ \text{SimUtil}_n(m) &= \frac{\text{Sim}_m(d)}{\text{Sim}_m(d) + \text{Sim}_n(d)}. \end{aligned} \tag{12}$$

Choosing Carrier. The decision on forwarding of the stored bundle is based on the utility calculation whenever a source or a carrier detects a new neighbour. If the new neighbour has a higher total utility compared to the given user, the bundle will be forwarded. The utilities are computed by pairwise comparison:

$$\text{CogPrivUtil}_n(m) = \frac{\text{CogPriv}_D(m)}{\text{CogPriv}_D(m) + \text{CogPriv}_D(n)}. \tag{13}$$

5. Experiment Setup and Results

5.1. Experiment Scenario and Datasets. We begin with describing two real-world data traces that we use in our experiments and then describe our methodology of running experiments and clarify our criteria before we give and discuss our results.

We base our experiments on the real-world data traces of different probes for mobile networks across 112 countries and over 200 mobile providers obtained by Netalyzr in [1]. Examples of the probes in [1] include Web probes such as *http_content_change*, *http_hdr_reorder*, *http_hdr_injection*, *invalid_host_name_vulnerability*, *http_enforcement*, *http_default_compression,* and *Transcoding* as well as DNS probes which include *dns_direct_mangled*, *dns_direct_proxy*, and *dns_direct_changed_id*.

We select traces of one country (Germany) as its number of mobile networks' providers best suits our real-world user communication trace [35] so that every user can be on the different network. For every mobile node, we obtain the probability for the network spying on the web traffic by calculating the percentage of test returning positive versus the total number of tests performed. For every mobile network, we obtain the probability of it spying on web traffic by averaging the values obtained by all individual mobile nodes on this particular network.

Table 1: Overview of middlebox distribution identified in a range of mobile providers in Germany.

Name	Probes	Web	DNS	Web %	DNS %
1&1	1	1	0	100	0
ALICE	1	0	0	0	0
BASE	12	0	12	0	100
BLAU	3	0	3	0	100
CONGSTAR	6	6	3	100	50
DEBITEL	1	0	1	0	100
E-PLUS	9	0	9	0	100
FONIC	1	0	1	0	100
FYVE	5	5	3	100	60
KABELBW	1	0	1	0	100
LIDL	2	0	0	0	0
MEDION	5	0	5	0	100
M-NET	2	0	1	0	50
NETZCLUB	1	0	0	0	0
O2	35	0	16	0	45.71429
T-Mobile	83	83	27	100	32.53012
Vodafone	36	36	10	100	27.77778

The table of mobile networks, probes, and analysis is given in Table 1.

We carry out performance evaluation of CogPriv versus cellular communication and local social opportunistic networks across a range of network conditions and user traffic types across a range of metrics.

Based on the real cellular networks in Germany (shown in Table 1), we average privacy levels into five evenly distributed privacy threat levels, for example, minimum (0%) such as ALICE and NETZCLUB, low (25%) such as M-NET, medium (50%) such as BASE and MEDION, high (75%) such as CONGSTAR, and maximum (100%) such as FYVE.

We developed extensions to the one simulator [36] that utilises data from Table 1 in order to return middleboxes presence probability discovered when performing probing of different cellular networks.

We run experiments with the entire time of real-world Facebook connectivity traces UNICAL [35] for maximum privacy requirements with five different levels of cellular network privacy to which users are connected. UNICAL contains Bluetooth device proximity data, collected by an ad hoc Android application, and the social profiles in terms of Facebook friendships and interests of a group of 15 students. Experimental data were collected at the campus of University of Calabria in Rende, Italy. In order to gather the proximity information, the aforementioned ad hoc application was installed on each student's smartphone. Each participant was

instructed to keep with themselves the device that ran the SocialBlueConn application. The experiment lasted one week during student's lessons, from January 28, 2014, to February 5, 2014, including only the working days. Unlike [37, 38] traces, [35] does not identify beginnings and ends of contacts but only sightings. We have assumed that the sightings last at least 60 seconds based on the interval duration between the most frequent sightings. Detailed analysis of mobile social networks and online social networks for UNICAL has been done in [35] and has shown high degree correlation which we exploit in our ad hoc local message forwarding in our experiments.

We assume that all sending nodes aim to send highly personal but not urgent messages (e.g., self-monitoring ongoing long-term health conditions) for large number of experiments, but we also investigate CogPriv performance in the face of varying privacy requirements. We assign varying privacy requirements to each bundle and each CogPriv node can check if the reported levels of middlebox presence in the network can be tolerated for each bundle based on the comparison of levels of middleboxes and privacy required.

In our experiments, we measure end-to-end achieved privacy levels, end-to-end delays, and number of hops between the end points. We run extensive experiments in three increments with steps of 4 (26% of all nodes), 8 (48% of all nodes), and 12 (80% of all nodes) which we repeat for 5 randomly selected combinations of sources and receivers for each cellular network privacy level. This is important for allowing us to get medium, minimum, maximum, and average for each metric. Our results showed that there are no significant differences between different percentages of nodes actively generating and sharing content for the privacy related metrics. We provide Figure 13 to show this. Regarding the resource metrics (retentiveness), we give Figure 19 that focuses on exploring differences between wide range of sending nodes and privacy requirements. Figure 19 does not show significant resource availability differences due to CogPriv utilising an effective congestion aware forwarding heuristics on retentiveness and receptiveness introduced in [28–31].

The following results show that adaptive Cognitive Privacy approach is fundamental for future pervasive applications where Personal Clouds need to communicate via different levels of network privacy for different applications. CogPriv module that is adaptive, real time, collaborative, and cooperative is the core component of future Personal Clouds and necessary extension of the virtualisation of the application storage and hosting. We show that CogPriv is able to gracefully and transparently adapt to local context (both social and network) and remote context (via probes and communication with the destination).

5.2. Results

5.2.1. Achieved End-to-End Privacy and Analysis. Figure 13 shows that end-to-end privacy levels remain higher for CogPriv approach than for cellular only and mobile social ad hoc communication independently of the level of presence of middleboxes in the cellular infrastructure, that is, ranging from no middleboxes to wide range of middleboxes; the performance of Cognitive Privacy drops from 100% privacy level to 85%. This is in contrast with the cellular network which drops end-to-end privacy linearly with the amount of the middleboxes in the cellular network. CogPriv approach also outperforms fully local social ad hoc approach because of the delays that are associated with the bundles time-out and invoke the nodes to utilise cellular infrastructure that may have privacy leaks.

In order to cover wide range of nodes and more conditions they may face (e.g., not to miss a node or nodes that are disconnected), we have done performance analysis for 27% (4 nodes out of 15), 53% (8 nodes out of 15), and 80% (12 nodes out of 15) of randomly selected nodes acting as senders and receivers and each experiment run has been repeated 5 times. We show that there are very minor differences in the performance in the three graphs in Figure 13. Figure 13 shows constant achieved end-to-end privacy for local ad hoc routing for each random selection of senders/receivers. This is due to the use of the real-world trace where the conditions in the node connectivity among the selected nodes do not change for one selection of the nodes for one experiment run as well as due to ad hoc local not detecting middleboxes in the cellular infrastructure and thus not changing its behaviour in the face of the increasing levels of middleboxes.

From Figures 13(a), 13(b), and 13(c), we can see that the differences in E2E privacy for local ad hoc network may slightly change for different numbers of senders and receivers but this difference is also low. This is due to the trace having strong mobile social network characteristic (as it is based on the real-world students traces) and us using local ad hoc routing which exploits social connectivity patterns for forwarding.

Figure 14 shows statistical analysis of end-to-end privacy levels for bundles (mean, max, and min) for different levels of presence of middleboxes in the cellular networks. We observe that there are no drastic oscillations in the level of end-to-end privacy and quality of services for the end-to-end nodes. This is because CogPriv approach adapts very effectively and is able to optimally utilise both local and infrastructure resources.

In order to better understand the influence on end-to-end privacy for different levels of centralities for mobile ad hoc local networks, we investigate a range of scenarios where the local ad hoc nodes have low, medium, and high centrality in the face of varying levels of cellular infrastructure surveillance. In offline analysis, we ordered the nodes' degree centralities and choose top 33% as high central nodes and medium (33–66%) as medium centrality and low centrality (below 33%). Due to the sparse connectivity of UNICAL dataset with peak degree connectivity of 6, these centralities result in 2 top ranked, 2 medium ranked, and 2 bottom ranked nodes. Figure 15 shows that, for all levels of connectivity degrees of the local ad hoc nodes, the achieved end-to-end privacy levels for CogPriv are significantly higher than those when cellular network is utilised. CogPriv performs more than 40% better compared to local ad hoc communications for all centrality levels.

In order to show how CogPriv approach adapts to different requirements for privacy, we have performed experiments

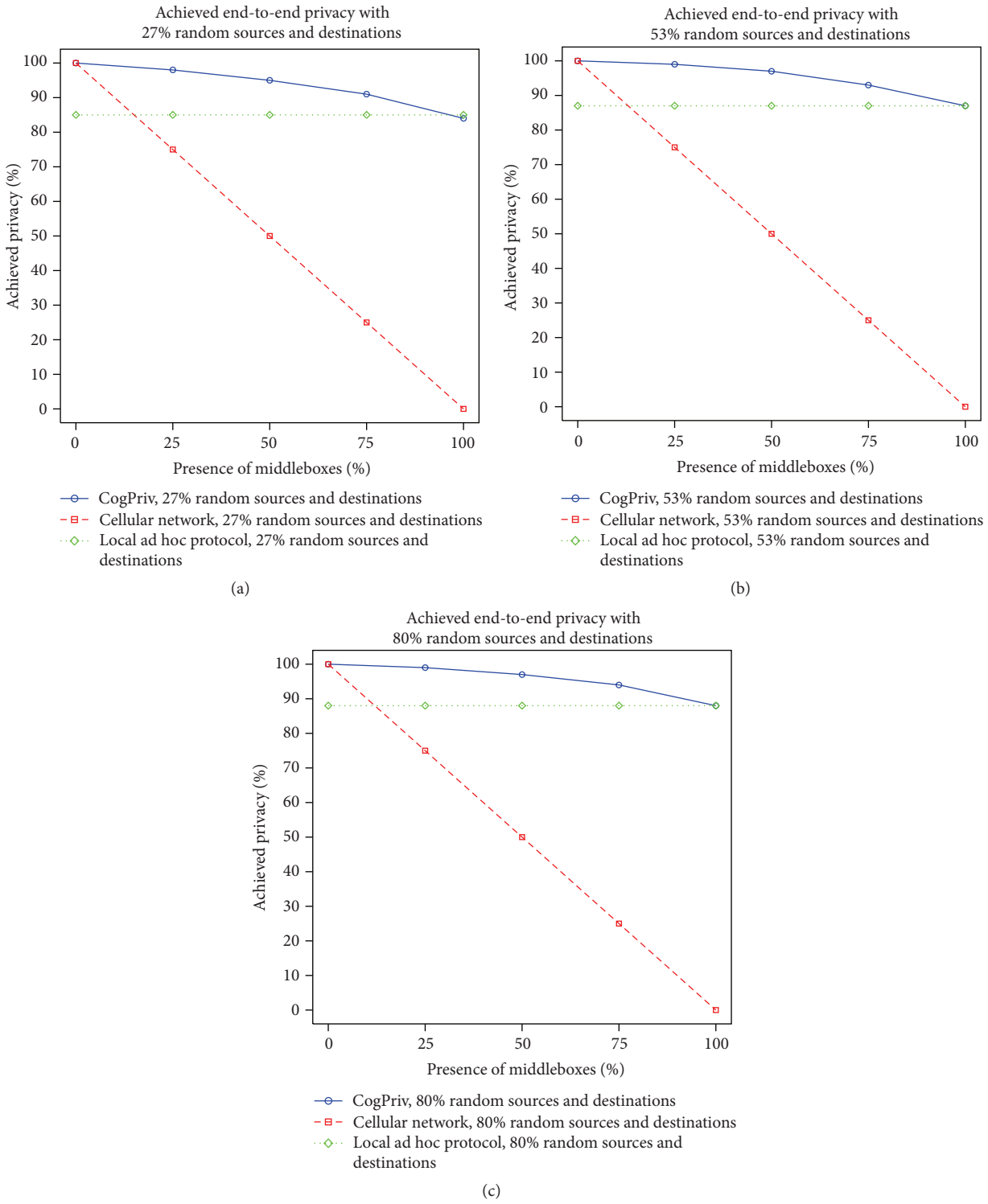

Figure 13: End-to-end privacy.

with different traffic types ranging from highly personal through intermediary and not personal types. We assign different privacy requirements to each bundle at the source. At each forwarding decision-making point, CogPriv nodes compare the bundle privacy requirement against the probability of leakage in a network that CogPriv returns. Bundles that have lower privacy requirements than the probability of leakage in a network can be sent via that network. Otherwise, the bundles will be sent via another network or stored at the node if no network meets the bundle privacy requirements. In Section 3, we explain that for bundles which are urgent, the bundles can be sent via cellular network if no trusted

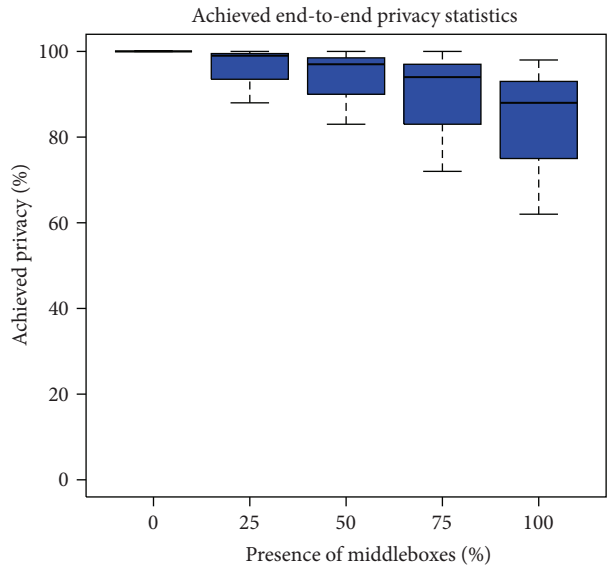

Figure 14: End-to-end privacy statistics.

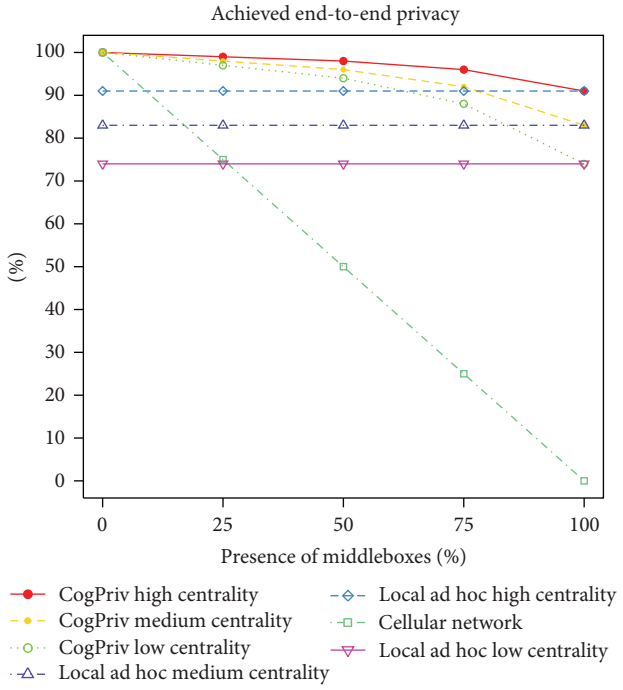

Figure 15: Security with varying centrality of the destination.

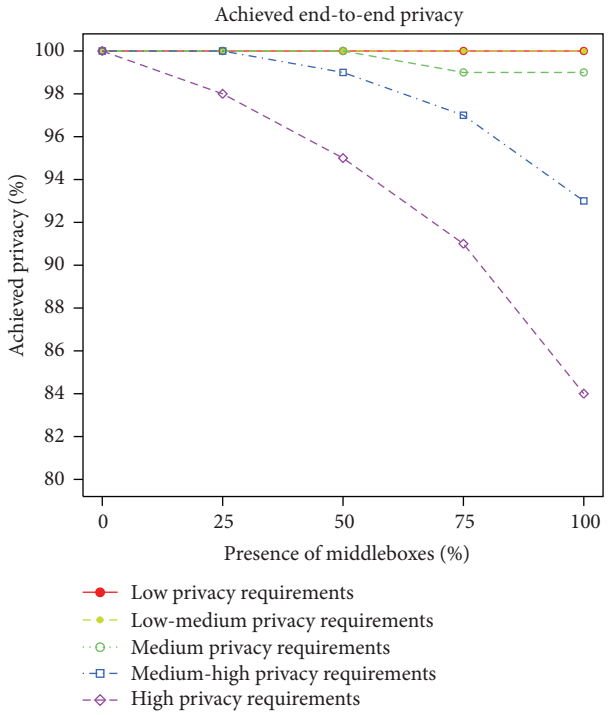

Figure 16: Security with varying privacy requirements.

local ad hoc route is found within a predetermined time-out period suitable for that bundle which is determined at the application level. Figure 16 shows that Cognitive Privacy approach manages to keep above 98% of achieved end-to-end privacy for medium personal traffic while it keeps above 92% for medium to high privacy traffic. For highly personal traffic, Cognitive Privacy manages to keep above 82% for all levels of middle boxes presence in the cellular network. As expected, we show that the higher the node centralities are, the higher the achieved end-to-end privacy levels are for all protocols. It is important to observe that the achieved end-to-end privacy levels for CogPriv are above 90% for all levels of degree centralities for low to medium-high level of middlebox presence in the cellular network. For high levels of middlebox presence in the cellular network and for high node centralities, the archived end-to-end privacy for CogPriv is still very high (96%). For medium and low node connectivity, CogPriv manages privacy of around 85% and 75%, respectively, in the face of high levels of middlebox presence in the cellular network. This is very important as it shows that even in both cases when the cellular network is highly compromised and the trusted local ad hoc network is very disconnected and sparse, CogPriv can keep high levels of privacy which converge to the performance of local ad hoc approach that utilises social network structure for forwarding.

5.2.2. End-to-End Delays and Retentiveness Analysis. Figure 17 shows that CogPriv end-to-end delays increase slowly until the infrastructure is fully compromised at which point the delays become the same as they are for the local ad hoc approach. The cellular network approach has the lowest delays but this is due to privacy being compromised and the traffic taking single hop (direct) cellular link between the end nodes.

Figure 18 shows delay distributions for highly private traffic bundles when the cellular infrastructure contains dramatically different amount of middleboxes. We observe that the delays are the lowest when the infrastructure is not compromised as the CogPriv approach takes cellular single hop router to the destination. As CogPriv discovers

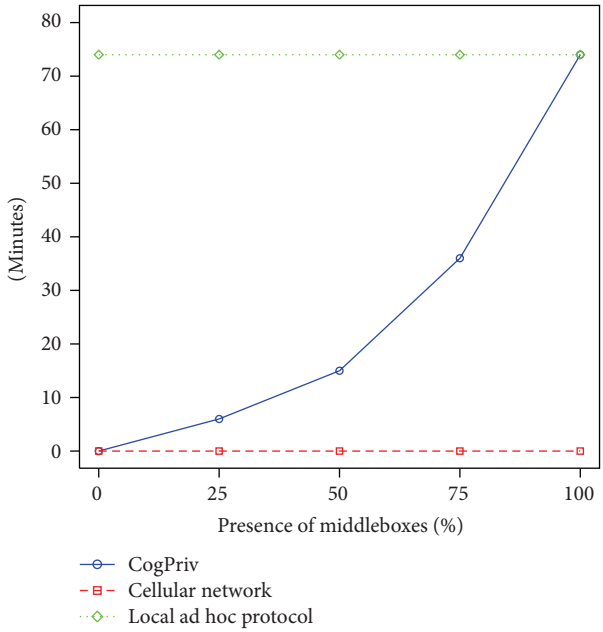

Figure 17: End-to-end delays.

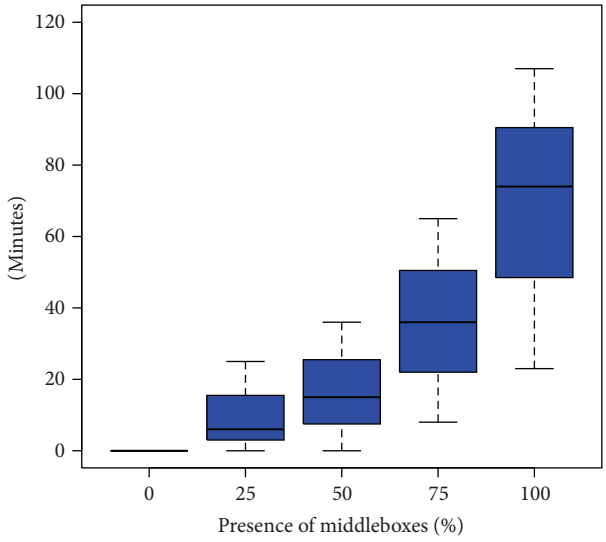

Figure 18: End-to-end delay statistics.

increasing number of middleboxes in the cellular networks, the delays increase but are significantly lower than the local ad hoc approach. Even though there are some bundles that may take up to 25 minutes until 50% of surveillance of the cellular network, the average still remains low and below 17 minutes. For the cellular network where there is 75% to 100% of middlebox presence, the delays range from 10 minutes (min) to 100 minutes (max) and from 3 minute to 75 minutes (average). These sorts of delays are appropriate for nonemergency applications where the users value their privacy and can tolerate delays such as regular daily checks for users with long-term medical conditions.

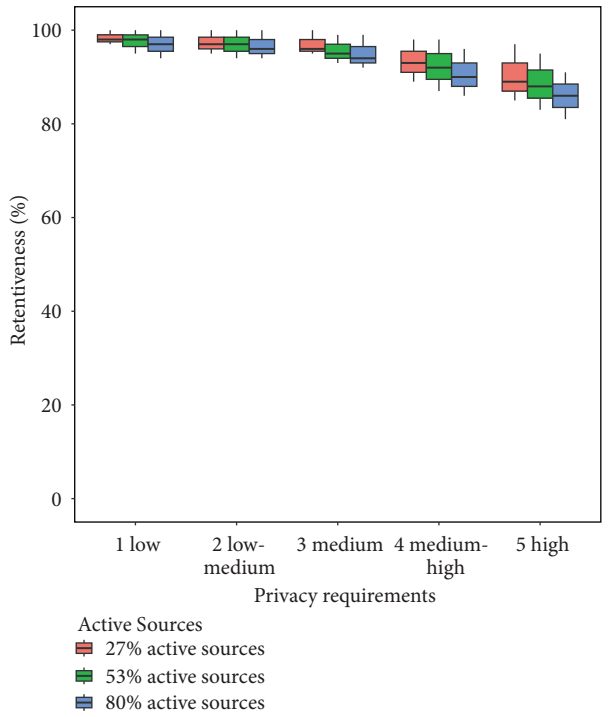

Figure 19: Retentiveness.

Figure 19 shows that CogPriv manages to maintain high levels of retentiveness (available storage) which is 85% for all levels of privacy requirements and for increasing number of active sources. It is important to investigate influence of different levels of privacy requirements as retentiveness gets measured only in ad hoc local forwarding (not cellular). More specifically, as privacy requirements increase and the more CogPriv chooses local forwarding over cellular forwarding which has middleboxes, we show that CogPriv does not significantly decrease available storage. Moreover, even for significant increase of active sources from 27% to 80%, the decrease in retentiveness is only around 1%. This is due to CogPriv utilising effective heuristics on congestion awareness and social graph analytics to predict the best next hop (the heuristic is described in Section 4). It is important to note that for the highest privacy requirements CogPriv will behave as local ad hoc protocol as it will always use only local ad hoc communications and not the cellular network infrastructure.

5.2.3. End-to-End Forwarding Hop Count and Transition Analysis. It is interesting to see in Figure 20 that CogPriv approach does not add additional number of hops compared to local ad hoc communication. We observe that end-to-end number of hops increases as the cellular network privacy decreases but remains lower than it is for local ad hoc forwarding. This is because CogPriv can effectively utilise an opportunity for middlebox-free cellular network whenever possible which allows it to connect to the destination via a single hop. This means that CogPriv does not add to delays compared to the local ad hoc approach while it increases the delays only when the cellular network significantly compromises user privacy.

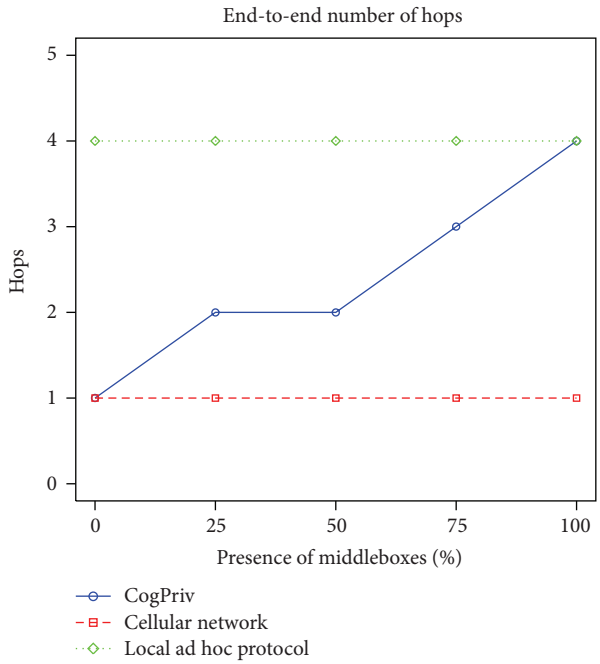

Figure 20: Number of hops.

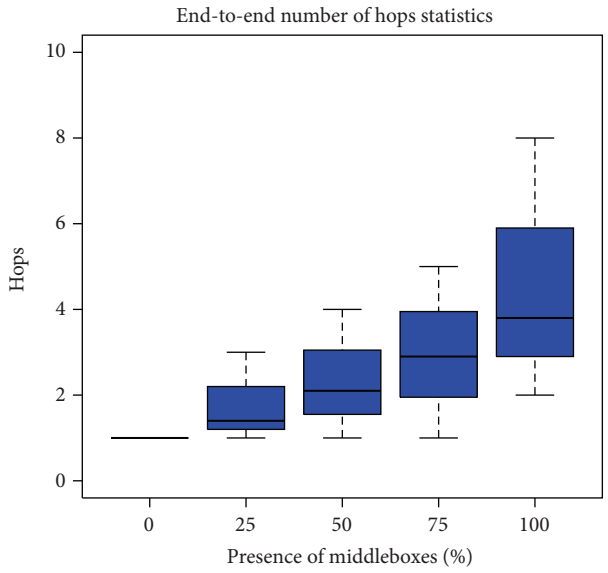

Figure 21: Number of hops statistics.

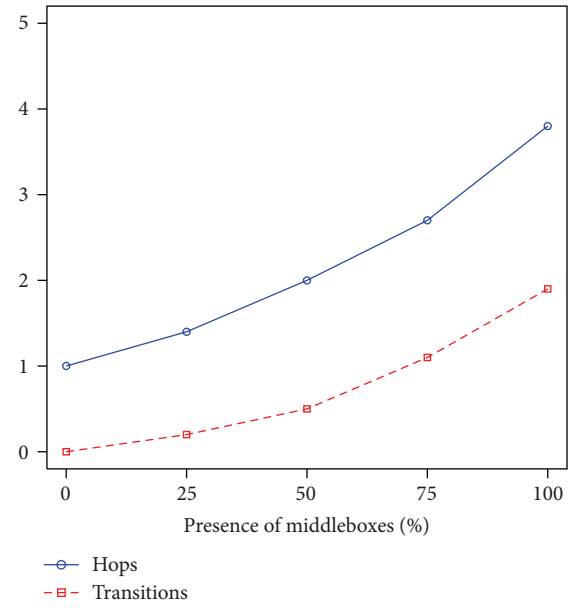

Figure 22: End-to-end number of transitions.

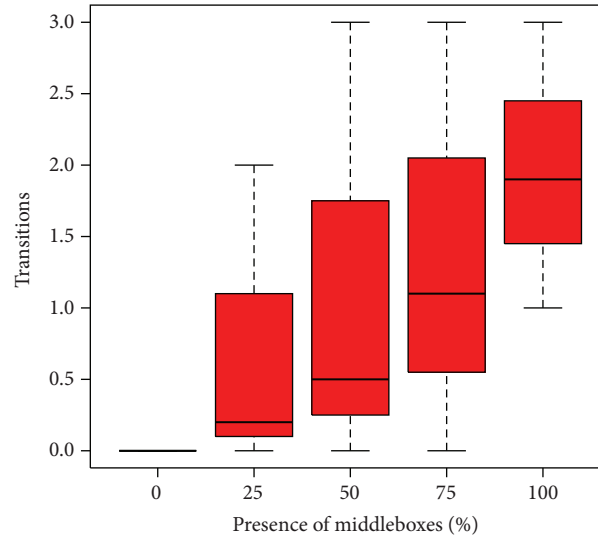

Figure 23: End-to-end transitions statistics.

Figure 21 shows statistical analyses of CogPriv number of hops with increased number of middleboxes in the cellular architecture. We observe that the numbers range between 1 and 4 across all levels of middleboxes presence.

In Figure 22, we show the number of transitions between infrastructure and local ad hoc protocol when the security of the cellular network decreases. It is interesting to see that while the number of hops is relatively low (reaching 4 for highly compromised cellular networks), up to 50% of these hops are transitions between the infrastructure and local communication. This shows that supporting adaptive transitioning between infrastructure and local communication is highly beneficial.

Figure 23 shows that the CogPriv approach keeps the average level of transitions below 2 for all levels of cellular network surveillance but occasionally peaks to 3 for high level of middleboxes in the network. This shows that CogPriv approach adapts well to the presence of middleboxes in the cellular networks while effectively utilising local communication to keep the end-to-end quality of service as high as possible.

The previous figures have shown that delays and hop by hop counts increase as CogPriv moves adaptively from fully

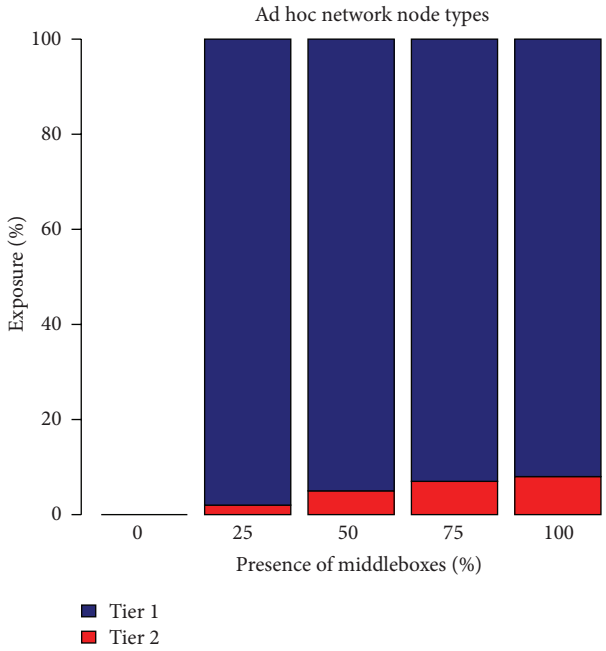

Figure 24: Exposure for increasing presence of middleboxes.

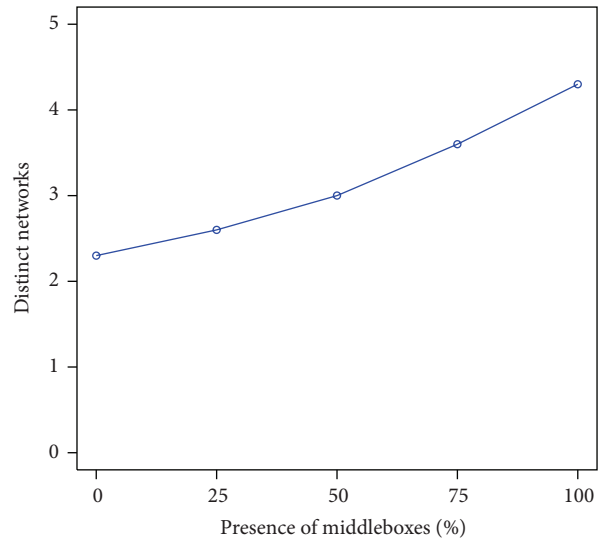

Figure 25: Exposure in end-to-end distinct cellular networks.

cellular mode to the fully opportunistic mode while managing very high levels of end-to-end privacy. More specifically, we show that the CogPriv achieves privacy of end-to-end connections which is almost constant while neither the delays nor the hop count is significantly increased.

5.2.4. Exposure Analysis. We are particularly interested in the issues of privacy being affected negatively despite the fact that no access control was violated. Emerging research shows that users of social media and remote health care applications increasingly prefer to have more control on who sees their data even among the users who are allowed to see their data via user access control rules. For example, while users may be happy that several closest friends of theirs can see and forward their data, they may not be happy that the other friends see some other data (e.g., social versus health related). Even in case of healthcare context, it has been argued that allowing local data control and privileges should be increasingly supported in addition to the central basic services. In this respect, more context sensitive policies can be enforced throughout the distributed communication cloud architecture.

Figure 24 shows percentage of data being exposed to the second tier of friends (those that are not the most trusted but who can still view the content) for increasing percentage of middleboxes in the cellular network. We observe that when percentage of middleboxes is lower than 25%, end-to-end traffic is not exposed to any second-tier friends. For increasing percentage of cellular network spying, we can see the increased reliance on all friends (both first- and second-tier) ranging from 1% to 7%. This is a very low exposure that shows the importance of local context driven data management.

Related research in social networks has shown that users consider their privacy violated when more different pieces of their data can be linked [39]. Towards this end, our proposal for adaptive privacy-aware forwarding is beneficial as it minimises multiple separate pieces of user data to be viewed, stored, and forwarded by the same node.

In Figure 25, we show the number of distinct networks on end-to-end routes that CongPriv takes for increasing levels of middlebox presence in the infrastructure. For medium to high level of privacy leakage in the cellular infrastructure, CogPriv utilises up to 4 distinct mobile networks and thus prevents the same compromised network provider from accessing and gathering different pieces of information about the user. For example, if we assume that a bundle gets forwarded via three mobile privacy providers with 25% privacy leakage, this does not add up to a total of 75% privacy leakage but remains in the low 25%.

6. Conclusions and Future Work

We proposed Cognitive Privacy (CogPriv) framework as an integral and core part of future Personal Clouds and pervasive communications. At the core of our proposal is the idea that, in mobile social world, privacy raises new challenges that go beyond typical binary allowed/forbidden access control and should take the form of cooperative, collaborative, and context dependent stochastic distributed decision-making. We argue that this new type of privacy can be called "Cognitive Privacy" as it on-the-fly senses and adapts to the infrastructure behaviour, strength/frequency of (mobile) social ties, and/or reputation of other nodes/people. Therefore, for different types of data and user context, the user may prefer to negotiate different levels of privacy.

We showed that CogPriv preserves end-to-end privacy levels to a high level across different network topologies and cellular network ad hoc middlebox distributions as well as different traffic types. As our future work, we plan to

deploy CogPriv and Personal Clouds in real-world scenarios in collaboration with Nottingham CityCare Partnership's initiatives to build healthier communities and improving long-term health and wellbeing of local people [40]. We plan to design new user-friendly interfaces that would improve usability of Personal Clouds particularly in respect of providing real time feedback to the user on the levels of privacy of their data. More specifically, we argue that it would be beneficial to allow users to disrupt some decisions of CogPriv at certain circumstances such as changed level of urgency, for example, when the user may prefer to wait longer and maintain higher level of privacy versus delivering the data to the destinations.

Competing Interests

The author declares that she has no competing interests.

References

[1] N. Vallina-Rodriguez, S. Sundaresan, C. Kreibich, N. Weaver, and V. Paxson, "Beyond the radio: illuminating the higher layers of mobile networks," in *Proceedings of the 13th Annual International Conference on Mobile Systems, Applications, and Services (MobiSys '15)*, pp. 375–387, ACM, Florence, Italy, May 2015.

[2] M. Radenkovic and N. Milic-Frayling, "Demo: RasPiPCloud: a light-weight mobile personal cloud," in *Proceedings of the 10th ACM MobiCom Workshop on Challenged Networks (CHANTS '15)*, pp. 57–58, Paris, France, September 2015.

[3] A. Y. Ding, J. Crowcroft, and S. Tarkoma, "Poster: SoftOffload: a programmable approach toward collaborative mobile traffic offloading," in *Proceedings of the 12th Annual International Conference on Mobile Systems, Applications, and Services (MobiSys '14)*, p. 368, Bretton Woods, NH, USA, June 2014.

[4] LXC—Linux Containers, https://linuxcontainers.org/.

[5] N. Vallina-Rodriguez, S. Sundaresan, C. Kreibich, and V. Paxson, "Header enrichment or ISP enrichment?: emerging privacy threats," in *Proceedings of the ACM SIGCOMM Workshop on Hot Topics in Middleboxes and Network Function Virtualization (HotMiddlebox '15)*, pp. 25–30, London, UK, August 2015.

[6] A. Y. Ding, B. Han, Y. Xiao et al., "Enabling energy-aware collaborative mobile data offloading for smartphones," in *Proceedings of the 10th Annual IEEE Communications Society Conference on Sensor, Mesh and Ad Hoc Communications and Networks (SECON '13)*, New Orleans, Lo, USA, June 2013.

[7] A. Balasubramanian, R. Mahajan, and A. Venkataramani, "Augmenting mobile 3G using WiFi," in *Proceedings of the 8th International Conference on Mobile Systems, Applications, and Services (MobiSys '10)*, pp. 209–222, San Francisco, Calif, USA, June 2010.

[8] K. Lee, J. Lee, Y. Yi, I. Rhee, and S. Chong, "Mobile data offloading: how much can WiFi deliver?" in *Proceedings of the 6th International COnference (Co-NEXT '10)*, Philadelphia , Pa, USA, 2010.

[9] A. Y. Ding, B. Han, Y. Xiao et al., "Enabling energy-aware collaborative mobile data offloading for smartphones," in *Proceedings of the 10th Annual IEEE Communications Society Conference on Sensing and Communication in Wireless Networks (SECON '13)*, pp. 487–495, New Orleans, La, USA, June 2013.

[10] N. Ristanovic, J.-Y. Le Boudec, A. Chaintreau, and V. Erramilli, "Energy efficient offloading of 3G networks," in *Proceedings of the 8th International Conference on Mobile Ad-hoc and Sensor Systems (MASS '11)*, pp. 202–211, IEEE, Valencia, Spain, October 2011.

[11] X. Zhuo, W. Gao, G. Cao, and Y. Dai, "Win-coupon: an incentive framework for 3G traffic offloading," in *Proceedings of the 19th IEEE International Conference on Network Protocols (ICNP '11)*, pp. 206–215, Vancouver, Canada, October 2011.

[12] E. Bulut and B. K. Szymanski, "WiFi access point deployment for efficient mobile data offloading," in *Proceedings of the 1st ACM International Workshop on Practical Issues and Applications in Next Generation Wireless Networks (PINGEN '12)*, pp. 45–50, ACM, Istanbul , Turkey, August 2012.

[13] J. Korhonen, T. Savolainen, A. Ding, and M. Kojo, "Toward network controlled IP traffic offloading," *IEEE Communications Magazine*, vol. 51, no. 3, pp. 96–102, 2013.

[14] S. Liu and A. Striegel, "Casting doubts on the viability of WiFi offloading," in *Proceedings of the ACM SIGCOMM Workshop on Cellular Networks: Operations, Challenges, and Future Design (CellNet '12)*, pp. 25–30, Helsinki, Finland, August 2012.

[15] E. Romero, J. Blesa, A. Tena, G. Jara, J. Domingo, and A. Araujo, "Cognitive test-bed for wireless sensor networks," in *Proceedings of the IEEE International Symposium on Dynamic Spectrum Access Networks (DYSPAN '14)*, pp. 346–349, McLean, Va, USA, April 2014.

[16] A. Razaghpanah, N. Vallina-Rodriguez, S. Sundaresan et al., "Haystack: in situ mobile traffic analysis in user space," http://arxiv.org/abs/1510.01419.

[17] E. Shi, T.-H. H. Chan, E. G. Rieffel, R. Chow, and D. Song, "Privacy-preserving aggregation of time-series data," in *Proceedings of the Network and Distributed System Security (NDSS '11)*, August 2011.

[18] M. Joye and B. Libert, "A scalable scheme for privacy-preserving aggregation of time-series data," in *Financial Cryptography and Data Security: 17th International Conference, FC 2013, Okinawa, Japan, April 1–5, 2013, Revised Selected Papers*, vol. 7859 of *Lecture Notes in Computer Science*, pp. 111–125, Springer, Berlin, Germany, 2013.

[19] K. Leontiadis, R. Elkhiyaoui, and R. Molva, "Private and dynamic time-series data aggregation with trust relaxation," in *Cryptology and Network Security*, D. Gritzalis, A. Kiayias, and I. Askoxylakis, Eds., vol. 8813 of *Lecture Notes in Computer Science*, pp. 305–320, 2014.

[20] M. Radenkovic and I. Vaghi, "Adaptive user anonymity for mobile opportunistic networks," in *Proceedings of the 7th ACM International Workshop on Challenged Networks*, pp. 79–81, ACM, August 2012.

[21] A. Grundy and M. Radenkovic, "Promoting congestion control in opportunistic networks," in *Proceedings of the 6th Annual IEEE International Conference on Wireless and Mobile Computing, Networking and Communications (WiMob '10)*, pp. 324–330, Niagara Falls, Canada, October 2010.

[22] M. Radenkovic, A. Benslimane, and D. McAuley, "Reputation aware obfuscation for mobile opportunistic networks," *IEEE Transactions on Parallel and Distributed Systems*, vol. 26, no. 1, pp. 230–240, 2015.

[23] H. Haddadi, H. Howard, A. Chaudhry, J. Crowcroft, A. Madhavapeddy, and R. Mortier, "Personal data: thinking inside the box," http://arxiv.org/abs/1501.04737.

[24] M. Y. Mun, D. H. Kim, K. Shilton, D. Estrin, M. Hansen, and R. Govindan, "PDVLoc: a personal data vault for controlled

location data sharing," *ACM Transactions on Sensor Networks*, vol. 10, no. 4, article 58, 2014.

[25] K. Scott and S. Burleigh, "Bundle protocol specification," RFC 5050, 2007.

[26] IBR-DTN, https://trac.ibr.cs.tu-bs.de/project-cm-2012-ibrdtn.

[27] S. Schildt, T. Lorentzen, J. Morgenroth, W.-B. Pöttner, and L. Wolf, "Free-riding the bittorrent DHT to improve DTN connectivity," in *Proceedings of the 7th ACM International Workshop on Challenged Networks (CHANTS '12)*, pp. 9–15, ACM, Istanbul, Turkey, August 2012.

[28] M. Radenkovic and A. Grundy, "Efficient and adaptive congestion control for heterogeneous delay-tolerant networks," *Ad Hoc Networks*, vol. 10, no. 7, pp. 1322–1345, 2012.

[29] M. Radenkovic and A. Grundy, "Framework for utility driven congestion control in delay tolerant opportunistic networks," in *Proceedings of the 7th International Wireless Communications and Mobile Computing Conference (IWCMC '11)*, pp. 448–454, Istanbul, Turkey, July 2011.

[30] M. Radenkovic and A. Grundy, "Congestion aware data dissemination in social opportunistic networks," *Mobile Computing and Communications Review*, vol. 14, no. 3, pp. 31–33, 2010.

[31] M. Radenkovic and A. Grundy, "Congestion aware forwarding in delay tolerant and social opportunistic networks," in *Proceedings of the 8th International Conference on Wireless On-Demand Network Systems and Services (WONS '11)*, pp. 60–67, Bardonecchia, Italy, January 2011.

[32] K. Fall, "A delay-tolerant network architecture for challenged internets," in *Proceedings of the 2003 Conference on Applications, Technologies, Architectures, and Protocols for Computer Communications (SIGCOMM '03)*, pp. 27–34, ACM, New York, NY, USA, 2003.

[33] M. Mondal, Y. Liu, B. Viswanath, K. P. Gummadi, and A. Mislove, "Understanding and specifying social access control lists," in *Proceedings of the 10th Symposium on Usable Security and Privacy (SOUPS '14)*, Menlo Park, Calif, USA, July 2014.

[34] E. M. Daly and M. Haahr, "Social network analysis for information flow in disconnected delay-tolerant MANETs," *IEEE Transactions on Mobile Computing*, vol. 8, no. 5, pp. 606–621, 2009.

[35] A. Socievole, F. De Rango, and A. Caputo, "Wireless contacts, Facebook friendships and interests: analysis of a multi-layer social network in an academic environment," in *Proceedings of the IFIP Wireless Days (WD '14)*, pp. 1–7, Rio de Janeiro, Brazil, November 2014.

[36] A. Keränen, J. Ott, and T. Kärkkäinen, "The ONE simulator for DTN protocol evaluation," in *Proceedings of the 2nd International Conference on Simulation Tools and Techniques (Simutools '09)*, article 55, p. 10, ICST (Institute for Computer Sciences, Social-Informatics and Telecommunications Engineering), Brussels, Belgium, 2009.

[37] J. Scott, R. Gass, J. Crowcroft, P. Hui, C. Diot, and A. Chaintreau, *CRAWDAD Dataset Cambridge/Haggle (v. 20090529)*, 2009.

[38] F. Benbadis and J. Leguay, "CRAWDAD dataset upmc/rollernet (v. 20090202)," February 2009, http://crawdad.org/upmc/rollernet/20090202.

[39] M. Mondal, P. Druschel, K. P. Gummadi, and A. Mislove, "Beyond access control: managing online privacy via exposure," in *Proceedings of the Workshop on Usable Security*, 2014.

[40] Nottingham CityCare Partnership, http://www.nottinghamcitycare.nhs.uk/.